TROPICAL CYCLONE INTENSITY CHANGE: EVALUATING THE EFFECTS OF INNER CORE PRECIPITATION PROPERTIES AND ENVIRONMENTAL INFLUENCES

by

George Robert Alvey

A thesis submitted to the faculty of
The University of Utah
in partial fulfillment of the requirements for the degree of

Master of Science

Department of Atmospheric Sciences

The University of Utah

August 2015

The University of Utah Graduate School

STATEMENT OF THESIS APPROVAL

The thesis of **George Robert Alvey**

has been approved by the following supervisory committee members:

Edward J. Zipser	, Chair	**12/10/2014** Date Approved
William James Steenburgh	, Member	**12/10/2014** Date Approved
Haiyan Jiang	, Member	**12/18/2014** Date Approved

and by **Kevin D. Perry** , Chair of

the Department of **Atmospheric Sciences**

and by David B. Kieda, Dean of The Graduate School.

ABSTRACT

Despite improvements in recent years, tropical cyclone intensity change, and in particular differentiating intensification rates (especially rapid intensification, RI), remains an unresolved issue. Studies have quantified the importance of both environmental and convective properties with respect to intensity change; however, conjoined analyses have been rare. Using 15 years (1998-2012) of analysis information for Atlantic and East Pacific storms, we analyze environmental conditions to determine a threshold in which intensification is plausible. In conjunction with the environmental dataset, an expansive collection of passive microwave satellite data is used to investigate the relative importance of various convective properties (specifically those proxies for convective intensity, symmetry, and area). The Tropical Cyclone - Passive Microwave dataset (TC-PMW) statistics, and in particular, the spatial distributions of precipitation and intense convection (proxied using 85-91 GHz polarization corrected temperatures), are related to environmental conditions in an analysis of storms that meet the "plausible" threshold.

Storms with higher intensification rates (including RI) are found to have more "intense" near center convection and more asymmetric distributions of precipitation prior to intensification onset (but also a greater overall areal coverage). The rate of symmetrization prior to and during intensification increases with increasing intensity change, and rapidly intensifying storms are more symmetric than slowly intensifying

storms after onset. While results clearly demonstrate important contributions from intense convection, it is concluded that hot towers, alone, are neither a necessary nor sufficient condition for RI. Of possibly greater importance, intensification is more strongly correlated to the evolution of the areal, radial, and symmetric distribution of precipitation. In addition, while intensification is sensitive to changes in environmental characteristics, these variables, alone, do not consistently offer predictive value in distinguishing 24-hour intensity changes in 10-kt increments (hence the emphasis on convective and precipitation characteristics).

CONTENTS

ACKNOWLEDGEMENTS

Honestly, the best part about completing my thesis is reflecting back on all those that have helped me get where I am today. So many people have made an impact that probably do not and may never know it, but you all helped me achieve something I have dreamed about since I was a kid. A truly amazing feeling and it makes me so grateful. To my awesome family, friends, and professors, past and present, mahalo! In particular, I would like to thank Dr. Ed Zipser for his invaluable advice and guidance throughout my Master's research project. To Dr. Haiyan Jiang and Dr. Jim Steenburgh, thank you for serving on my committee and providing critical feedback. For mentorship and support I am grateful for the time Jon Zawislak put aside to help me. I am also thankful for the advice and assistance provided by members of the Zipser research group, and in particular, Sarah Bang. None of this would be possible, however, without the support of my family and the unwavering love and encouragement from my parents, Bonnie and George.

CHAPTER 1

INTRODUCTION

While improvements have been made in recent years, tropical cyclone intensity changes, and in particular, forecasting intensification rates (including rapid intensification, RI) remains an unresolved issue. Bister and Emanuel (1998) defined a theoretical maximum steady-state intensity (maximum potential intensity, MPI) a storm can reach based upon sea surface temperature (SST) and storm top environmental temperature. Most tropical cyclones (TC), however, fail to reach their MPI due to inhibiting environmental effects including vertical wind shear and insufficient SSTs (often induced cooling via upwelling). Previous studies have quantified the importance of these large-scale environmental characteristics on tropical cyclone (TC) intensity changes (Holliday and Thompson 1979; Bosart et al. 1999; Hong et al. 2000; Black et al. 2002; Emanuel et al. 2003; Kaplan and DeMaria 2003, 2010; Hendricks et al. 2010). DeMaria and Kaplan (1994) developed a Statistical Hurricane Intensity Prediction Scheme (SHIPS) that utilizes predictors including the difference between MPI (a function of SST) and current intensity, vertical wind shear of the horizontal wind, and persistence, to provide a statistically significant improvement over climatology and persistence models for the Atlantic Basin. Since then several important contributions have been made to SHIPS including the addition of new environmental and convective variables (using infrared satellite). Kaplan and DeMaria (2003) investigated the frequency distributions of

24-hour intensification periods in the Atlantic Basin. From these data they defined RI as the 95th percentile of intensity changes, or approximately 30 kt (15.4 m/s). Kerry Emanuel (personal communication, June 28, 2014) stated that "histograms of intensification rates…all show perfect, bell-shaped probabilities of intensification, with absolutely no lumps or deviations." From a strictly scientific standpoint RI does not exist, it is simply defined into existence. Despite this sentiment, the majority of intensity change studies currently use RI as a threshold, often out of necessity to synthesize results.

Additional studies investigating environmental conditions have found that while important, these variables alone do not satisfy the intensity change problem. Although SHIPS improved upon climatology and persistence, the forecasts only explain approximately 50% of variability in observed TC changes (DeMaria and Kaplan 1994). Barnes et al. (2008) stated that "perfect" environments for RI are rare and many TCs undergo RI in the presence of less than ideal conditions. The synoptic environments surrounding TCs often do not provide unambiguous guidance for RI. Hong et al. (2000), in a study of Hurricane Opal (1995), hypothesized that only ~25% of the pressure fall during Opal's RI could be explained by a warm eddy. Hendricks et al. (2010) found that the environments of RI and slower intensification rates were similar, and thus concluded that on average the rate of intensification may be only weakly dependent on environmental conditions.

In response to the limited predictability of intensification rates using environmental parameters, several studies have examined the convective and precipitating properties of TCs. Studies examining the azimuthal distribution of convection in TCs have almost unanimously found that vertical wind shear is the

dominant factor in placement of precipitation (Rogers et al. 2003; Wingo et al. 2010; Hence et al. 2011; DeHart et al. 2014). These studies investigated the rainfall and associated convective distributions with similar results: Precipitation tends to maximize in the downshear-left quadrant. Hence et al. (2011) and DeHart et al. (2014) explored vertical reflectivity profiles (Tropical Rainfall Measuring Mission, TRMM, precipitation radar and airborne Doppler radar) and found that convection tends to initiate downshear-right; updraft frequency maximizes downshear-left before decreasing upshear-left. The upshear-right quadrant contains a "dearth" of intense reflectivity: Largest particles from the downshear-left quadrant have already fallen out and initiation generally does not occur until downshear-right.

Numerous additional studies have considered the effects of convection on intensity change (Rodgers et al. 1998; Cecil and Zipser 1999; Eastin et al. 2005; Montgomery et al. 2006; Nolan et al. 2007; Price et al. 2009; Sitkowski and Barnes 2009; Guimond et al. 2010; Jiang 2012; Kieper et al. 2012; Chen and Zhang 2013; Ramirez et al. 2013; Rogers et al. 2013, 2014; Zagrodnik et al. 2014). Gray (1998) found that TCs will not intensify without outbreaks of organized deep convection even when all environmental conditions are favorable for intensification. Rodgers et al. (1998, 2000), Price et al. (2009), and Guimond et al. (2010), analyzed several TCs in which convective bursts (CBs) with intense convection preceded or were coincident with the start of RI. It has been hypothesized that convective bursts moisten the midtroposphere so that deep convection can occur symmetrically within the inner core, contracting the eyewall (Nolan et al. 2007; Montgomery et al. 2006). Others have attempted to quantify warm-core contributions from CBs and associated subsidence (Holland et al. 1984; Heymsfield et al.

2001; Rogers et al. 2002; Guimond et al. 2010). Shea and Gray (1973) emphasized the importance of the "inner radar radius" and its close proximity to the radius of maximum winds (RMW) in the most intense TCs. More recently, Rogers et al. (2013, 2014) composited airborne Doppler observations and concluded that CBs in intensifying TCs are preferentially located inside the RMW. The question still remains, however, are CBs a cause of TC intensification or are they a reflection of vortex scale processes that enable CBs; and do intensifying TCs (particularly RI) have a higher proportion of CBs within the inner core?

Despite what appears to be a plethora of evidence supporting the importance of CBs with respect to intensity change, several studies, particularly those with the use of passive microwave (PMW) imagery, have hypothesized differently. Spencer et al. (1989) first determined that PMW properties could be used as a proxy for convective and precipitation intensity. Because ice has a much smaller absorption coefficient than water and a higher single scattering albedo, it produces the lowest brightness temperatures (Tb) at 85 GHz. Small depressions (10° - 30° C) are still possible, though, with liquid precipitation alone. Unfortunately, surface water bodies have low emissivities at 85-91 GHz also causing low Tbs; however, the emissivities are a strong function of polarization for oblique viewing angles. Because ice scattering has a much smaller polarization effect, it allows a calculation of brightness temperatures that removes ambiguities, hereafter referred to as polarization corrected temperatures (PCT). Using the 85 GHz channel, Spencer et al. (1989) determined that PCTs below 250-260 K have a good probability of being influenced by precipitation; thus, they created a threshold of 255 K to delineate rain areas with rates greater than or equal to 1-3 mm/hr. Similarly, Cecil and Zipser (1999)

used 85 GHz PCT as a proxy for updraft strength and precipitation intensity; more specifically, they used 250 K as a proxy for areas precipitating at least 1-3 mm/hr. Mohr and Zipser (1996) used 225 K PCT as a proxy for deep convection with lower PCTs (below 200 K) considered indicators of more "intense" convection. Using PCT to categorize mesoscale convective system (MCS) properties, they defined an "intense" MCS as a sufficiently large area less than 200 K with a minimum PCT less than 175 K.

Looking at PMW statistics as a proxy for convective intensity, Cecil and Zipser (1999) examined special sensor microwave imager (SSMI) 85 GHz PCT statistics and found a lack of relationship between indicators of intense convection and tropical cyclone intensification. Jiang (2012), using an 11-year TRMM tropical cyclone precipitation feature (TCPF) database, concluded that extremely intense convection in the inner core increases the chance of RI, but the increase is not substantial. Ramirez et al. (2013) used the same dataset to conclude that RI storms always have larger raining area and volumetric rain in the inner core; convective intensity (at the highest end of the spectrum), though, is not significantly greater for RI storms than slow or neutral intensification. In these studies it is believed that axisymmetric latent heat release is more crucial for vortex intensification than asymmetric heating.

This study utilizes a 15-year (1998 - 2012) passive microwave dataset (TC-PMW database) coincidentally with environmental statistics obtained from the Statistical Hurricane Intensity Prediction Scheme (SHIPS) and the National Centers for Environmental Prediction (NCEP) Final (FNL) analysis in the Atlantic (ATL) and Eastern Pacific (EPAC) Basins. Using the TC-PMW dataset, we aim to quantitatively compare the precipitation and convective characteristics with TC intensification rates. In

addition, an attempt is made at examining environmental characteristics in more detail (similar to Kaplan and DeMaria 2003, 2010). The temporal and spatial evolution of the environmental variables coincident with PMW snapshots are investigated before and during intensification periods in an attempt to further understand the complicated relationships between the environment and precipitation during TC intensity change.

CHAPTER 2

DATA AND METHODS

2.1 Extended Best Track Database

Using the National Hurricane Center (NHC) extended best track database, 6-hourly center positions at 0000, 0600, 1200, and 1800 coordinated universal time (UTC) are obtained for all tropical depressions and tropical cyclones (which will hereafter be solely referred to as tropical cyclones) in the Eastern Pacific and Atlantic Basins from 1998 - 2012. The database includes maximum sustained winds using the U.S. 1-minute average in kts for each time period along with storm classification (tropical, subtropical, extratropical, etc.). Figure 2.1 displays the distributions of 6-hourly intensities separated by basin for all tropical cyclones. Only storms with a tropical designation and classification of at least depression status are considered for the purpose of this study. Additional variables (archived by the NHC) include each storm's estimated radius of maximum winds; and the estimated maximum radius for 34 kt, 50 kt, and 64 kt sustained winds.

2.1.1 Best Track Population

Data are from 256 tropical cyclones of at least tropical depression status in the Atlantic Basin, comprising 5718 6-hourly best track times. After removing those periods with land interaction or extratropical transition (designated by the NHC) within the +24

hour timeframe, 4021 remain. The total number of cases divided into 5-kt increments for 24-hour intensity change represents a Gaussian distribution, as shown in Figure 2.2. The Atlantic Basin (solid black) is slightly left skewed, attributed to the large number of periods removed during which storms undergo extratropical transition in the Central and North Atlantic. When all cases with land interaction are removed the distribution becomes further left skewed.

Data from 241 tropical depressions and tropical cyclones in the Eastern Pacific total to 4661 6-hourly best track times. This reduces to 3621 after removing those with land interaction during the +24 hour period. The Gaussian distribution for the East Pacific is shifted slightly left from the Atlantic (Fig. 2.2). Removing land interaction periods in the East Pacific does not significantly alter the distribution; this indicates land interaction and extratropical transition are not as significant a source of TC weakening in the Eastern Pacific as in the Atlantic. Figure 2.3 displays tropical cyclone tracks for all periods used in this study and helps verify this hypothesis.

2.2 Environmental Database

The environmental variables encompass data from the Statistical Hurricane Intensity Prediction Scheme (SHIPS) reanalysis and the NCEP Final (FNL) model analysis. The SHIPS reanalysis includes the archived 00-hour forecast analysis for all tropical cyclones (6-hourly increments coinciding with the NHC best track) in the Eastern Pacific and Atlantic Basin. Archived data from the years 1998-2012 coincident with best track times in the ATL and EPAC are synthesized for this study.

2.2.1 SHIPS Dataset

All fields in the SHIPS reanalysis use the NCEP global analyses (DeMaria 2014) and NHC best track for center locations. The variables obtained from the SHIPS reanalysis file include the following variables (additional descriptions can be found at rammb.cira.colostate.edu/research/tropical_cyclones/ships/developmental_data.asp). *Distance to land* outputs the distance in kilometers to the nearest major landmass. *24-hour intensity change* is calculated for all 24-hour periods during which no land interaction occurs. SHIPS uses the Reynolds *sea surface temperature* (SST) methodology from a real-time global SST analysis. SHIPS also outputs *relative humidity* (RH) for 3 atmospheric layers using a 200 - 800 km annulus from the best track center: low-level (850 - 700 hPa), midlevel (700 - 500 hPa), and upper-level (500 - 300 hPa). Multiple *vertical wind shear* outputs from SHIPS are used: A vortex removal method in which the 0 - 500 km average wind shear is calculated as a layer difference (850 - 200 hPa) after the "vortex" has been artificially removed; additionally, a standard 200 - 800 km wind shear calculated as a layer difference without vortex removal is used. *Shear direction* (in degrees) for both shear methodologies, *ocean heat content* (OHC) using satellite altimetry data, and *maximum potential intensity* (MPI) using Kerry Emanuel's equation are additional variables.

Ocean heat content (OHC) is the integrated heat content excess per unit area relative to the 26 °C isotherm i.e., the integrated depth of the 26 °C isotherm to the surface. This helps combine SST and upper-ocean temperatures, which are important because of mixing, into one parameter (Mainelli et al. 2007).

Potential intensity is a function of SST, storm-top environmental temperature, and air-sea thermodynamic disequilibrium (Emanuel et al. 2003). MPI is defined as the maximum steady-state intensity a storm can reach based upon the thermodynamic efficiency of heat input from oceanic evaporation and dissipative heating balanced by the mechanical dissipation in the boundary layer (Bister and Emanuel 1998); in simplified terms, an open-cycle heat engine. Equations 2.1 and 2.2 are solved iteratively to determine MPI. Variables are as follows: V_m is the maximum gradient wind speed, T_s is the ocean temperature, T_0 is the mean outflow temperature, C_k is the exchange coefficient for enthalpy, C_D is the drag coefficient, $CAPE^*$ is the convective available potential energy of saturated air lifted from the sea surface, p_0 is the ambient surface pressure, and p_m is the surface pressure at the radius of maximum winds (RMW).

$$V_m^2 = \frac{T_s}{T_0}\frac{C_k}{C_d}[CAPE^* - CAPE]\Big|_m \tag{2.1}$$

$$c_p T_s \ln\frac{p_0}{p_m} = \frac{1}{2}V_m^2 + CAPE\Big|_m \tag{2.2}$$

2.2.2 Additional Variables and FNL Analysis

In addition to the SHIPS analysis, variables are calculated (and some duplicates from SHIPS) using the NCEP FNL analysis. The analysis uses additional observational data with the GFS initialization on 1-degree by 1-degree grids. This provides a sufficient resolution for the calculation of synoptic variables such as vertical wind shear of the horizontal wind and environmental relative humidity.

A Group for High Resolution Sea Surface Temperature (GHRSST) produces daily analyses at 1/4° resolution using optimal interpolation (OI) from the Advanced Very

High Resolution Radiometer (AVHRR). From these data, 1° and 2° centered averages are created. In Figure 2.4, SST calculated using the 1° method is compared to the SHIPS Reynolds SST. The slight difference in means can be attributed to the "point selection" method for SHIPS versus the 1° average. The 1° average is predominantly used for this study as a more representative measure for the inner core. Vertical wind shear is also calculated from the FNL analysis using the 200 - 800 km 850 - 200 hPa methodology and compared to the SHIPS (same calculation method). Figure 2.5 demonstrates the correlation coefficient of .95 and difference in means of -.04 m/s, verifying that no biases exist, and either calculation is sufficient.

2.2.3 Environmental Sensitivity

The importance of environmental parameters is examined using probability density functions (PDF), cumulative distribution functions (CDF), and box plots. Statistics are inspected for each basin separately. The environmental parameters deemed most important for 24-hour intensity changes remain the focus for the remainder of the study: Vertical wind shear (200 - 800 km 850 - 200 hPa), ocean heat content (OHC), low-level relative humidity (RH), midlevel relative humidity (RH), sea surface temperatures (SST), and maximum potential intensity - current intensity (VMPI - $V_{current}$). Using these six environmental variables, thresholds under which intensification is "plausible" are quantified for each basin.

Outliers for the variables are determined using the "box plot" method described below. All periods with a +24 hour intensity change greater than 0 kts are classified as "intensifiers." An environmental value qualifies as an outlier if it falls below (above for shear) 1.5 times the inner quartile range for the intensifiers. For each 6-hourly best track

period, a storm meets the threshold for plausible intensification if all six environmental conditions are satisfied; i.e., if all the conditions are above the "outliers" (or below for shear). Figure 2.6 demonstrates the above methodology using a flow chart.

2.3 Passive Microwave Dataset

A multiplatform dataset consisting of passive microwave overpasses coincident with tropical cyclones from 1998-2012 in the Eastern Pacific and Atlantic Basins is compiled for this study; the dataset is hereafter referred to as the Tropical Cyclone - Passive Microwave dataset (TC-PMW). It includes the special sensor microwave imager/sounder (SSMI-[S]), advanced microwave scanning radiometer for EOS (AMSR-E), and TRMM microwave imager (TMI); Table 2.1 displays the satellite characteristics. Best track centers are interpolated for each passive microwave overpass using the phase speed calculated between each 6-hourly time period. The best track wind speed and pressure, however, are not interpolated; instead, the nearest 6-hourly time is used. Only passes containing 100% coverage within 1° of the interpolated best track center are considered. Polarization-corrected brightness temperatures (85-91 GHz PCT) are assembled for the calculation of various passive microwave parameters, statistics, composites, and sensitivities. PCTs are used rather than brightness temperatures in order to help distinguish between brightness temperature depressions due to ice scattering or those due to low sea surface emissivity (Spencer et al. 1989; Cecil 2002).

Despite differing frequencies (85-91 GHz) all the overpasses are examined jointly for this study. From a climatological and composite standpoint the differences between brightness temperatures at these frequencies are small and do not alter the overall results. In addition, the different resolutions among the satellites do not affect the composites,

means, fractional areas, etc. The minimum brightness temperatures are the only statistics adversely affected by resolution: The highest resolution overpasses (TMI) have a higher frequency of the coldest PCTs at the extreme end of the spectrum (< 150 K), as shown by Figure 2.7. The degraded version of AMSR-E (appx. 11 km resolution) is used in this figure only to demonstrate the statistical affects of higher resolution (TMI) versus lower (AMSR-E degraded and SSMI-S). Figure 2.8 demonstrates the resolution affects for an overpass of Hurricane Katrina '05. The overall "means" are not affected, however, the minimums are significantly colder at higher resolution.

2.3.2 Passive Microwave Population

A total of 12788 passive microwave overpasses from Atlantic Basin tropical cyclones are compiled; 9643 remain after removing those with a "nontropical" designation and those with less than a 100% coverage (within 1° of interpolated best track center). A total of 6741 overpasses remain after removing all periods with land interaction in +24 hours.

An additional 9034 images are obtained from the Eastern Pacific for this study; 7075 remain after removing those with "nontropical" designation and less than 100% coverage, and numbers reduce to 5432 after removing those with land interaction. Figure 2.9 shows the distribution of passive microwave overpasses with respect to 24-hour intensity changes.

From the 12173 overpasses that have a tropical designation, 1525 are from AMSR-E, 3122 from TMI, 5293 from SSMI platforms, and 2227 from SSMIS platforms. Figure 2.10 reveals the spatial distribution for all passive microwave overpasses used in this study. This differs from the track climatology shown in Figure 2.3 in that we have

since removed cases with significant land interaction during the +24 hour period.

2.3.3 Passive Microwave Parameters

Statistics are calculated for 85-91 GHz within the inner core region of all passive microwave snapshots. The inner core region encompasses the center or "eye," eyewall (full or partial), and any near center convection. Previous studies have subjectively determined the inner core for each passive microwave overpass. Jiang and Ramirez (2011) determined a mean inner core radius of 82 km from the center with a standard deviation of 18 km. For this study we use a radial distance of 1° from the interpolated best track center as an objective restriction to define the inner core. As previously stated, only those passes with 100% coverage within the 1° radius are included.

Similar to previous studies (Jiang 2012, Jiang and Ramirez 2013) a minimum 85-91 GHz is calculated for each passive microwave overpass. This calculation outputs the lowest single pixel value within the inner core, which can be used as a proxy for the strength of the most intense convection. In addition, the mean and median PCTs for the inner core are computed. Fractional areas with 85-91 GHz PCT less than 250 K, 210 K, and 160 K indicate the areal coverage of various proxies for convective intensities within the inner core.

Composites are constructed to represent the temporal and spatial distributions of PCTs for different 24-hour intensity change criteria. The composites use corresponding shear direction information previously stored to rotate each centered overpass relative to the shear vector. An example of this methodology can be seen using a passive microwave overpass from Hurricane Wilma in Figure 2.11. Additional plots are constructed using various environmental constraints and criteria including the threshold method. The above

methodologies follow closely with several previous studies (Rogers et al. 2002; Lonfat et al. 2003; Wingo and Cecil 2009), but with a larger dataset and more comprehensive approach that includes a high temporal resolution before and during intensification events. This unique "timeline" approach allows for a detailed investigation of convective and environmental evolution with respect to intensity change. The onset of the 24-hour intensification period is hereafter referred to as the "0 hour" with periods during intensification referred to as +6, +12, +18, and +24 hours. Periods prior to onset span from the "-18 hour" to "-6 hour."

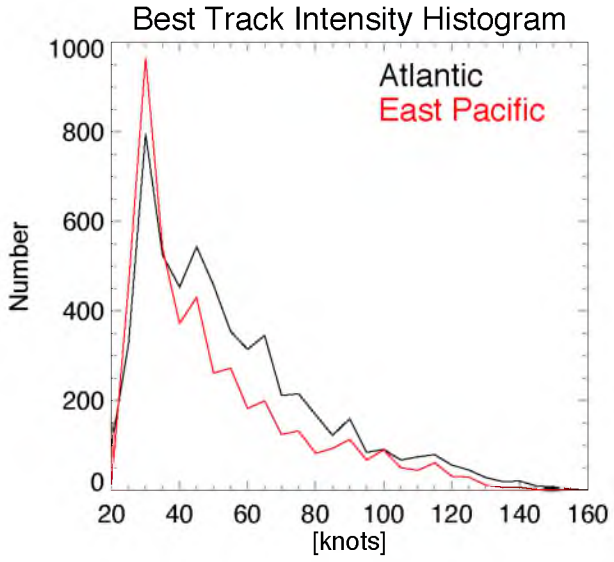

Figure 2.1. NHC best track 6-hourly intensities for all tropical depressions and tropical cyclones.

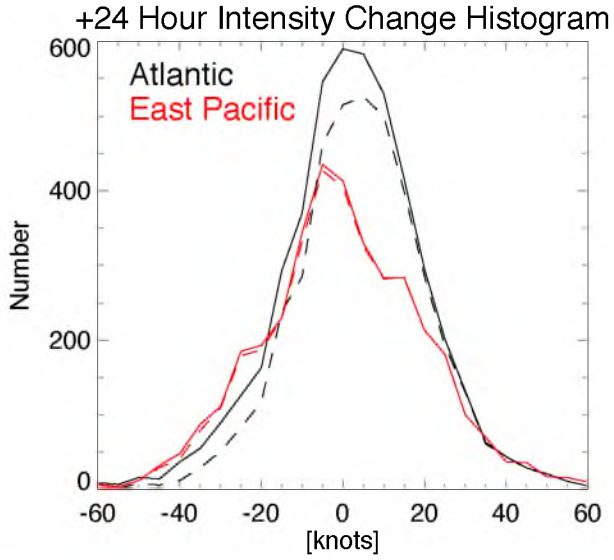

Figure 2.2. 24-hour intensity changes using NHC Best Track intensity for all tropical cyclones in the Atlantic Basin (solid black) and East Pacific (solid red). Dashed lines represent 24-hour intensity changes with all land interaction periods removed.

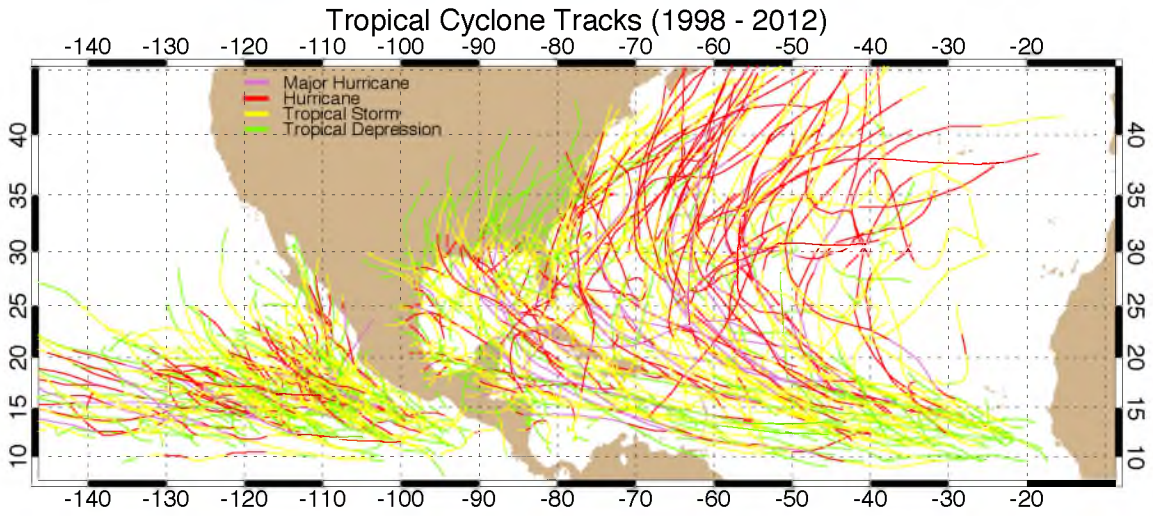

Figure 2.3. All tropical cyclone tracks from 1998 - 2012 in the ATL and EPAC.

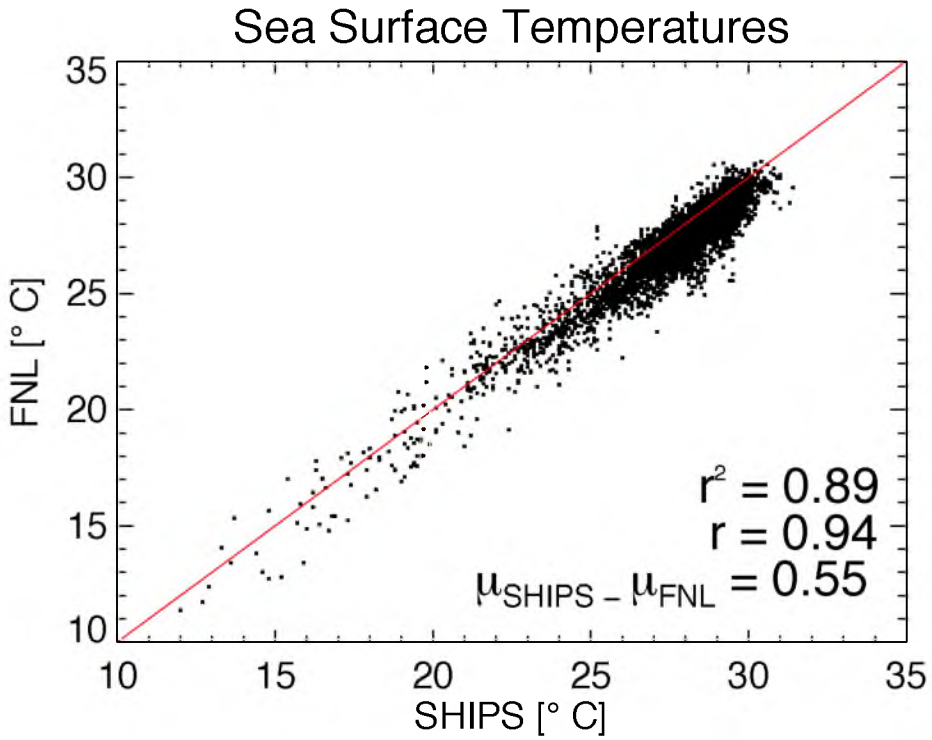

Figure 2.4. Atlantic Basin correlation between SHIPS Reynold's SST calculation (x-axis) and GHRSST analysis (y-axis).

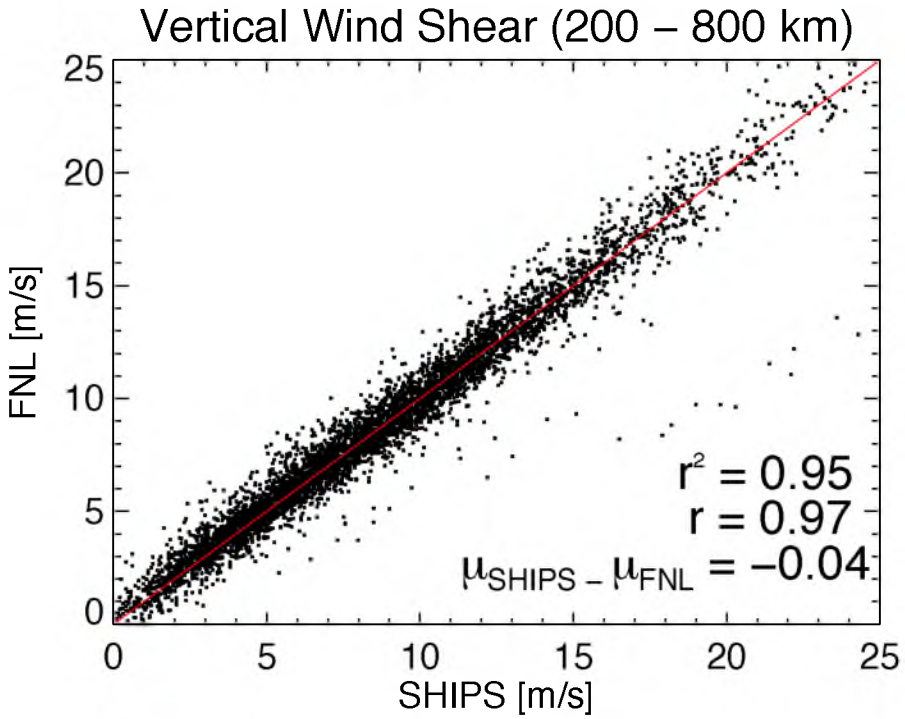

Figure 2.5. Atlantic Basin correlation between SHIPS vertical wind shear calculation and NCEP FNL (same methodology).

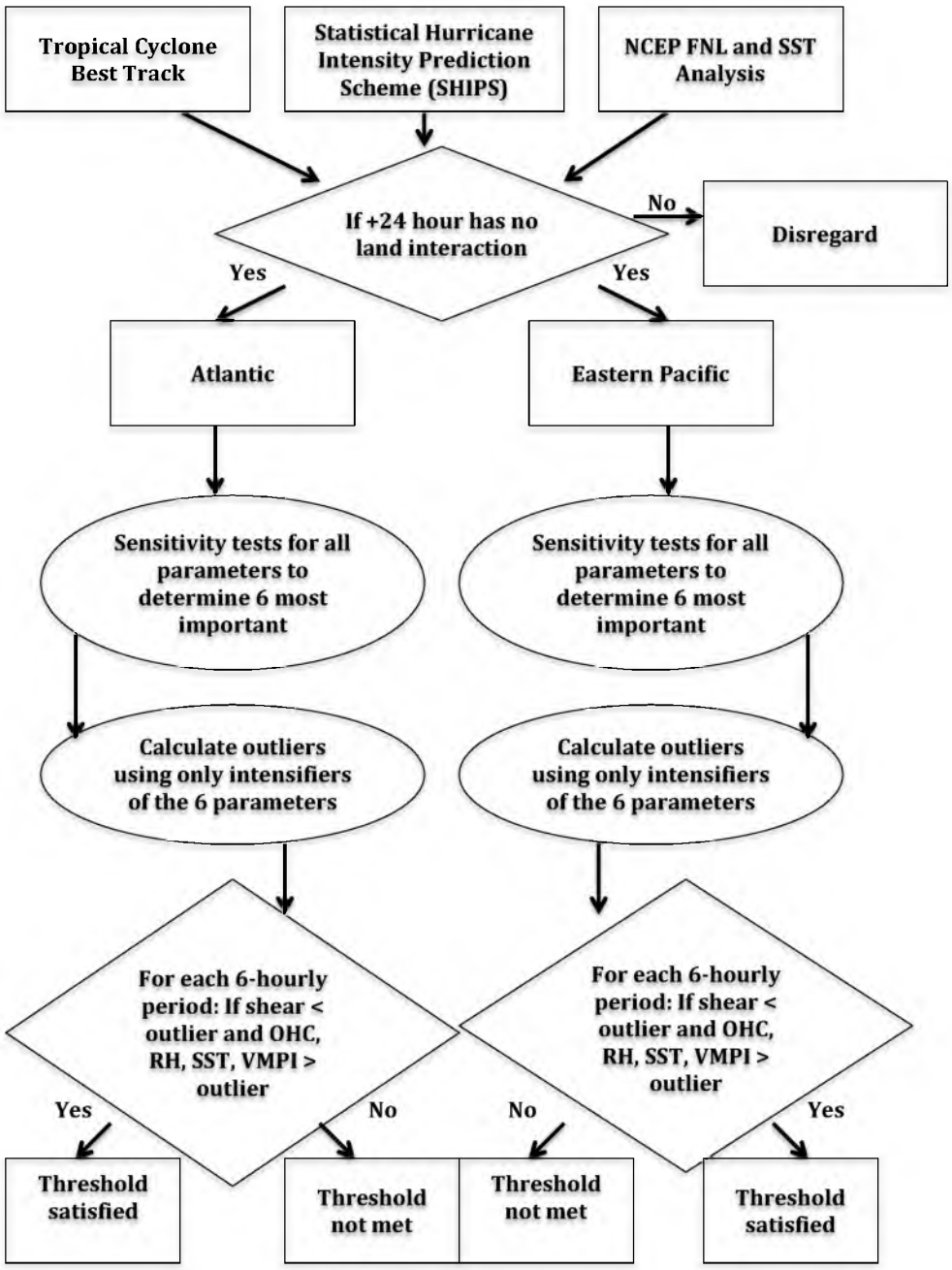

Figure 2.6. Flow chart showing the "outlier" methodology.

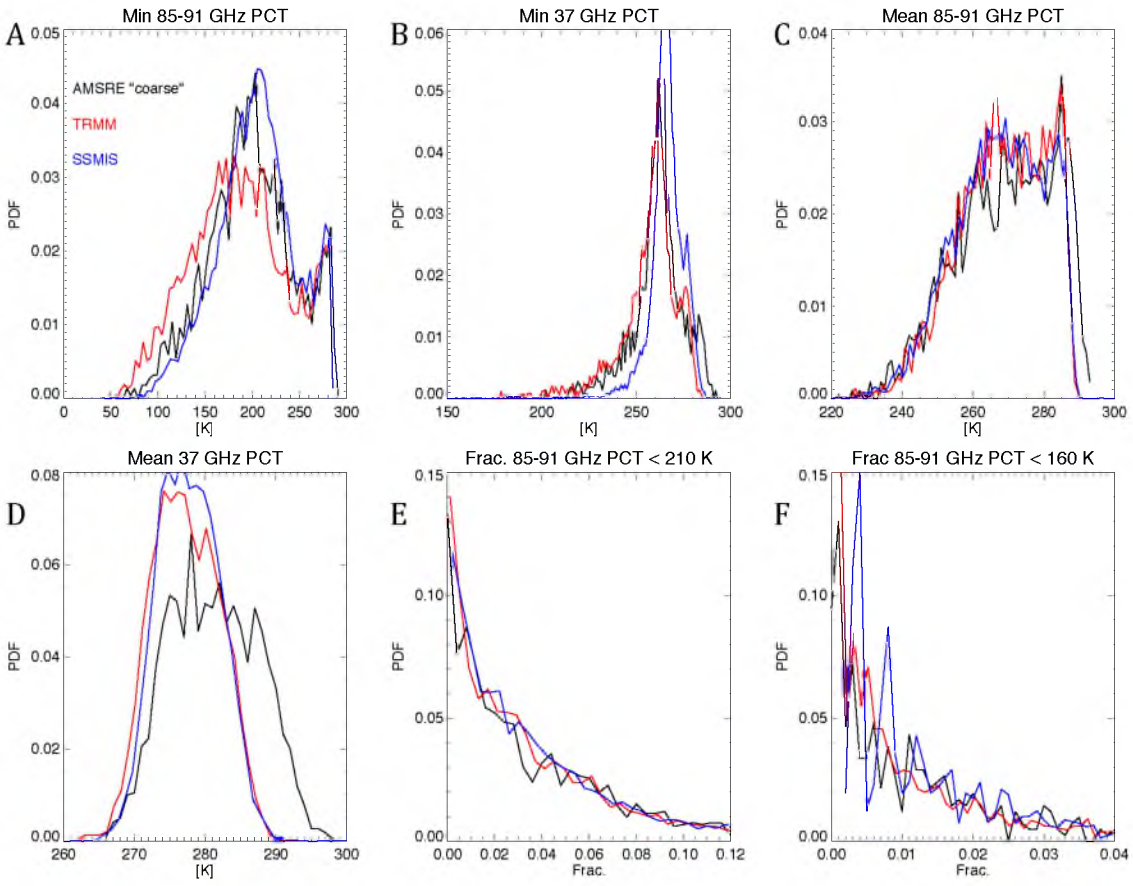

Figure 2.7. Probability density function (PDF) of all AMSRE (degraded resolution), TRMM, and SSMIS overpasses. Minimum 85-91 GHz PCT and 37 GHz PCT within 1° of the center (A, B) PDF of the mean 85-91 GHz PCT and 37 GHz PCT within 1° of the center (C, D). PDF of the fractional area less than 210 K (E) and 160 K (F).

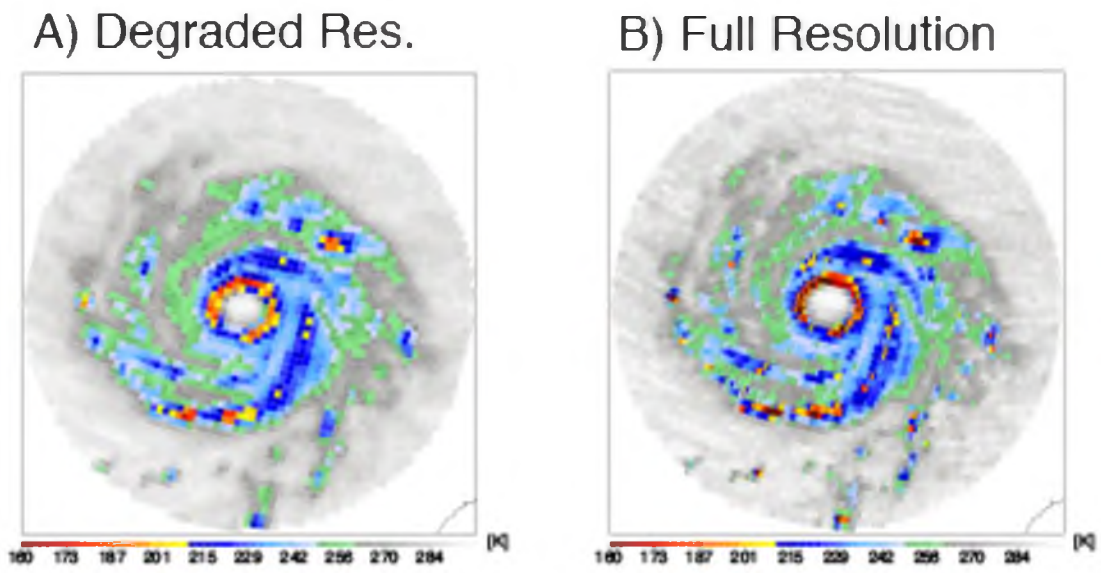

Figure 2.8. Hurricane Katrina 8/28/05 AMSRE overpass 89 GHz PCT. Degraded Resolution (A) has an inner 1° mean PCT of 239 K and minimum PCT of 167 K. Panel B (Full resolution) has an inner 1° mean PCT of 239 K and minimum PCT of 118 K.

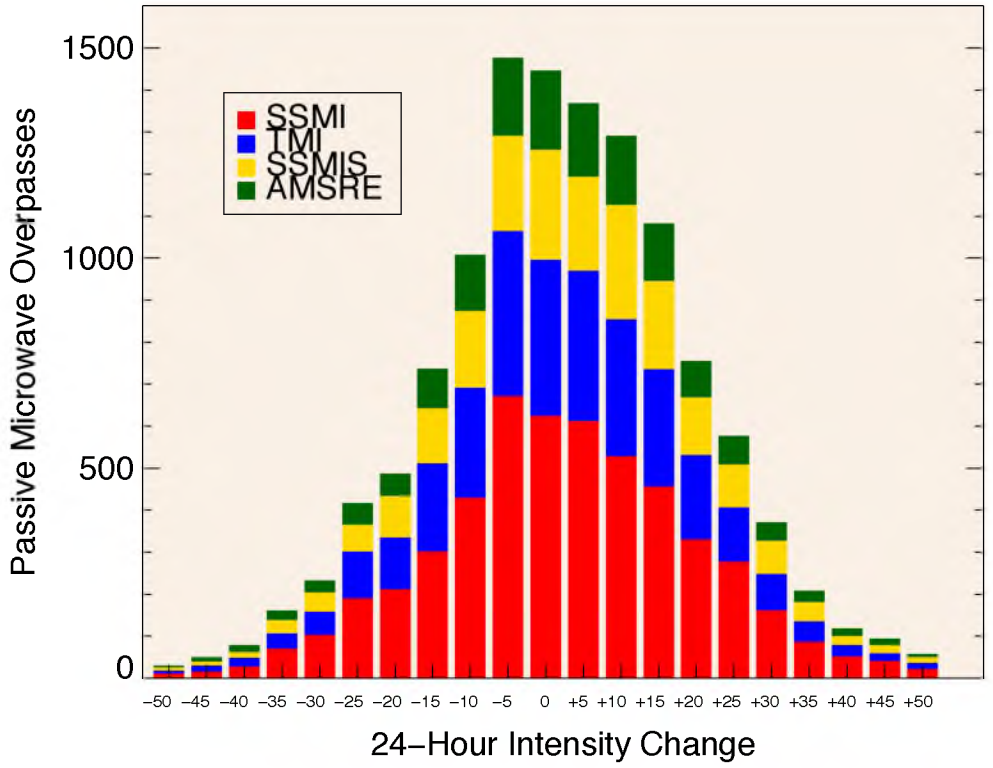

Figure 2.9. Overlapping bar plot of all passive microwave images and the associated 24-hour intensity change.

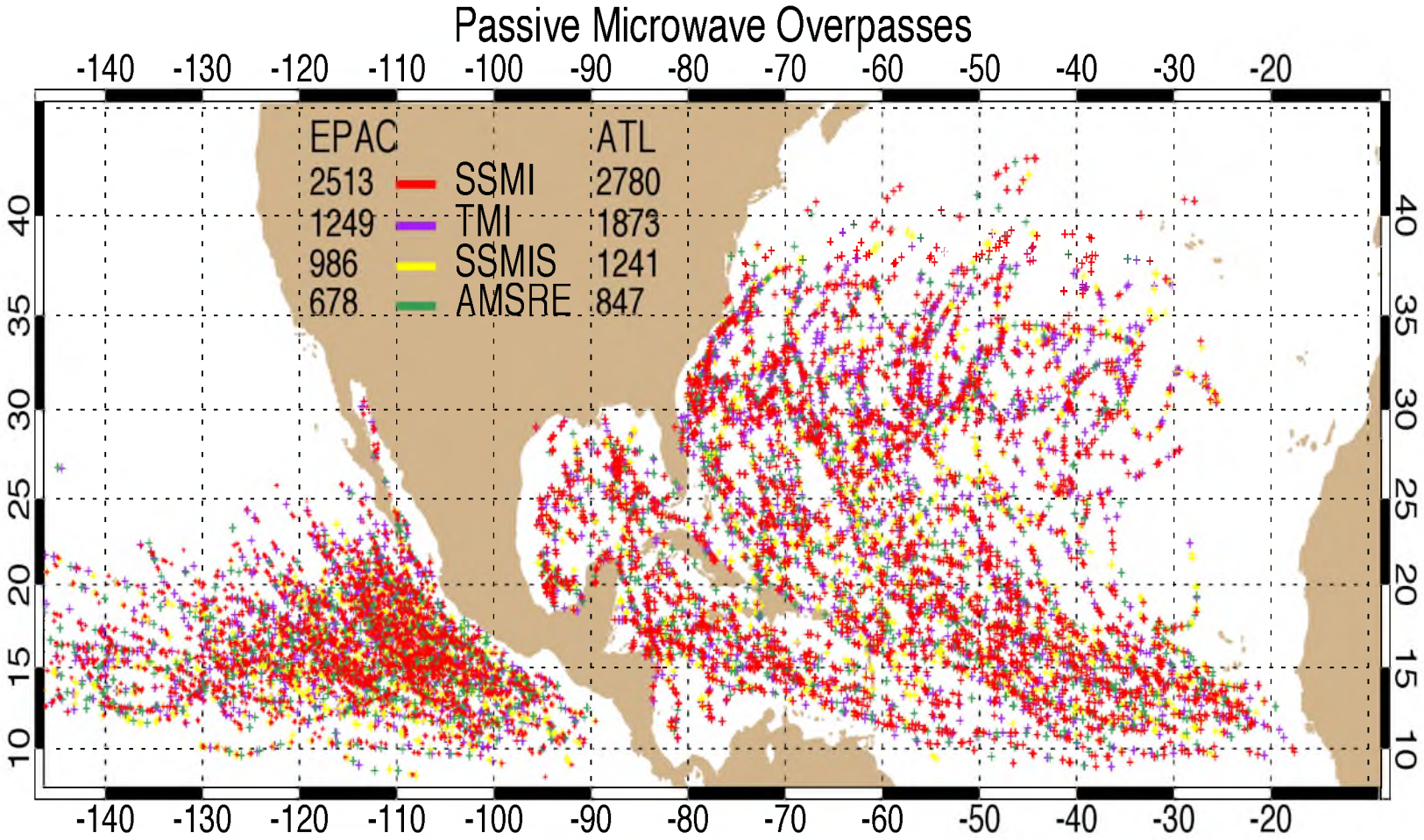

Figure 2.10. Spatial distribution of all tropical cyclone PMW overpasses.

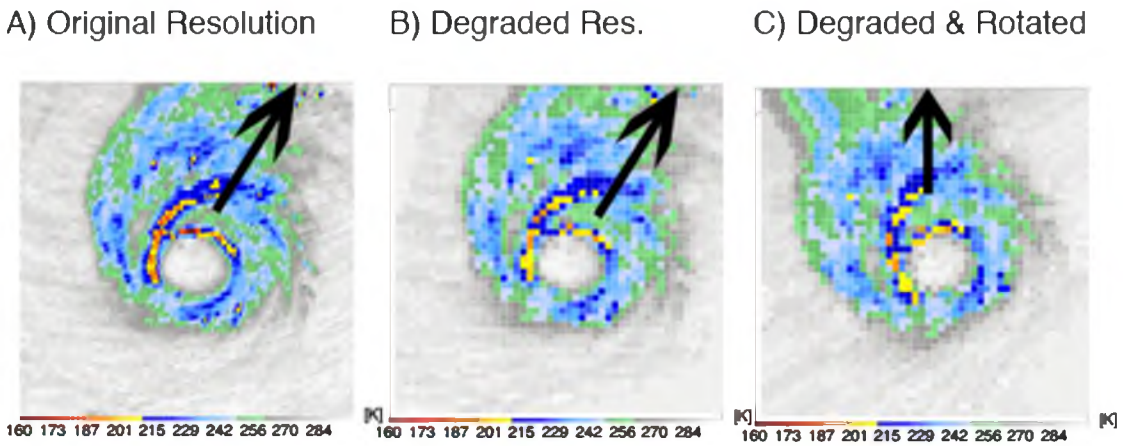

Figure 2.11. Hurricane Wilma 10/24/05 AMSR-E overpass of 89 GHz PCT. Black arrow indicates the vertical wind shear vector.

Table 2.1. Passive microwave satellite specifications.

Satellite	Spatial resolution	Frequencies Used	Year start - Year end
SSMI (F13 - F15)	12.5 km	85 GHz	1995 - present
SSMI-S (F16 - F18)	12.5 km	91 GHz	2003 - present
AMSR-E	5.4 km	89 GHz	2002 - 2011 (now AMSR-2)
TMI	5.1 km	85 GHz	1997 - present

CHAPTER 3

CHARACTERISTICS OF ENVIRONMENTAL PROPERTIES WITH RESPECT TO INTENSITY CHANGE

DeMaria and Kaplan (1994) and Hendricks et al. (2010) demonstrated the importance of environmental variables for predicting tropical cyclone intensity changes. In this study environmental variables from the extended best track dataset, SHIPS reanalysis, and FNL analysis are examined in order to distinguish those that offer the most predictive value for intensification.

Kaplan and DeMaria (2003) analyzed rapidly intensifying (RI) storms and found that they tend to be farther from their MPI than slower intensifying storms. In the mean RI cases also feature warmer SSTs, higher low-tropospheric humidity, and weaker vertical wind shear of the horizontal wind than non-RI cases. Despite these differences, only a very small fraction of RI cases actually exhibit all thresholds; numerous tropical cyclones undergo RI in less than ideal conditions (Sitkowski and Barnes, 2008). Throughout the chapter, the findings of previous studies are compared using both similar and different methodologies.

3.1 Spatial Distribution

Examination of the environmental parameters for the Atlantic and East Pacific using extended best track characteristics, the Statistical Hurricane Intensity Prediction

Scheme (SHIPS) reanalysis, and the NCEP Final (FNL) analysis, reveals statistically significant differences between the two basins. Figure 3.1 demonstrates the spatial variability of 24-hour intensity changes for all tropical depressions and tropical cyclones excluding those with land interaction. The East Pacific features more uniform spatial variability, which appears to be latitudinally dependent. Storms south of approximately 15°N have a more frequent occurrence of intensification (and RI). Coincidentally, the sea surface temperatures (Fig. 3.2) follow a similar spatial pattern of longitudinal homogeneity (especially at more westward longitudes) and decreased SSTs with increased latitude. A few areas appear to have an increased likelihood of intensification in the Atlantic: Bay of Campeche, Gulf of Mexico, Caribbean Sea, and parts of the Main Development Region (MDR). Intensification and even rapid intensification, though, remains plausible in all parts of an active basin. The Atlantic's irregular spatial variability, and in particular the close proximity of rapid intensification events to land, emphasizes the need for efforts to better explain, and forecast, short-term (24-hour) intensity change.

Given how well the spatial distribution of SST in the EPAC aligns with the variability seen in Figure 3.1, the data suggest a strong, coherent relationship between SST and intensification. The Atlantic also reveals interesting spatial characteristics; almost all tropical depressions and tropical cyclones south of 25°N and between 100°W and 50°W have SSTs of at least 28°C. Sea surface temperature, compared to the East Pacific, has a less obvious connection with distinguishing intensification rates in the Atlantic (though still appears useful for distinguishing "weakeners" from "intensifiers"), and thus must not be the main contributor.

The spatial patterns of vertical wind shear (SHIPS 200 - 800 km) reveal important differences between the basins (Fig. 3.3). The East Pacific, as a whole, has lower values (typically averaging 10 m s^{-1} or less) than the Atlantic. Vertical wind shear also has much higher spatial variability in the Atlantic with values increasing (in the mean) at higher latitudes as a result of prevalent interactions with the midlatitude jet stream.

Given the spatial variability observed in each basin, simply binning statistics by basin as a whole, as nearly every previous study has done (Kaplan and DeMaria 1998; Emanuel et al. 2003; Hendricks and Peng 2010), may not be the best methodology; creating further subsetting within the Atlantic Basin may potentially lead to more robust results, and improved prediction when considering the environmental parameters. This study will proceed without subsetting each basin, but this issue is further examined later in the chapter.

3.2 Extended Best Track Dataset - Intensity and Size Characteristics

Figure 3.4 reveals numerous characteristics regarding initial intensities of 24-hour intensity changes. In spite of differences in sample size distribution, the boxplots for the Atlantic and East Pacific are reasonably similar. Storms with higher rates of weakening tend to have greater initial intensities. A majority of those storms with a 30-kt decrease in 24 hours have initial intensities of at least minimal hurricane status. Interestingly, those storms that intensify most rapidly ($\geq$ 40 kts) tend to also have higher initial intensities than those that intensify 5-35 kts in 24 hours.

A recent study (Carrasco et al. 2014) using the extended best track dataset revealed that tropical cyclone size (34-kt wind radius as a proxy) might aid intensity

forecasts. Results using the datasets in this study reveal a similar relationship; those storms with a rapid weakening rate tend to have a larger 34-kt radius in both basins (Fig. 3.5). In the Atlantic the weakening periods coincident with a larger 34-kt radius tend to occur at higher latitudes; the East Pacific, however, reveals no latitudinal dependence. The periods of 24-hour intensification have smaller 34-kt wind radii than neutral or weakening periods in the mean. The median size actually increases slightly for both basins for the most rapid intensifiers; concurrently, the variances within the distributions decrease.

3.3 Environmental Variables

Environmental variables that have the strongest correlation with intensity change are examined further in this section: Vertical wind shear, low and midlevel relative humidity (RH), sea surface temperatures (SST) and ocean heat content (OHC), and maximum potential intensity (MPI). Figure 3.6 displays the histograms for all 6-hourly periods of these variables in both the Atlantic and East Pacific.

3.3.1 Vertical Wind Shear

The vertical wind shear calculations are from the SHIPS database. Different methodologies exist for examining wind shear (Black et al. 2002; Hanley et al. 2001): In this study, the two most popular calculations for deep-layer shear (850-200 hPa) are used, both output by SHIPS; one averaged over the 200-800 km annulus (hereafter referred to as "annulus shear"), and another averaged over 0-500 km from the center (this calculation removes the modeled TC vortex, and hereafter will be referred to as "vortex removal shear"). The distribution of vortex removal shear follows a similar pattern to annulus

shear; the biggest difference being that the values as a mean are slightly lower. Given their similarity, for the remainder of the thesis, only annulus shear will be used.

The distribution of annulus shear for all periods in the Atlantic and East Pacific is shown in Figure 3.7. In the Atlantic, vertical wind shear values have a strong tendency to decrease with increasing 24-hour intensity changes. Those storms that intensify more rapidly tend to have lower vertical wind shear. There is, however, significant overlap between all intensity change categories; and thus this variable alone does not offer significant predictive value in distinguishing 24-hour intensity change in 10-kt increments.

There is one significant difference between Atlantic and East Pacific vertical wind shear: East Pacific storms in the mean have significantly lower values. The biggest differences exist for weakening storms; those in the Atlantic tend to have much higher values. Atlantic storms with higher shear values are often at higher latitudes and thus experience more impacts from the midlatitudes (Fig. 3.8). The mean latitude for all 6-hourly positions in the Atlantic is 24°N with a standard deviation of 8.2°; in the East Pacific the mean is only 17°N with a standard deviation of 3.8°. Overall, vertical wind shear in the East Pacific has less variability with respect to intensity changes, and offers a seemingly less predictive value for the weakening cases.

3.3.2 Low and Midlevel Humidity

Relative humidity, particularly in the lower and middle troposphere, plays an important role in the formation, maintenance, and intensification of tropical cyclones. Two separate pressure layers are examined in this study: A low-level (850-700 hPa) and midlevel (700-500 hPa). For these two layers we utilize the SHIPS 200 - 800 km annulus

calculation and a 0 - 500 km calculation for the NCEP FNL analysis; these are hereafter referred to as "SHIPS annulus" and "FNL inner" methodologies.

We test the correlations between the different methodologies and their associated 24-hour intensity changes. The variables themselves do not have a perfectly linear response with respect to intensity change (Fig. 3.9). This is expected though, because of the numerous multiscale environmental factors that affect tropical cyclones. For statistical analysis we use a linear Pearson's correlation coefficient; this is sufficient because we are interested in the direct relationship between layer-mean relative humidity and intensity change. Although the FNL inner calculation for the midlevels (700-500 hPa) has the highest correlation coefficient, it is closely followed by the SHIPS annulus. For this study, the SHIPS annulus calculation will be used since it better portrays the surrounding environmental humidity and is not "contaminated" by the typical high humidity of the inner core. The low-level moisture calculations have lower correlations, but, as shown by Kaplan and DeMaria (2003), they still have potential for predictive value. Additionally, the correlation between relative humidity and intensity change has some latitudinal dependency: Tropical cyclones at higher latitudes (greater than 20°N) have a lower correlation between intensity change and layer-mean relative humidity than those at lower latitudes (less than 20°N).

Atlantic Basin distributions have slightly lower medians for the "slow weakeners" (24-hour decrease of 10 to 20 kts) than for the "rapid weakeners" (24-hour decrease of 30 kts or greater). Figure 3.9 reveals that the strongest correlation between intensity change and relative humidity occurs with the intensifiers. While the medians amongst the rapid intensifiers (+24-hour change of 30 kts or greater) do not significantly change, the

variances decrease with increasing intensity change.

Although the East Pacific follows a similar distribution to the Atlantic, the mean relative humidity is higher in the EPAC. This result is, however, skewed higher due to the fact that the Atlantic has a disproportionately higher amount of storms north of 25°N (2655 6-hourly periods) compared to the EPAC (only 138 cases above 25°N); lower relative humidity is more likely to be found at higher latitudes (Fig. 3.10).

3.3.3 Sea Surface Temperature and Ocean Heat Content

Several previous studies have also cited the importance of sea surface temperatures (SST) for the formation, maintenance, and intensification of tropical cyclones (Palmen 1948; Miller 1957; Emanuel 1986). In addition, ocean heat content (OHC) provides an important role, and offers operational forecasters a discriminator that takes into account upwelling (Mainelli et al. 2007; Shay et al. 2000).

The relationships between SST and 24-hour intensity change are drastically different in the Atlantic and East Pacific. Storms tend to weaken from different mechanisms in the two basins (as previously discussed in section 3.1). TCs in the EPAC weaken almost exclusively from cooler SSTs north of 15-20°N. In the Atlantic, a much larger number of storms weaken due to land interaction or interaction with midlatitude troughs. These differences cause the correlation between SST and intensity change to be significantly higher for the EPAC than the Atlantic. When only the intensifiers are examined, however, the EPAC still has a significantly higher correlation. OHC, being a similar metric to SST, also follows similar trends in the two basins.

While the OHC in the Atlantic varies little for neutral and weakening periods (Fig. 3.11), intensifying storms do have a higher linear correlation with increasing

intensity change. The EPAC, on the other hand, features a much higher correlation for the "slow weakeners" and neutral intensification periods. OHC tends to decrease with increasing weakening rates excluding the storms that weaken most rapidly (< -30 kts +24 hour intensity change). The EPAC "weakeners" also contain lower OHC variances and medians than the Atlantic by nearly an order of magnitude. Interestingly, for intensifiers, median OHC values are lower in the EPAC than the Atlantic despite higher SSTs in the EPAC; one potential hypothesis is simply the uncertainty in thermocline and associated OHC measurements.

3.3.4 Maximum Potential Intensity (MPI)

The maximum potential intensity (VMPI in kts) has statistically significant predictive value; VMPI minus the current intensity ($V_{current}$ in kts), though, offers an even stronger correlation with +24 hour intensity change. As previously discussed in Data and Methods, MPI is predominately determined by SST; and thus the two variables have a very high correlation. The storms that weaken most rapidly in the East Pacific have a median value of 0 (VMPI-$V_{current}$), meaning they have reached their MPI (Fig. 3.12); storms in the Atlantic tend to reach their MPI less frequently. A strong correlation exists between VMPI-$V_{current}$ and 24-hour intensity change for those storms weakening and slowly intensifying. A much weaker correlation occurs amongst the intensifiers in both basins, though the variances decrease with more rapid intensifiers.

3.4 Multivariate Interactions

3.4.1 Shear and Relative Humidity

Figure 3.13 confirms the multivariate interaction between vertical wind shear and midlevel relative humidity for all storms with at least a 10 kt 24-hour intensity change. A large majority of storms in the Atlantic (Fig. 3.13a.) intensify when surrounded by very high relative humidity. Although this figure indicates that even storms with higher vertical wind shear still intensify, due to the relatively small sample size of storms containing both high relative humidity and high wind shear, the distribution in the upper right is questionable. At best, this figure indicates that as long as (midlevel) humidity is sufficiently high (70%), on rare occasion, a storm embedded in a high vertical shear environment can undergo some intensification. The East Pacific (Fig. 3.13b.) also reveals a multivariate response, but the overall frequency distribution is lower. The bottom left sharply cuts off in response to a very low number of cases with relative humidities less than 50%. Spurious maxima above 10 m s^{-1} are also attributed to small sample sizes; as previously demonstrated (Fig. 3.7), the East Pacific's shear distribution is lower and less variable than in the Atlantic.

3.4.2 Shear and Divergence

The multivariate interaction between vertical wind shear and 200 hPa divergence is most evident in the East Pacific. Figure 3.14 demonstrates the frequency distribution (%) of those storms with a +24 hour intensity change greater than 5 kts. The Atlantic does not reveal any significant correlation for the two variables with respect to intensity change. The East Pacific, however, reveals a pattern in which increasing divergence along with low wind shear (2 - 6 m s^{-1}) increases the probability of intensification.

3.5 Environmental Thresholds

In order to create a "threshold" for which intensification is plausible, we examine the distributions of the above parameters and their periods under which 24-hour intensification occurs. Using the procedure described in Data and Methods (Fig. 2.6), the outliers are removed, then the threshold is determined based on the maximum value (wind shear) and minimum values (relative humidity, SST, OHC, and MPI) under which intensification occurs. Due to significant differences between the basins for several of the environmental variables (previous sections), a separate threshold for the Atlantic and East Pacific is determined.

Intensification thresholds for the Atlantic are as follows: Intensification is plausible when wind shear is less than 14.9 m s^{-1}, SST greater than 25.4 °C, midlevel RH greater than 31%, low-level RH greater than 49%, and VMPI-$V_{current}$ greater than 25 kts. After periods not meeting this set of thresholds are removed from the dataset, 2917 6-hourly periods from the 4021 total in the Atlantic remain. The distributions of the thresholds and nonthresholds (NT) are shown in Figure 3.15. Applying the threshold does help remove several weakening cases and shifts the PDF slightly to the right. This indicates that the environmental variables add some predictive value, at least in terms of weakening versus strengthening. Distributions in the EPAC reveal a potentially higher predictive value, though are more sensitive to smaller changes in environmental values.

Figure 3.16 follows the same methodology as Figure 3.15, except for the EPAC. Similar to the results shown in previous sections, the vertical wind shear threshold is lower than in the Atlantic; RH, SST, and VMPI-$V_{current}$ threshold values are all higher than those of the Atlantic. The CDFs and PDFs also reveal significantly greater

separation than those in the Atlantic. This is partially attributed to the differing weakening mechanisms between the basins that were previously discussed. In addition to the threshold for all intensifiers, thresholds have been created for all +24 hour intensification periods in 10-kt increments (Table 3.1). These are used in the next chapter in conjunction with passive microwave statistics and distributions.

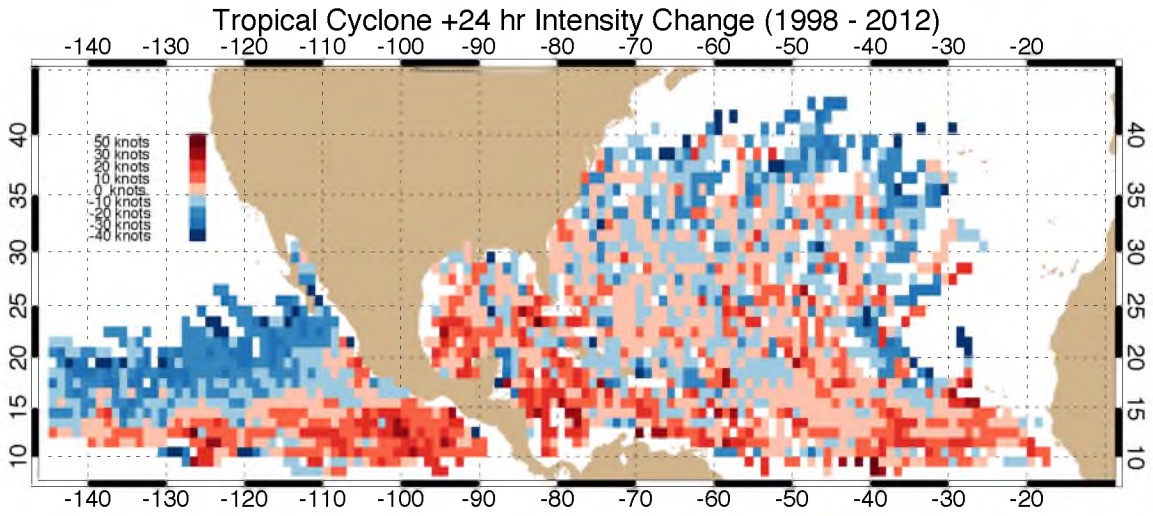

Figure 3.1. One degree boxes for all +24 hour intensity changes from 1998-2012. Boxes are averaged if more than one 24-hour period exists at a particular point. All periods with major land interaction have been removed. The following two figures follow this methodology.

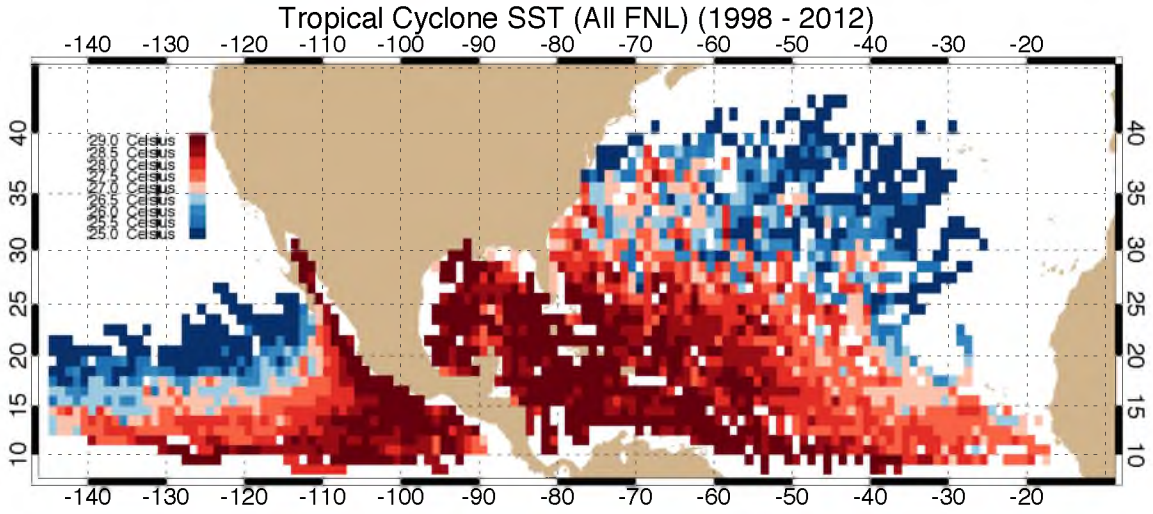

Figure 3.2. One degree boxes of sea surface temperatures for all 6-hourly periods from 1998-2012.

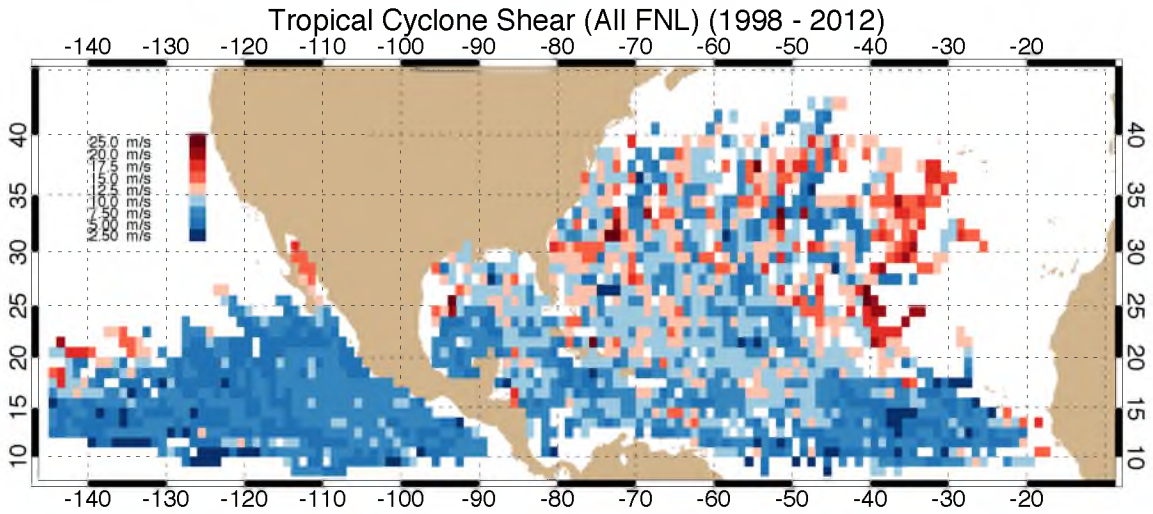

Figure 3.3. One degree boxes of 850-200 hPa wind shear using a 200-800 km annulus (SHIPS reanalysis) for all 6-hourly periods.

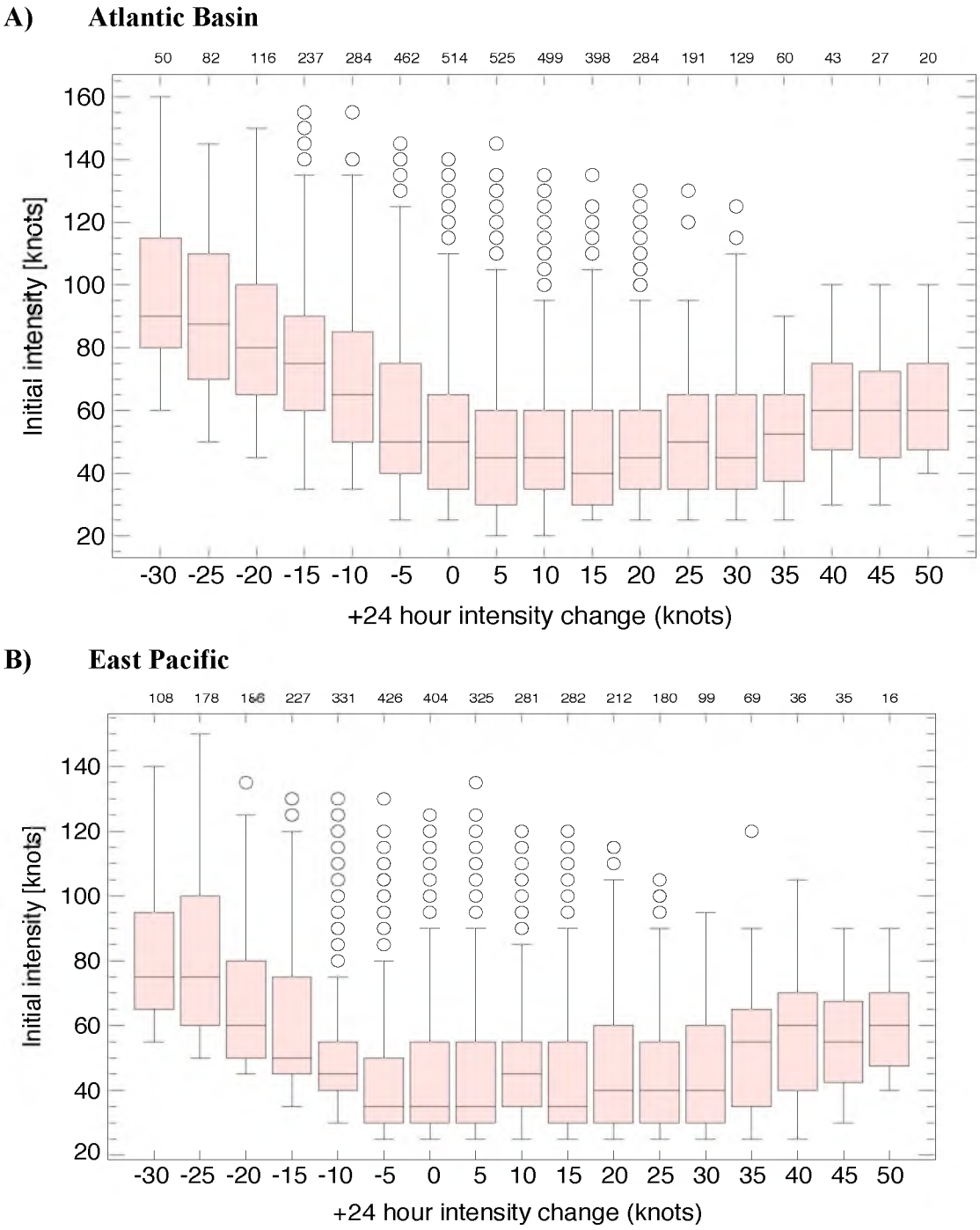

Figure 3.4. Boxplots of 00 hour initial intensity for all +24 hour intensity change periods. Numbers above boxplots indicate the sample sizes for each 5-kt increment of +24 hour intensity change. Center lines in each pink box represent the median; upper and lower lines enclosing the box indicate the upper (25% of data are greater than this value) and lower quartiles (25% of the data are less than this value). Lines extending outward (whiskers) indicate the maximum and minimum values excluding outliers. Outliers are represented by the open circles.

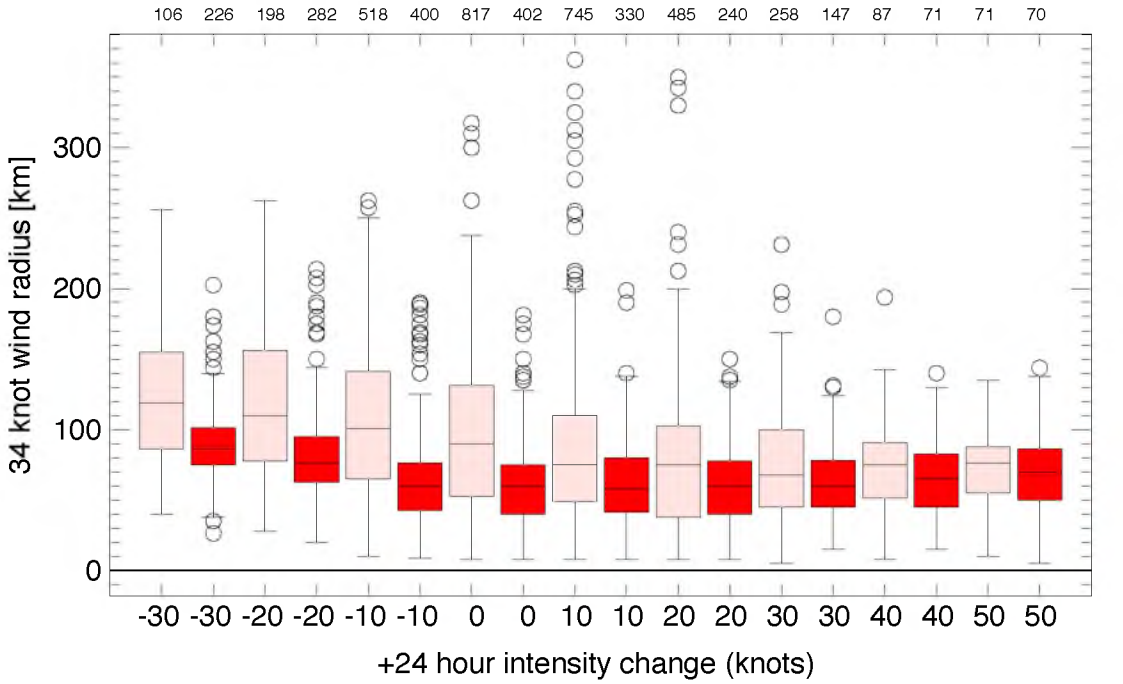

Figure 3.5. Boxplots of 34-kt wind radii for all +24 hour intensity change periods. Pink boxes indicate distribution in the Atlantic; red boxes in the East Pacific. The number above each intensity change classification indicates sample size. Center lines in each box represent the median; upper and lower lines enclosing the box indicate the upper (25% of data are greater than this value) and lower quartiles (25% of the data are less than this value). Lines extending outward (whiskers) indicate the maximum and minimum values excluding outliers. Outliers are represented by the open circles. Remaining box plot figures follow this methodology.

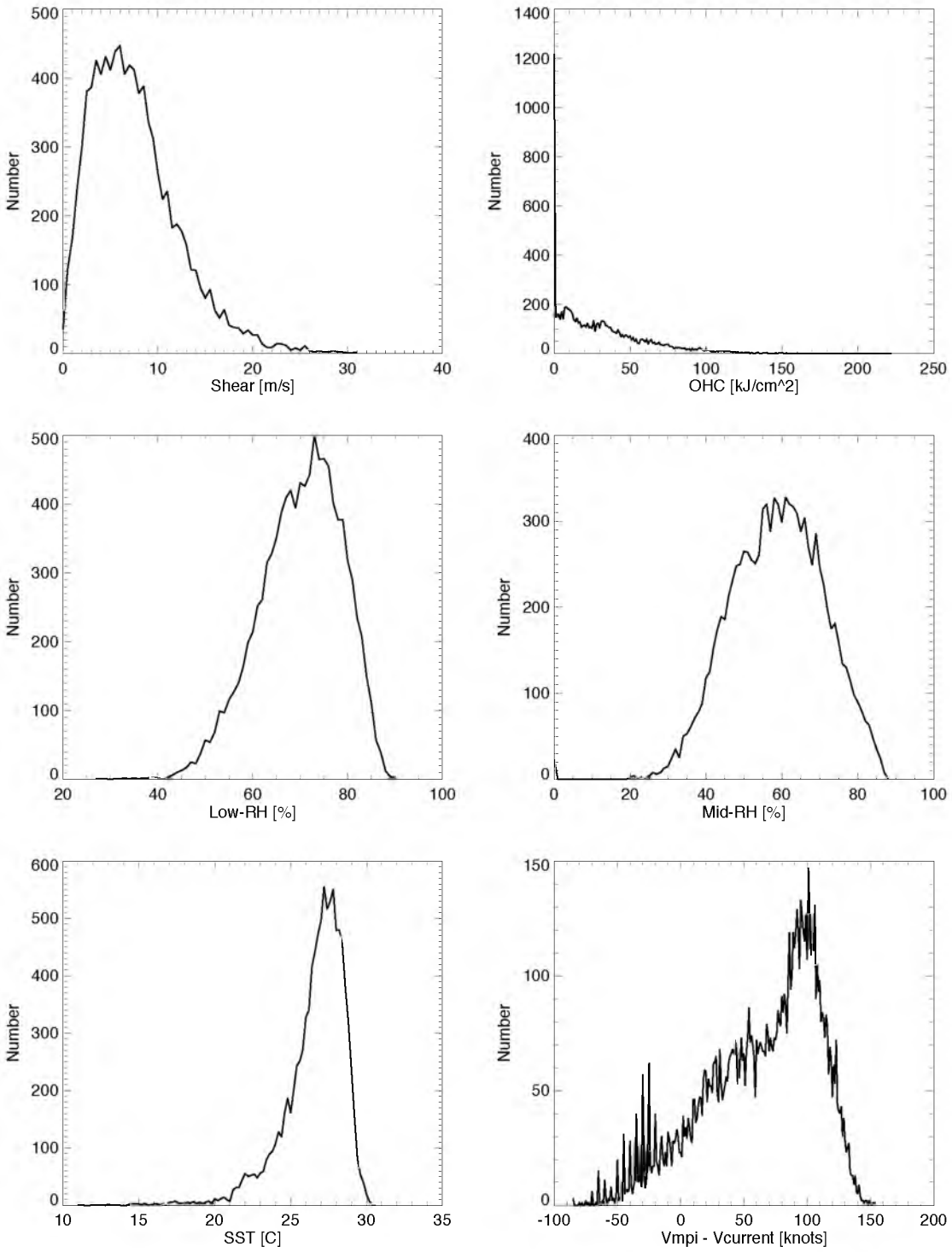

Figure 3.6. Environmental histograms for all 6-hourly periods in the Atlantic and East Pacific. From the upper left panel to the bottom right, the figure displays the number of 6-hourly periods for all shear, ocean heat content (OHC), and low-level relative humidity (Low-RH), midlevel relative humidity (Mid-RH), sea surface temperatures (SST), and values of the maximum potential intensity minus current intensity.

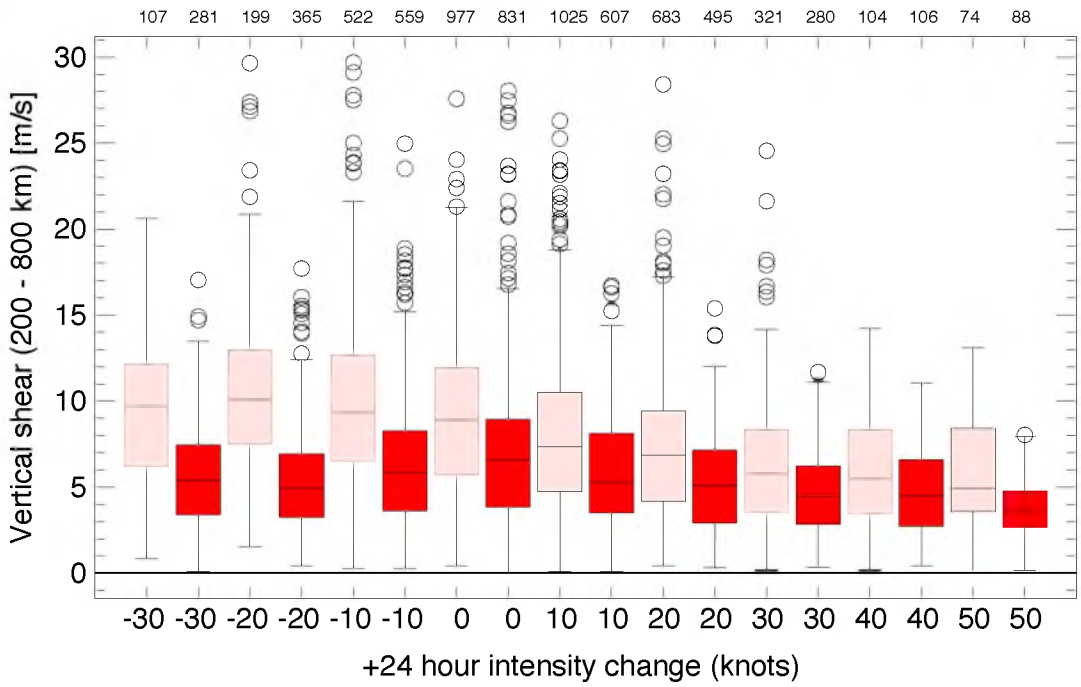

Figure 3.7. Boxplots of annulus vertical wind shear (SHIPS) for +24 hour intensity change periods in the ATL (pink) and EPAC (red).

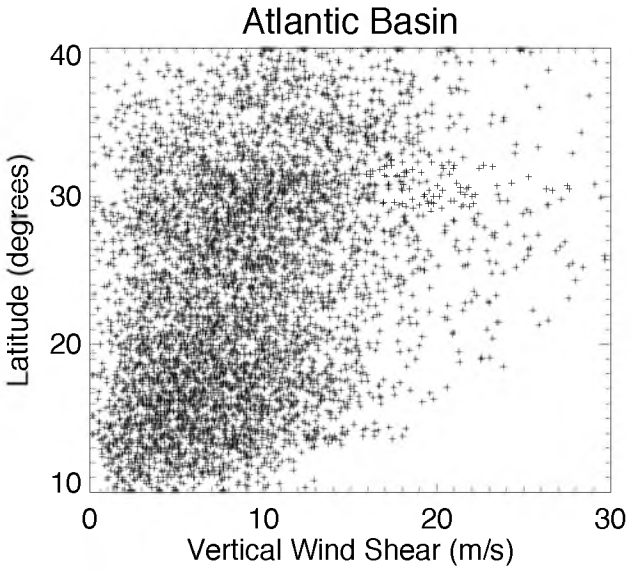

Figure 3.8. Scatterplot of SHIPS annulus shear and latitude for all 6-hourly periods in the Atlantic.

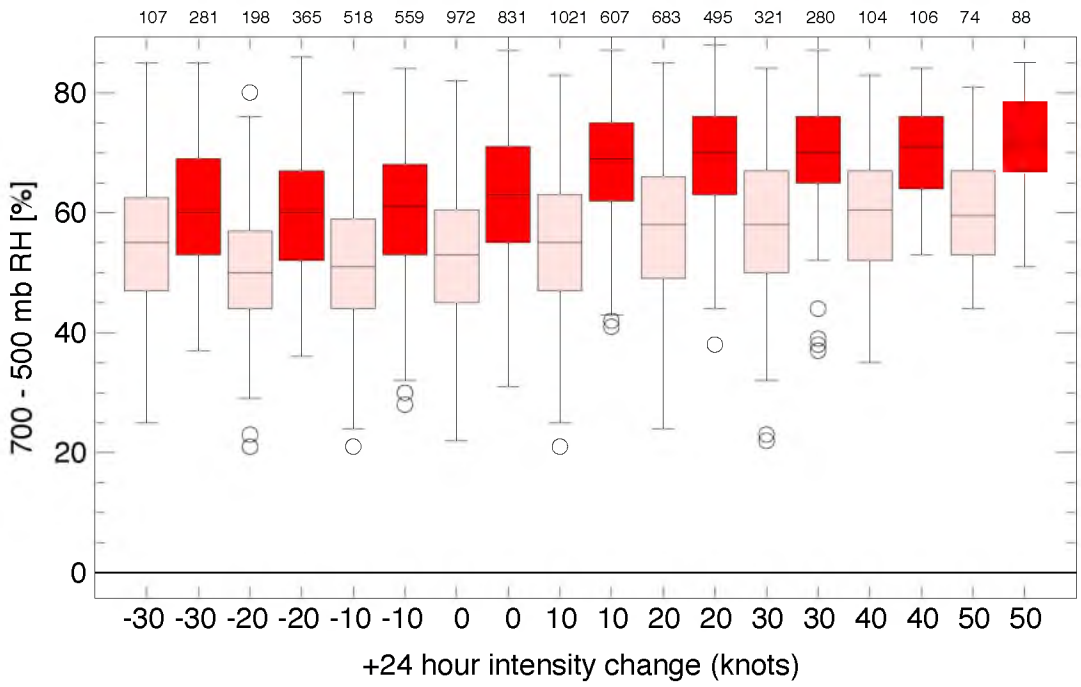

Figure 3.9. Boxplots of SHIPS annulus midlevel relative humidity and 24-hour intensity changes. Pink is Atlantic cases and red is East Pacific.

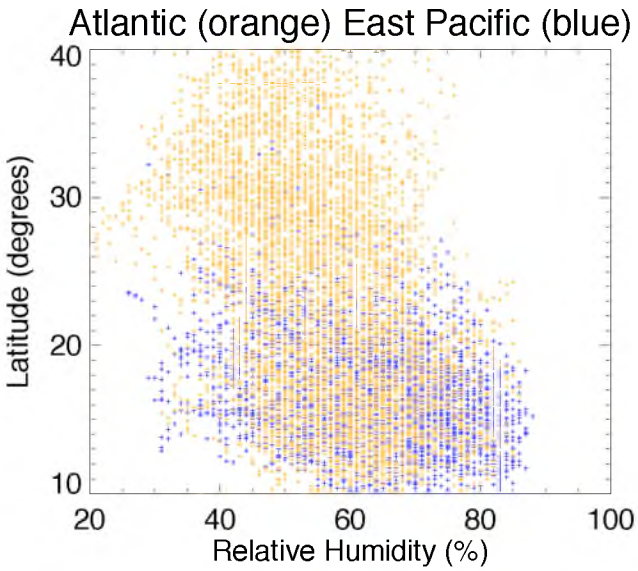

Figure 3.10. Scatterplot of midlevel relative humidity and latitude for the Atlantic (orange) and East Pacific (blue).

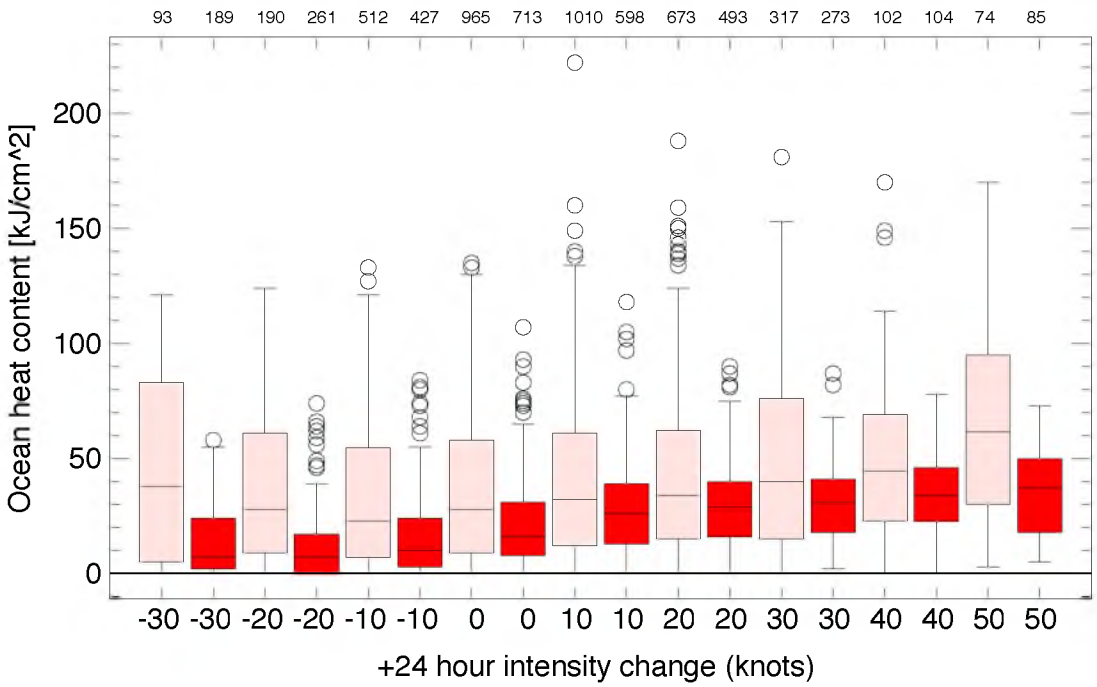

Figure 3.11. Boxplot of ocean heat content and +24 hour intensity change with the Atlantic in pink and East Pacific in red.

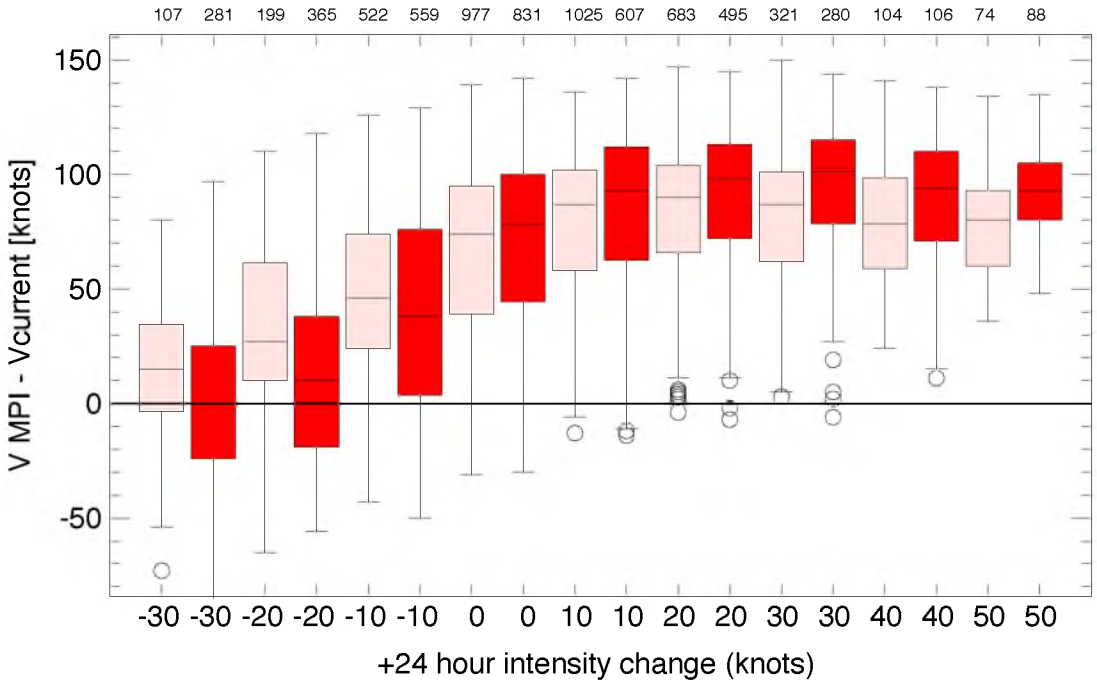

Figure 3.12. Boxplot of the MPI minus the current intensity and +24 hour intensity change with the Atlantic in pink and East Pacific in red.

A) Atlantic Basin

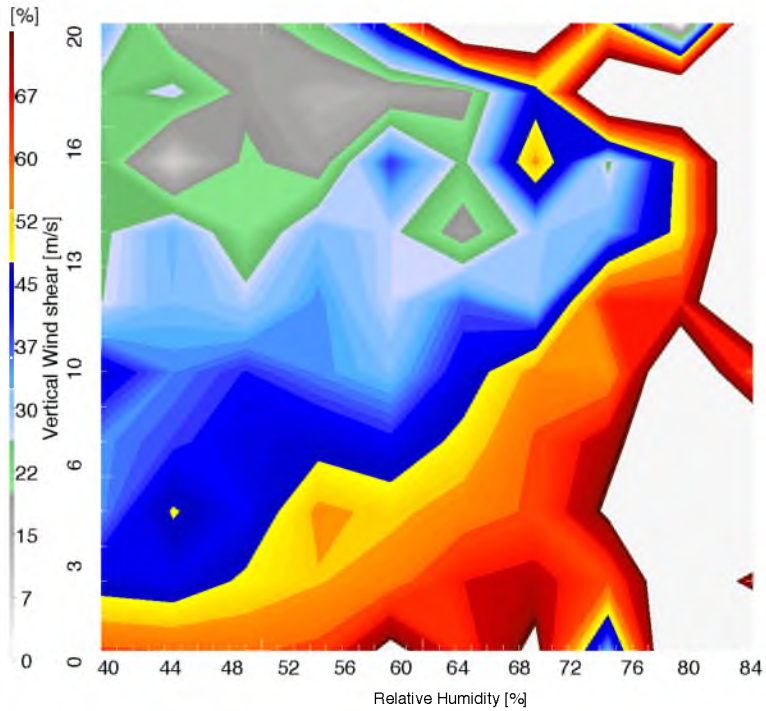

B) East Pacific

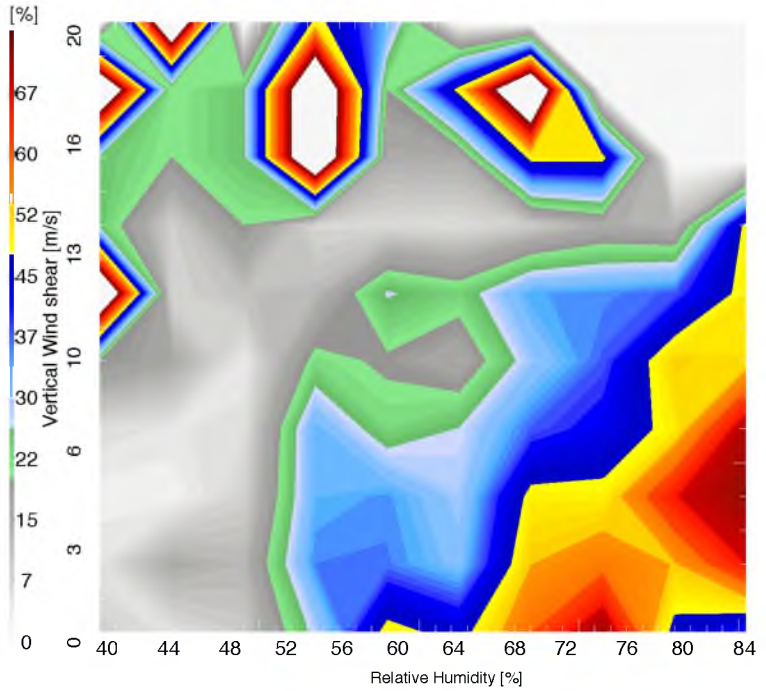

Figure 3.13. Frequency distribution [%] of storms that have a +24 hour intensity change of 10 kts or greater. SHIPS annulus shear (850 - 200 hPa) is plotted on the y-axis, and 700 - 500 hPa relative humidity is plotted on the x-axis.

A) Atlantic

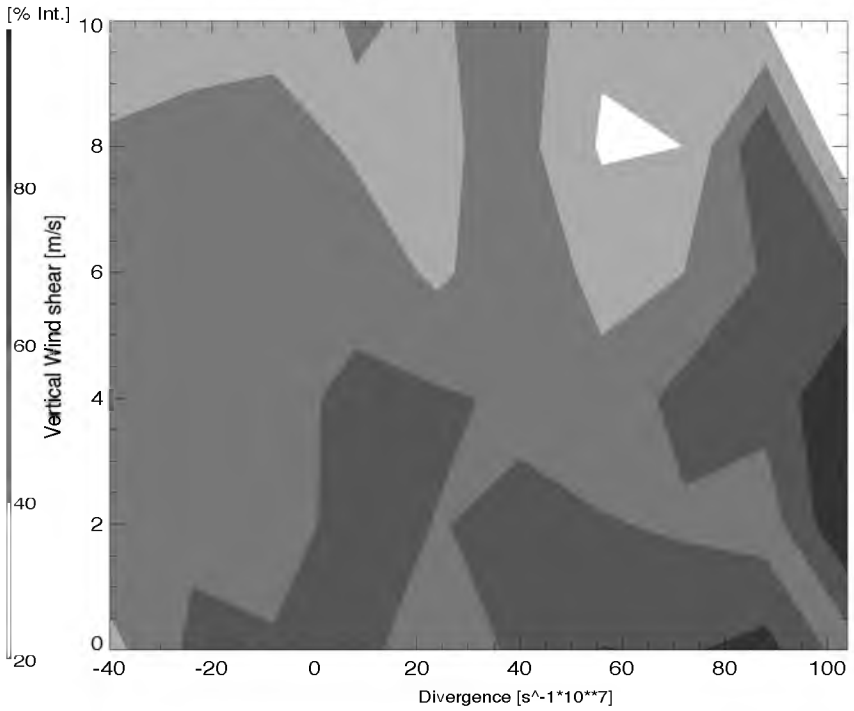

B) East Pacific

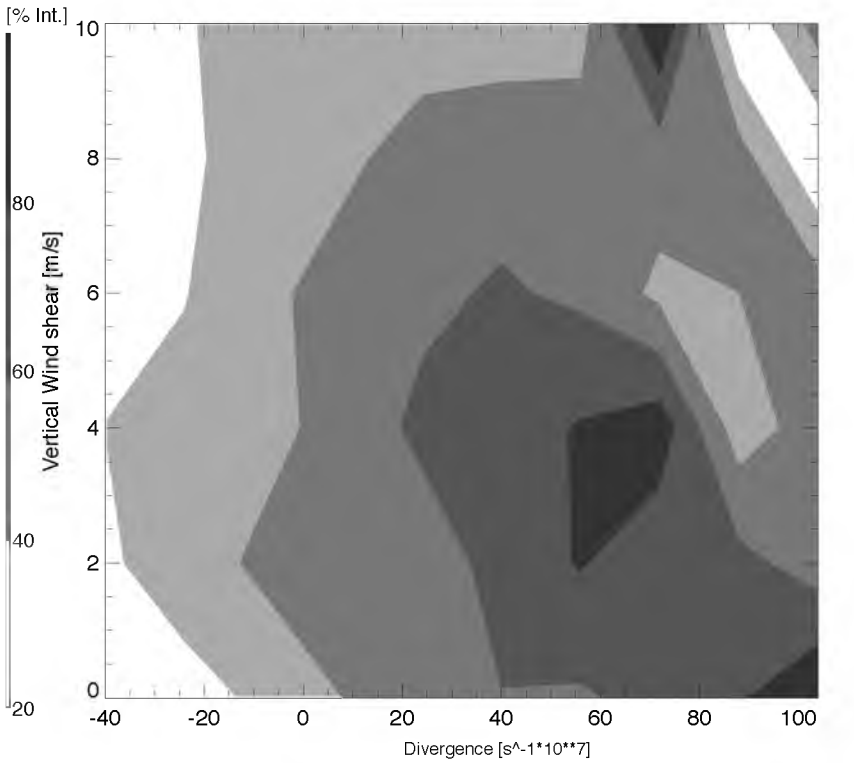

Figure 3.14. Frequency distribution [%] of storms that have a +24 hour intensity change of 10 kts or greater. The y-axis is 850 - 200 hPa annulus shear, and x-axis displays the 200 hPa divergence calculated at 200 - 800 km from the storm center.

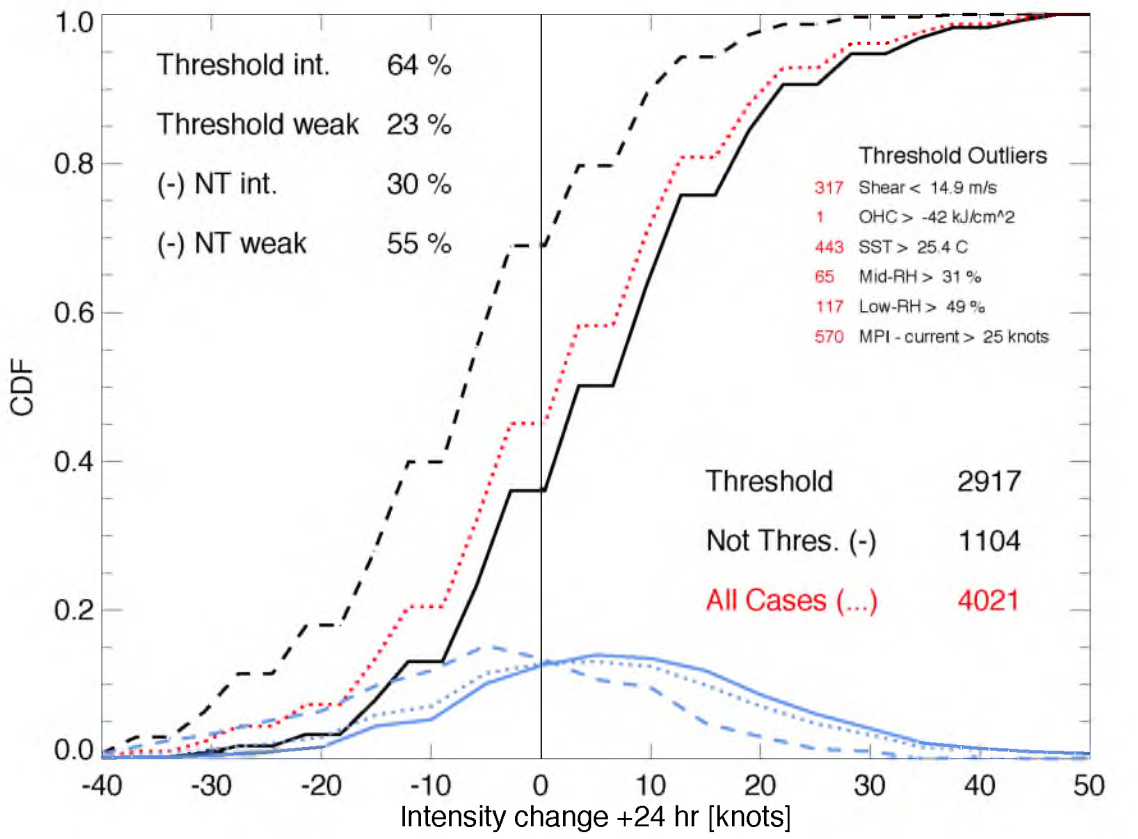

Figure 3.15. Cumulative distribution function (CDF) for all Atlantic storms (dotted red), all storms that meet the threshold for plausible intensification (solid black), and those that do not meet the threshold (dashed black). Blue lines follow the above, however, they display the PDF. Sample sizes are indicated in the bottom right. Numbers in the upper right indicate the threshold values (black) and number of 6-hourly periods removed by the particular variable's threshold.

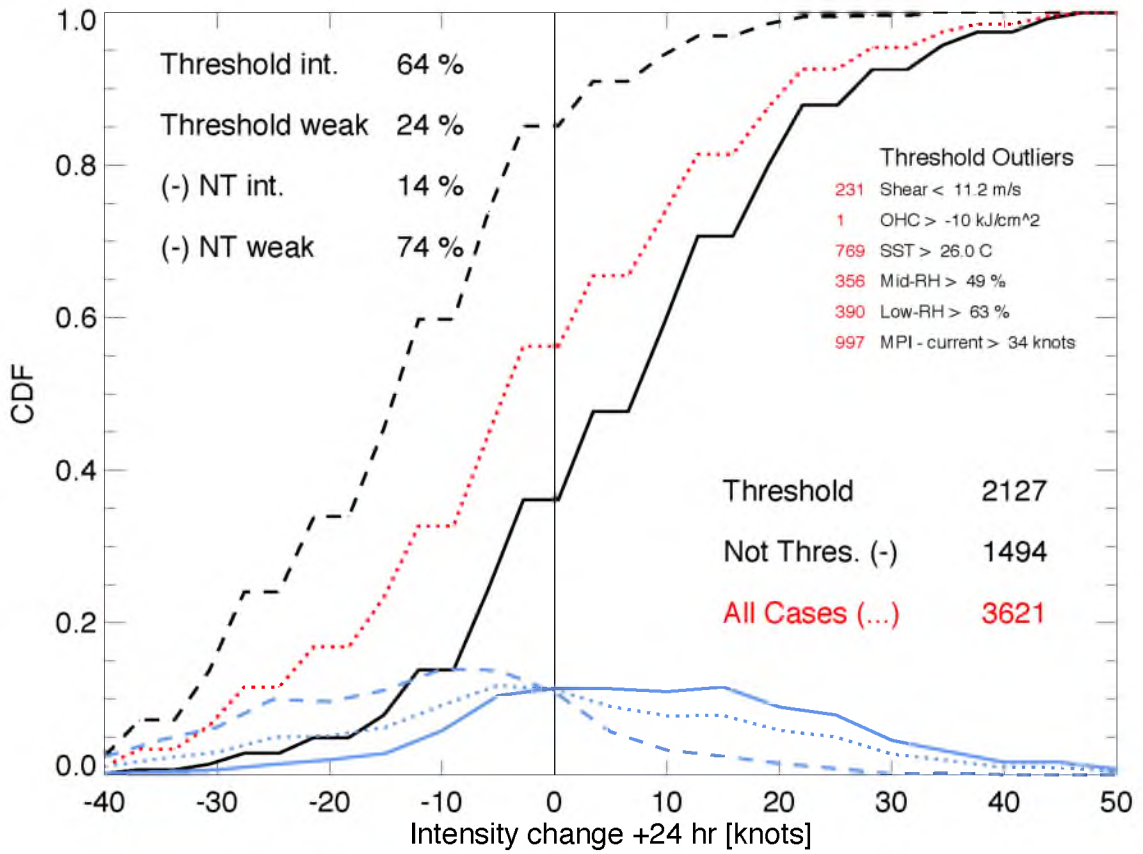

Figure 3.16. Cumulative distribution function (CDF) for all East Pacific storms (dotted red), all storms that meet the threshold for plausible intensification (solid black), and those that do not meet the threshold (dashed black). Blue lines follow the above, however, they display the PDF. Sample sizes are indicated in the bottom right. Numbers in the upper right indicate the threshold values (black) and number of 6-hourly periods removed by the particular variable's threshold.

Table 3.1. Thresholds for variables of all intensification periods in the Atlantic (black) and EPAC (red).

+24 hour intensity [knots]	Vertical shear [m/s]	SST [C]	VMPI – Vcurrent [knots]	Low-RH [%]	Mid-RH [%]
> 0	14.9	25.4	25	49.5	31.5
	11.2	26	34.5	63	49
> +10	14.4	25.6	25.5	52	30
	10.9	26.2	37	63	49
> +20	13.3	25.9	26	53	33.5
	9.7	26.5	42.5	63	51
> +30	12.5	26.1	27	57	35
	8.9	26.9	45.5	64	53
> +40	12.3	26.7	22.5	58.5	34.5
	7.7	27.2	47.5	64	53
> +50	11.9	26.9	20	55.5	35.5
	6.5	27.3	60	65.5	57

CHAPTER 4

PRECIPITATION PROPERTIES OBSERVED DURING INTENSITY CHANGE

Kaplan and DeMaria (2003), along with the results in Chapter 3, have shown the importance of environmental conditions for tropical cyclone intensity change; however, the synoptic environment surrounding a TC alone often does not provide distinguishable skill for intensification rates or RI prediction (Sitowski and Barnes, 2008). The intensification of tropical cyclones, instead, is related to the individual and collective interactions between the large-scale environment, storm-scale processes, and ocean-atmosphere coupling (Bosart et al. 1999). This chapter focuses on the inner core distribution of convection and rainfall, using passive microwave radiometer data, and their relationships with environmental properties and intensity change.

The primary energy source for a tropical cyclone's secondary circulation is the release of latent heat of condensation (Malkus and Riehl, 1959). Gray (1998) reiterated that outbreaks of organized deep convection are required for TC intensification. "Near center" convection is particularly important. Shea and Gray (1973) emphasized the importance of the location of the inner radar eye radius (IRR) with respect to the radius of maximum winds (RMW). The IRR tends to occur inward of, or very near, the RMW for the most intense storms; weaker storms have a larger difference, and thus less concentrated latent heat release and subsidence. Uncertainties remain regarding TC intensification mechanisms. Numerous studies have emphasized the importance of near-

axisymmetric net latent heating (Shapiro and Willoughby, 1982; Cecil and Zipser, 1999; Nolan and Grasso, 2003; Kieper and Jiang, 2012), while others point to the effect of asymmetric latent heating on intensification (Montgomery and Kallenbach, 1997; Nolan and Montgomery, 2002; Guimond et al. 2010), especially the contributions of intense convection or "convective bursts."

In situ data with adequate spatial and temporal resolution in tropical cyclones remains limited, however, infrared and passive microwave satellite sensors offer another viable tool to examine the convective evolution. Geostationary satellites provide nearly continuous infrared imagery, but are limited to providing information about cloud top properties (temperature and height); cold IR cloud tops, such as from a cirrus anvil, can be misinterpreted as active deep convection, and do not necessarily represent the precipitation organization. In contrast, passive microwave sensors (often on polar orbiting satellites), though offering considerably less frequent snapshots, provide a more direct relationship to precipitation (Cecil and Zipser, 1999). This chapter attempts to quantify the importance of precipitation properties, such as symmetry around the center, areal coverage, and intensity, for tropical cyclone intensification using 85-91 GHz brightness temperatures. Given the relative infrequency of overpasses for any individual storm, this thesis provides robust results by evaluating a large sample of storms over 15 years (1998-2012) in multiple basins (Atlantic and East Pacific).

4.1 Temporal and Spatial Evolution of Convection with Respect to Intensity Change

Varying footprints is one particularly important aspect to consider when compositing data from different passive microwave sensors. This is most critical when

analyzing the convective intensity, which is approximated by the minimum 85-91 GHz PCT (previously demonstrated in Fig. 2.7). High resolution sensors (AMSRE and TMI, ~5km) are more likely to capture particularly depressed pixels associated with intense convective towers. Figure 4.1 shows the cumulative distribution function (CDF) of minimum 85-91 GHz PCTs for the "native high-resolution" (Table 2.1) data. Compared with the "degraded resolution" (approximately 13 km), the minimum PCTs are approximately 10 K lower between 140 and 170 K. Hereafter composites will consist of the degraded resolution data. The 25^{th} - 50^{th} percentile of the degraded resolution of minimum 85-91 GHz PCT, approximately 170 K - 190 K, is defined in this work as the threshold for the most "intense" convection. "Weak" to "moderate" convection is defined by thresholds of PCT less than or equal to 250 K, which has previously been found to closely relate to at least a 3 mm/hr rain rate (Spencer et al. 1989).

Jiang (2012), using a dataset of TRMM overpasses from 1998 - 2008, found that predictability of intensification rate, and particularly RI, may be further improved by using PMW and PR convective parameters. The TRMM Tropical Cyclone Precipitation Feature (TCPF) database (Jiang et al. 2011) was used in a similar study that reiterated the importance of axisymmetric convection and associated heating for tropical cyclone intensification. They also demonstrated that intense convection (sometimes referred to as "hot towers") does not substantially increase the probability of RI. This section further investigates the hypotheses and findings from these previous studies using the large TC-PMW dataset, and using new methodologies for examining the distributions and evolution of convection during intensity change. Due to the lesser importance of basin convective differences (which will be shown in section 4.2) and in the interest of brevity

in the synthesis of results, the EPAC and Atlantic are combined.

4.1.1 Areal Coverage and Spatial Symmetry of Precipitation and "Weak" to "Moderate" Convection

Figure 4.2 shows the spatial frequency distribution of 85-91 GHz PCT less than 250 K with respect to intensity change for the "0 hour" of all overpasses in the Atlantic and EPAC. TC quadrants are referenced with the following abbreviations: downshear-left [DL], downshear-right [DR], upshear-right [UR], upshear-left [UL]. Storms that weaken the most rapidly (+24 hour intensity change of < -20 kt) have the second highest occurrence (behind only the most rapid intensifiers) of 85-91 GHz PCT < 250 K in the DL quadrant (Fig. 4.2); these cases also have the highest median initial storm intensity, > 70 kts. Composites of steady state TCs (+24 hour intensity changes of -10 to +10 kt) have the lowest areal coverage of PCT < 250 K. The DR quadrant also features a minimum in frequency with 10% or less. As intensification rates increase, the coverage of PCT < 250 K increases in all quadrants. The most significant increase in coverage occurs for rapid intensification (+24 hour intensity changes of $\geq$ 30 kts); the frequency increases by > 15% in the DL quadrant, and > 20% in the UR quadrant. Overall, the cases that intensify most rapidly also feature the greatest symmetry at the 0 hour. In addition, the location of maximum occurrence also changes slightly. Maxima in the occurrence of PCT < 250 K tends to shift upshear with greater intensification rates. Overall, these results indicate that the occurrence of inner core precipitation at the onset not only increases with intensification rate in all quadrants, but also that the symmetry (measured by the occurrence in the upshear quadrants) distinguishes those that undergo RI (greater symmetry) versus those that undergo SI (less symmetry).

As the previous paragraph analyzed only the beginning (or onset) of the +24 hour intensity change, this section investigates the time evolution prior to, and during, the intensification period. Figure 4.3 shows the time evolution of the frequency of 85-91 GHz PCT < 250 K in 6-hourly increments for all RI cases (+24 hour intensity change of ≥ 30 kts). Within the 18 hour period leading up to RI, areal coverage of PCT < 250 K ("precipitating area") increases slightly; notably, this includes the upshear quadrants, which indicates that the *symmetry is already increasing prior to the onset of RI.* Coincidentally, the median TC intensity also increases by 10 kts during this period. The observation that rapidly intensifying storms are already intensifying at the beginning of RI onset was also found by Zagrodnik and Jiang (2014). During the +6 hour and +12 hour period after RI onset, the occurrence of PCT < 250 K increases more substantially in *all quadrants*. The period +12 to +24 hours ("RI continuing" stage) after RI onset features the highest PCT frequencies and symmetry. Given that the vertical shear magnitudes change very little during the entire 42-hour period, the increase in precipitation symmetry during RI is not attributed to decreasing wind shear.

Figure 4.4 summarizes Figure 4.3 for all intensity change categories by showing Hovmöllers of frequency. The TCs that weaken most rapidly have the highest best track intensities and the highest mean distribution of PCT < 250 K during the -18 to 0 hour period. As stated before, this category is almost exclusively biased towards mature TCs. As one would expect, the percent coverage of PCT < 250 K (raining area) tends to decrease with time in all quadrants for the weakening TCs.

Intensifying TCs tend to have an increasing occurrence and coverage of PCT <250 K in the DL quadrant in the 18 hours prior to the intensification period. Perhaps

importantly, a similar increase is observed in the UL quadrant preceding only the strongest intensification rates ($\geq$ 20-25 kts); as shown previously, this is an indication that precipitation symmetry is already increasing prior to the defined onset of RI. This can be attributed largely to storms that, by the onset, are already beginning to undergo intensification and have a higher initial intensity. Removing those storms already intensifying (> 5 kts) in the 18 hours prior reveals similar results; this could be explained by the fact that storms without pre-onset intensification have a nearly identical VMPI-$V_{current}$ to those already intensifying. Finally, the maximum in coverage of PCT < 250 K, as shown in Figure 4.3, actually increases and rotates from DL towards the upshear quadrants during RI. This result is in agreement with recent case studies of Hurricane Earl (2010) by Stevenson et al. (2014), Rogers et al. (2014), and Susca-Lopata et al. (2014), which determined a convective burst DL rotated upshear and may have contributed to vortex alignment (and RI).

To further quantify symmetry with respect to intensity change, a symmetry index is created by differencing the mean 85-91 GHz PCT (within 60 radial km of the center; polar coordinates) in each shear-oriented quadrant (i.e., downshear left [DL] - upshear right [UR] and downshear right [DR] - upshear left [UL]). Figure 4.5 shows the time evolution of precipitation symmetry for only slowly intensifying storms. Overall, the symmetry, according to the mean PCT in each quadrant, changes very little from the -18 hours period to onset to 24 hours after. Additionally, all three indices are fairly small, ranging from -4 to 1 K. The rapid intensifiers (Fig. 4.6) differ in that they initially (during the -18 hour to 0 hour timeframe) have a much more asymmetric PCT distribution than the slow intensifiers. During the 0 to +24 hour timeframe, however, the PCT distribution

rapidly symmetrizes to a nearly axisymmetric distribution in all quadrants. Overall, these results indicate that the rate of symmetrization increases with increasing intensity change.

In addition to the symmetry index shown in Figures 4.5 and 4.6, quadrant based 85-91 GHz PCT < 225 K standard deviations are investigated (Fig. 4.7) with respect to intensity change. In order to remove the steady state TCs that are likely already mature hurricanes, all cases with VMPI-$V_{current}$ $\leq$ 60 kts are removed. PCT standard deviation for all pixels < 225 K is used as another approach (compared to the difference of means method used in the previous paragraph) to investigate the symmetry and occurrence of at least "moderately-deep" convection. Figure 4.7 reveals that storms with lower intensification rates, when examining only those pixels less than 225 K, have a greater variability (or higher standard deviation) at the onset. Those TCs with higher intensity changes, however, tend to have lower standard deviations, an indication that they have a more axisymmetric convective distribution.

4.1.2 Investigation of "Intense" Convection in TC Inner Cores

Observational studies (Sitkowski and Barnes, 2008; Guimond et al.,2009) and, more frequently, modeling experiments (Hendricks and Montgomery, 2003; Montgomery and Kallenbach, 1997), have demonstrated the importance of "intense" convection in the form of "vortical" hot towers within the inner core for tropical cyclone formation and intensification. Although the definition varies, for this study, 85-91 GHz PCT 190 K is used as a threshold to identify "intense" convection.

Figure 4.8 shows the spatial frequency of 85-91 GHz PCT < 190 K. The highest occurrence of PCT < 190 K in the TCs that weaken most rapidly is in the DL and UL quadrants, maximizing at approximately 3.5%. The higher occurrence UL, is consistent

with the fact that the initial intensity of TCs included in this sample are typically already at hurricane strength (median intensity 80 - 85 kts). TCs with a slow intensification rate (+24 hour intensity change of 0 to +20 kts) have the lowest occurrence of "intense" convection in all quadrants. As intensification rate increases, however, occurrence of "intense" convection noticeably increases as well. Not unlike the 250 K threshold, those storms that intensify most rapidly have the highest occurrence of PCT < 190 K in the DL quadrant. This appears to verify the radar results of Hence and Houze (2012) and DeHart and Houze (2014) that convection matures DL. For unknown reasons, the distribution of the 30-40 kt intensity change category has a double maximum: one almost directly aligned with the shear vector and another 90 degrees left of shear. The TCs with a +24 hour intensity change greater than 40 kts have a lower fractional occurrence than the 30-40 kt category; this, however, is likely attributed to the limited sample size (192 total cases versus 536 cases).

Whereas Figure 4.8 showed the spatial frequency distribution of "intense" convection with respect to intensity change, Figure 4.9 shows the time evolution of that frequency distribution, except for RI only. Figure 4.9 reveals interesting characteristics for rapidly intensifying storms; the period 18 hours prior to the onset of rapid intensification features a higher fractional occurrence of intense convection (PCTs < 190 K) nearest to the center (within 50 km) than all other periods prior to onset. Examining the spatial frequency of only those PCTs < 170 K (not shown) reveals the period 18 hours prior to onset features the highest fractional occurrence of more intense convection nearest to the center of all periods. This maximum in occurrence approximately 90° left of shear in the inner core decreases slightly with time prior to onset. In addition, from 18

hours prior to onset, to the onset time, there is a marked increase in the frequency of intense convection straddling the shear vector at radii greater than 50 km. This maximum rotates slightly left of shear with time (though more significantly with PCTs < 170 K); and appears legitimate, as one would expect convection to migrate with time in an axisymmetric flow regime. Rogers et al. (2014) and Stevenson et al. (2014) found a similar convective evolution prior to and during Earl's (2010) RI. Within the 12 hours after the onset of RI, the overall areal coverage of intense convection (PCT < 190 K) changes very little. These results indicate that the frequency of intense, near-center convection does not increase after RI onset, and actually decreases slightly when investigating more intense convection (PCT < 170 K). The reinvigoration of the maximum in occurrence 90 degrees to the left of the shear vector during the "continuing RI" period (12 to 24 hours after onset) is clearly demonstrated; this maximum rotates farther upshear at the end of the +24 hour intensification period. This "burst" may be the result of diurnal variations, the consolidation and inward development of an eyewall, or simply a reflection of varying pathways towards RI with different environmental interactions.

Figure 4.10 summarizes the time evolution of the radial distribution of intense convection (PCT < 190 K) within the inner core for all intensity change categories. As shown before, the rapidly weakening TCs have a maximum occurrence closer to the center initially (radial distance of 20-40 km from the center) during the period within 18 hours of the onset of weakening; however, this maximum, and the overall frequency of intense convection, rapidly dissipates as the TC weakening ensues. Slow intensifiers feature an increase in the occurrence of intense convection at a radial distance of 40 - 80

km during the intensification period, however, it does not contract radially inward towards the center as intensification proceeds. The +20 to +40 kt intensification periods see the most significant increase in occurrence during the -18 to -12 hour timeframe. Differing from the slow intensifiers, the intense convection in rapid intensifiers tends to be more frequent and occur closer to the center (with the maximum occurrence near 20 - 60 km by +24 hours). The frequency of intense convection near the center within the 18 hours *before intensification onset* appears to be strongly correlated with the +24 hour intensification rate. In addition, not surprisingly, for the greater intensification rates, there is a definitive inward contraction of intense convection as the intensification proceeds.

4.2 Comparison of Atlantic and East Pacific Convective Characteristics

Significant variability in the relationship between TC intensity change and convective intensity may exist amongst the different basins (Jiang, 2011). While Jiang's study did not focus on these differences, several possibilities were cited including sampling issues, best track quality differences, and TC-environment interactions. This section investigates basin differences and relationships between convective intensity and TC intensity change.

The distributions of minimum and fraction of < 250 K for 85-91 GHz PCT within 1° of the center in the EPAC and Atlantic in Figure 4.11 reveal no discernible differences between the areal coverage of rainfall, nor convective intensity, within the inner core of TCs. This is to be expected: The processes driving convection do not change from basin to basin. An analysis of convective properties with respect to intensity change, though, reveals differences attributed to environmental variables (SST, mid-RH, vertical wind

shear). The most significant differences for statistics exist with those storms that weaken, which is not the focus of this study. Additional comparisons were made using spatial distributions similar to Figures 4.2 and 4.8, but because additional conclusions with practical importance could not be drawn, the results are not shown. Overall, the convective statistics feature minimal differences, thus justifying the methodology of combining basins in section 4.1.

4.3 Environmental and Convective Evolution with Respect to Intensity Change

This section focuses on the relationship between convective and environmental properties during slow and rapid intensity change. Basins are examined individually for this section due to the previously determined environmental differences (section 3.5 and Table 3.1).

Figure 4.12 shows the temporal evolution of the median environmental and convective parameters within a degree of the center in the Atlantic during, and prior to, slow and rapid intensity changes. For the slow intensifying TCs, overall, the environmental variables change very little during the entire period (18 hours prior to onset to 24 hours after onset); the median SST remains near 28°C, the median vertical wind shear has only a slight increase of less than 1 m s^{-1} during the 0 to +24 hour period, and the midlevel RH decreases, but only by 2-3 %. The convective properties, however, feature more significant fluctuations. Minimum 85-91 GHz PCT decreases approximately 10 K (becoming more intense) throughout the period, while the fractional coverage of 85-91 GHz PCT < 250 K increases (and does so most significantly from onset to 18 hours

after onset). Additionally, the average best track intensity remains at minimal tropical storm strength prior to onset, after which slow intensification occurs.

Rapid intensification cases feature similarly small rates of change in environmental parameters during the entire period (Fig. 4.12, right panels), though storms that rapidly intensify generally have higher median midlevel RH (~60%), higher median SST (~28.3°C), and lower median shear (~6 m s^{-1}) than storms that slowly intensify. These results indicate a potentially important conclusion: The period leading up to RI appears more favorable than SI. Storms that undergo RI begin with a more humid environment over warmer waters and in lower vertical wind shear, which may be favorable for more efficient latent heating. The more rapid decrease in midlevel RH during RI can be attributed to the formation of an eye. Convective parameters for rapidly intensifying TCs also feature a distinguishably greater rate of change than the slow intensifiers. The fractional coverage of 85-91 GHz PCT < 250 K within 1° of the center during the entire period is greater (~5-10% during pre-RI and 10-20% post-onset) than the SI period. The maximum rate of change occurs during the -6 hour to +12 hour timeframe. Minimum 85-91 GHz PCT features a greater change from -18 hours to +24 hours for rapidly intensifying cases than for slowly intensifying TCs; RI TCs also tend to initially have more intense convection (~5 K colder) than slow intensifiers. RI TCs also feature a significantly higher rate of change not only during the 6 hours after the onset, but as was mentioned in a previous section, also show an obvious tendency of intensification during the 12 hours prior to the onset of the 24 hour RI period. All of these results are consistent with the more favorable pre-intensification environment (higher RH and SST, lower shear) seen for rapidly intensifying TCs.

EPAC slow intensifiers (Fig. 4.13, left panels), despite having different magnitudes, feature some similar environmental rate of change characteristics to the Atlantic cases. Median vertical wind shear and midlevel RH only change slightly from -18 hours to +24 hours. The initial values, though, prior to intensification onset are lower (higher) for vertical wind shear (midlevel RH) than the Atlantic. In light of statistically significantly higher initial SSTs and a sharper SST gradient (Chapter 3), EPAC median SST decreases during intensification are greater than .5°C, a stark contrast to the Atlantic cases. The rapid intensifiers in the EPAC have the largest SST decrease in the period (> .5°C). Both the EPAC and Atlantic feature environmental differences with respect to intensification rate; while these differences alone cannot definitively distinguish intensity change, the pre-intensification environment can help discern future intensity changes.

Despite the EPAC and Atlantic having similar rates of change (mid-RH decreases ~5% and vertical wind shear fluctuations ~1 ms^{-1}) in environmental parameters (excluding SST), differences still exist when examining the convective evolutions (Fig. 4.13). In the median, EPAC slowly intensifying TCs have a much smaller increase in fractional coverage of 85-91 GHz PCT < 250 K than Atlantic cases. It is important to note, however, that EPAC TCs, compared to the Atlantic, tend to already exhibit a greater fraction (area) in the 18 hours prior, and that fractions are ultimately similar at the conclusion of the +24 hour intensification period. The median intensity (minimum 85-91 GHz PCT) changes very little in the EPAC (-18 to +24 hours), and has slightly lower initial values than Atlantic cases. Even more interesting, intensification (both slow and rapid) in the EPAC also features very little change in median intensity despite intensification occurring; in contrast, the Atlantic exhibits a noticeable increase in

intensity during the period.

Environmental thresholds (Table 3.1) previously discussed in Chapters 2 and 3 are applied in order to remove outlier cases. Applying the thresholds and comparing the convective statistics to results in sections 4.1 and 4.2 (no thresholds) also helps give an indication of the sensitivity to the environmental parameters. Figure 4.14 demonstrates the difference in distribution of 85-91 GHz PCT < 250 K between the original composites (no threshold applied, Figure 4.2) and those cases where thresholds are satisfied. The Atlantic distributions for all cases with a 24-hour intensity change > 0 and > 10 kts feature an interesting "half-annulus" around the center, where the threshold occurrence of PCT < 250 K is lower than when the threshold is not applied. This occurs in all quadrants except DR. In conjunction with the asymmetries previously examined (Fig. 4.5), it is determined that when applying the environmental thresholds, there is an increase in the frequency in the DR quadrant, which indicates further symmetry in the convective/precipitation area. This makes sense given that applying the threshold removes cases with "high" (> 12-15 m s^{-1}) vertical wind shear. Those storms in the Atlantic that intensify more rapidly see an even greater magnitude difference between threshold and nonthreshold cases, a possible indicator that the precipitation distribution of storms with higher intensification rates also have a higher sensitivity to the surrounding environment. PCT occurrences are lower left of shear and particularly in the UL quadrant when the threshold is applied. All other quadrants (in particular the DR), however, see an increase in occurrence with the threshold. Given these differences, it is hypothesized that applying the environmental thresholds for RI increases the symmetry with increasing intensification rates in the Atlantic.

The EPAC intensifiers > 0 and > 10 kts feature a similar distribution to the Atlantic differences, though with a much lesser magnitude. Those storms that intensify most rapidly (≥ 40 kts) feature the greatest differences between threshold and non-threshold composites, but still to a much lesser extent than the Atlantic. This indicates that the Atlantic features a stronger environmental sensitivity to convective evolution and intensity change than the EPAC.

Overall, applying the thresholds results in differences in the spatial occurrence and magnitude of 85-91 GHz PCT; these differences, however, are relatively small in both basins (~ 2 - 3 % for PCT < 250 K) and precipitation characteristics, while sensitive to changes in the environment, are not dependent upon environmental characteristics. These results also help support the hypothesis that, environmental variables, alone, do not offer significant predictive value in distinguishing 24-hour intensity change in 10-kt increments.

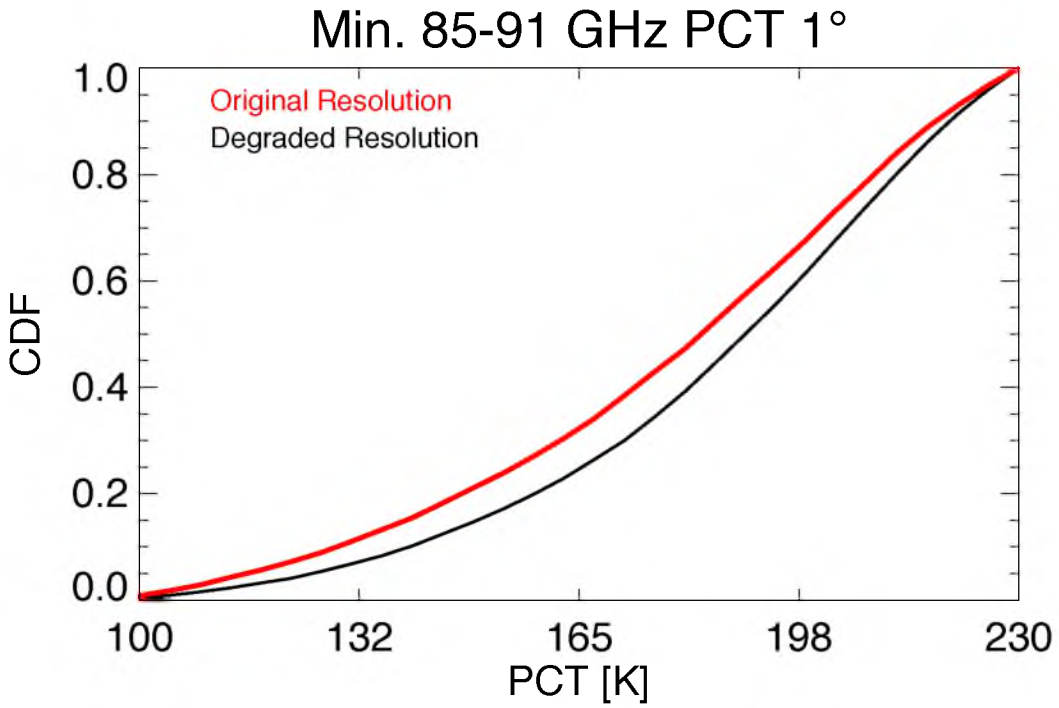

Figure 4.1. CDF of the minimum 85-91 GHz PCT within 1° of the center for original "high" resolution PCTs and the degraded PCTS (appx. 13 km resolution).

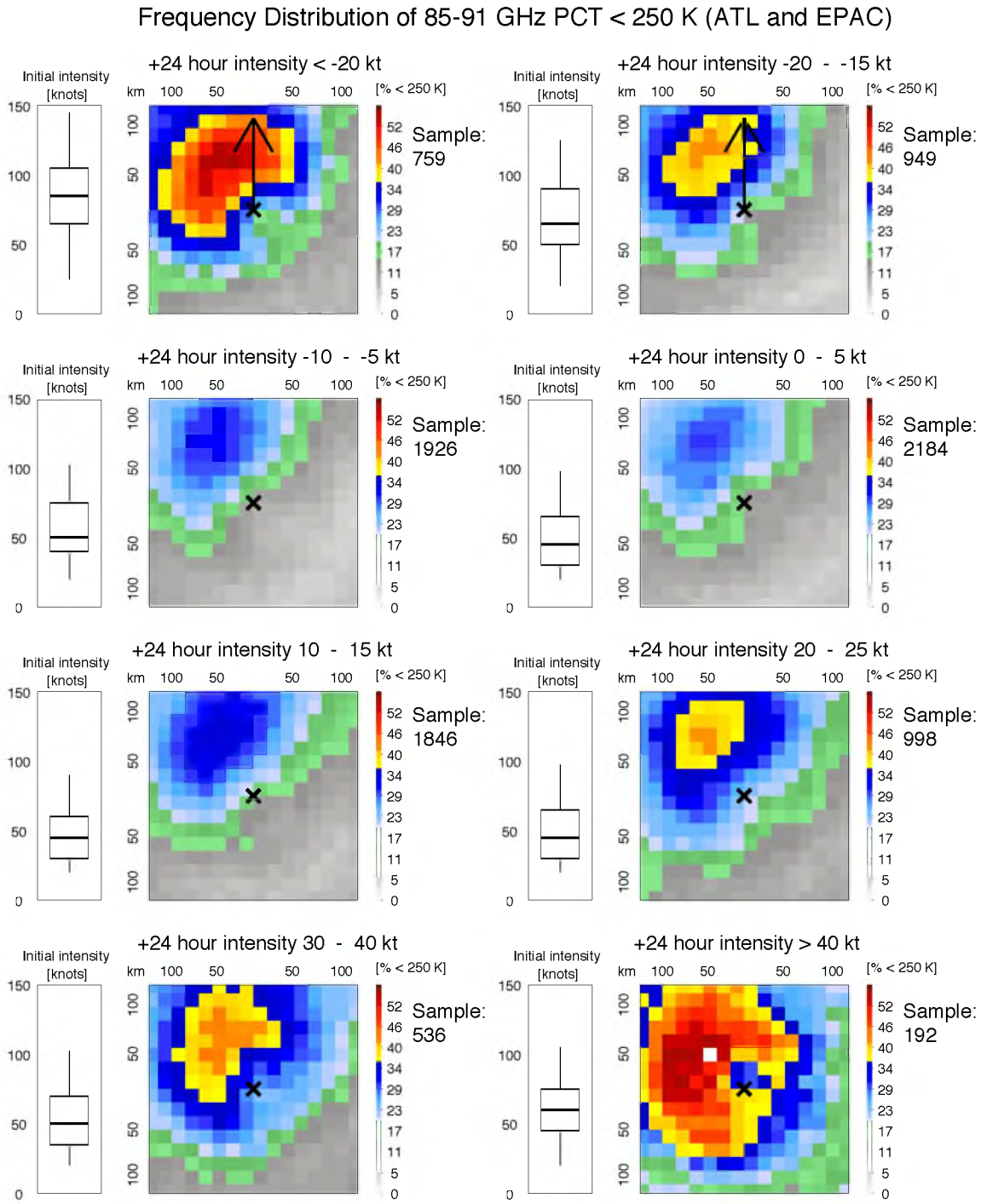

Figure 4.2. Eight-panel image of the frequency distribution of 85-91 GHz PCT < 250 K for all intensity change categories at onset (0 hour). All composites are constructed relative to the shear vector (pointing straight up). Boxplots of the initial intensities for each intensity change category are displayed.

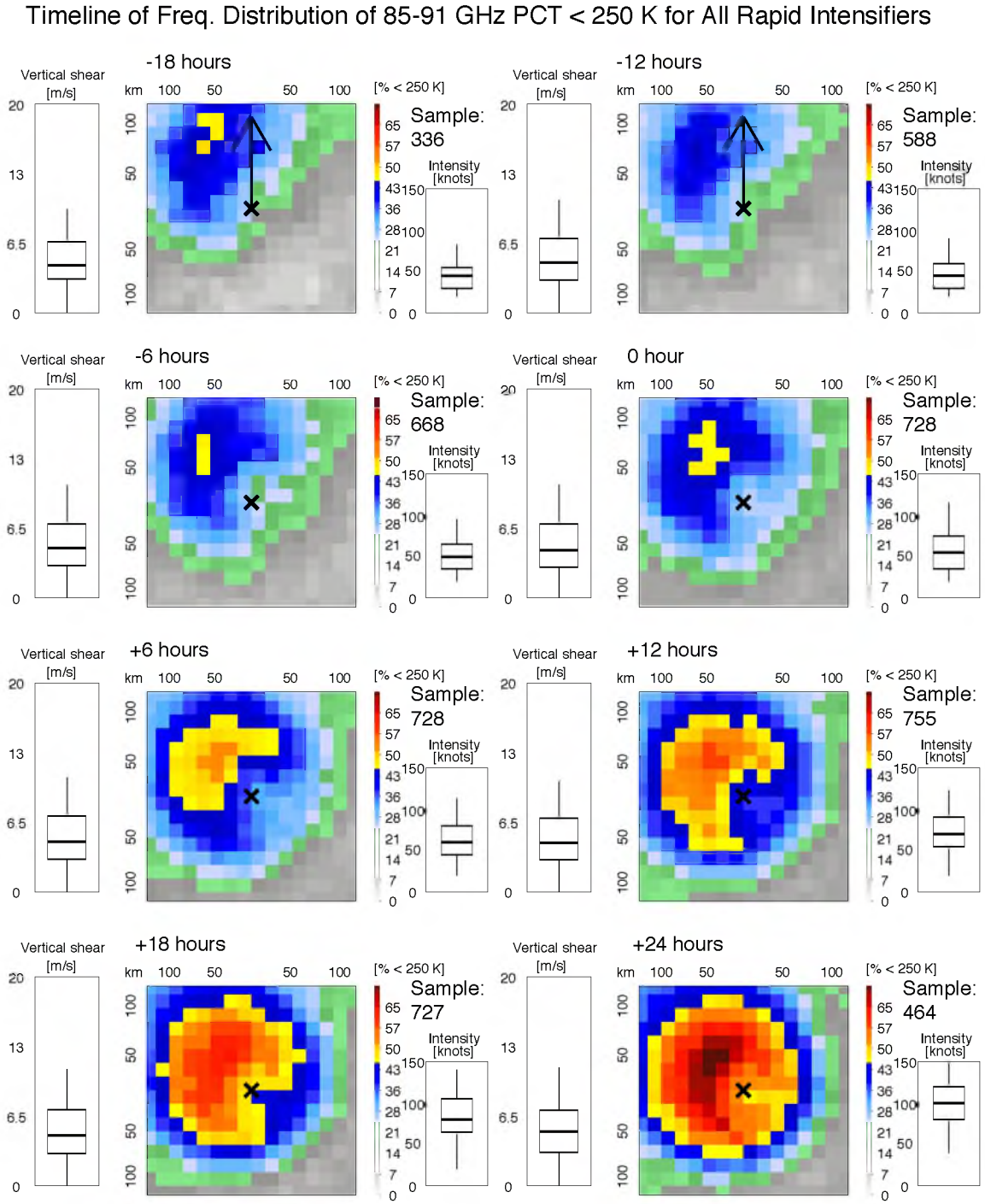

Figure 4.3. Eight-panel image of the frequency distribution timeline of 85-91 GHz PCT < 250 K for all rapid intensifiers. All composites are constructed relative to the shear vector (pointing straight up). Boxplots of the TC intensity and shear are displayed for each 6-hour interval. The 0-hour is the start of the +24 hour intensity change.

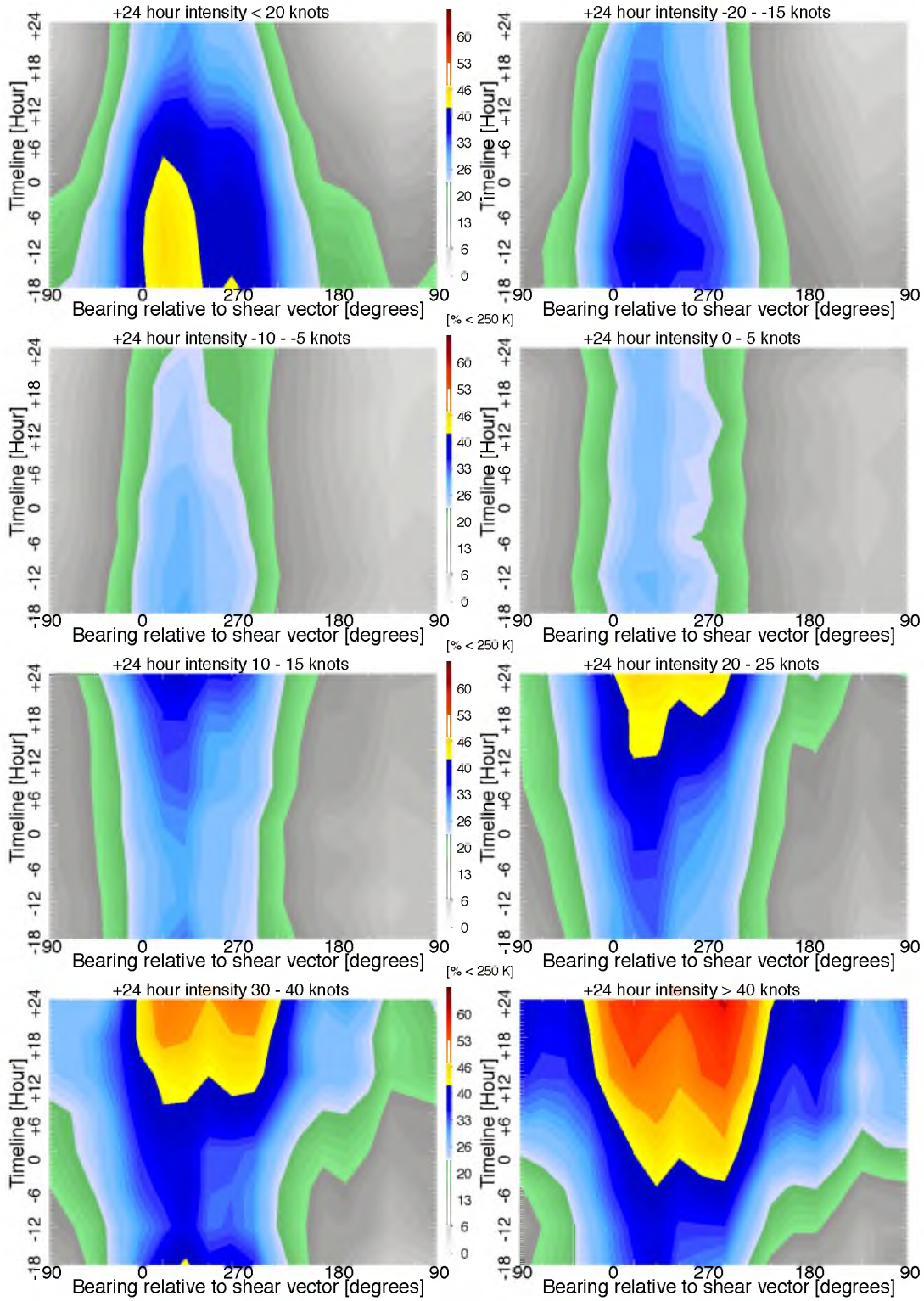

Figure 4.4. Hövmollers of 85-91 GHz PCT frequency distribution <250 K azimuthally averaged within 1° of the center for all intensity change categories. The methodology to compute the statistics for this figure uses the PCT distributions (Fig. 4.3) and averages them for 20° azimuthal increments within 1° of the center for all intensity change categories.

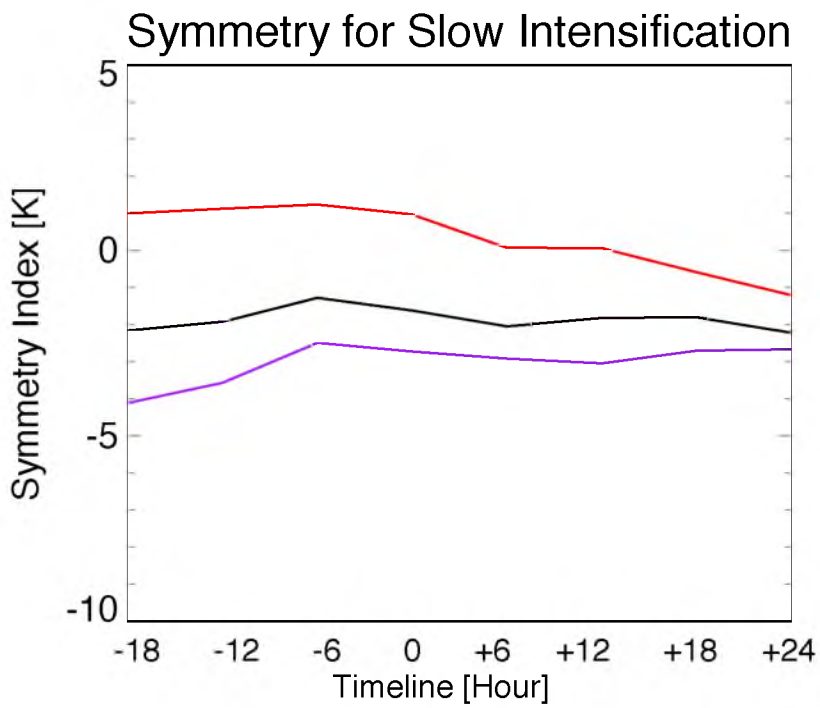

Figure 4.5. Symmetry for all TCs with a +24 hour intensity change of 10 - 25 kts using quadrant differences of mean 85-91 GHz PCT within 60 km of the interpolated best track center. Quadrants are oriented with respect to the shear vector; UL - DL (black), UL - DR (red), UR - DL (purple).

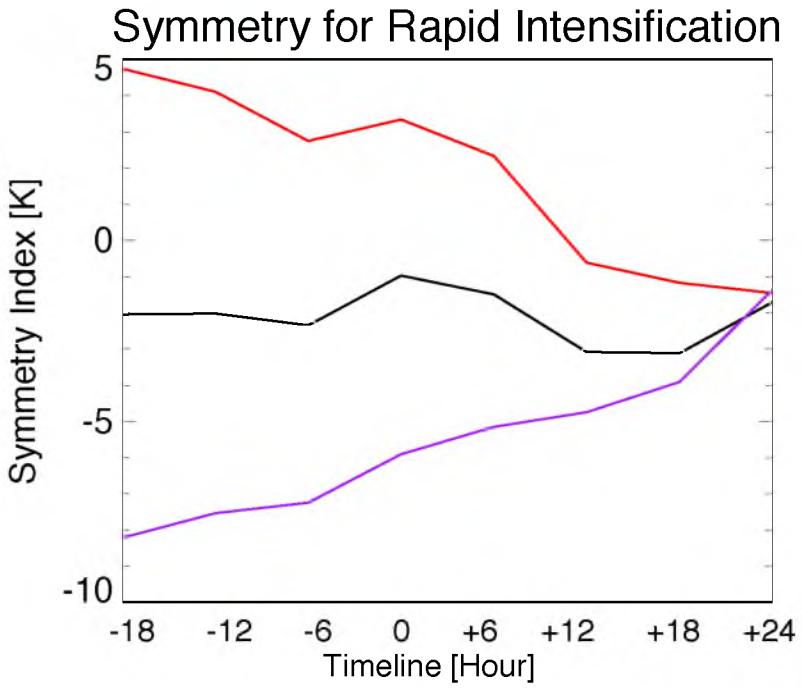

Figure 4.6. Symmetry for all TCs with a +24 hour intensity change of $\geq$ 30 kts using quadrant differences of mean 85-91 GHz PCT within 60 km of the interpolated best track center. Quadrants are oriented with respect to the shear vector; UL - DL (black), UL - DR (red), UR - DL (purple).

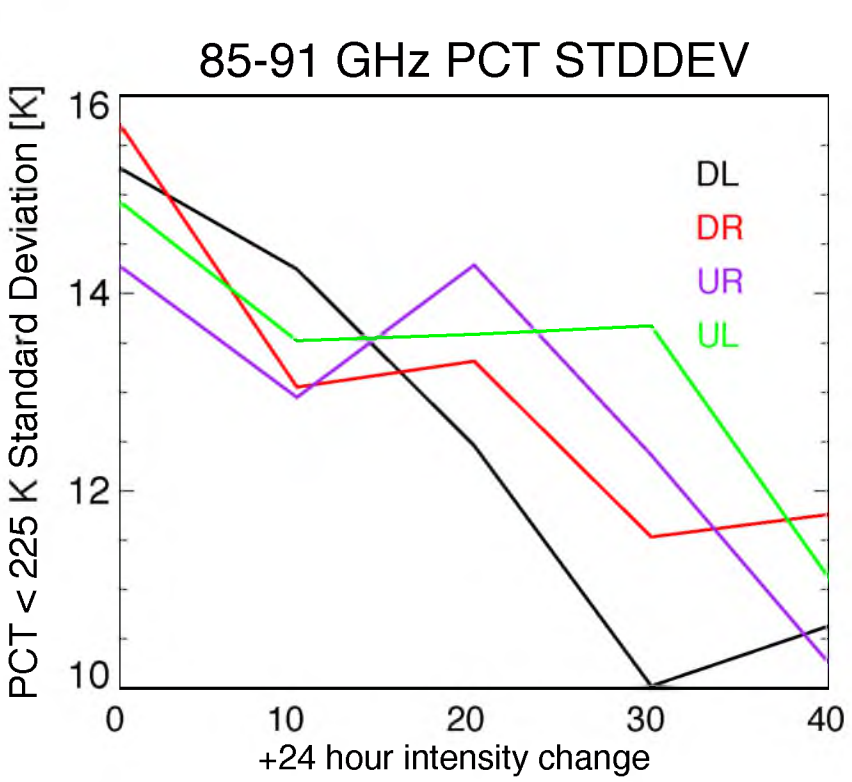

Figure 4.7. The standard deviation (using only 85-91 GHz PCTs < 225 K within 60 km of the center) of the shear-oriented quadrant of each pmw image is calculated. Mean quadrant standard deviations for all the snapshots with a VMPI-$V_{current}$ > 60 kts are plotted with respect to intensity change at onset (0 hour).

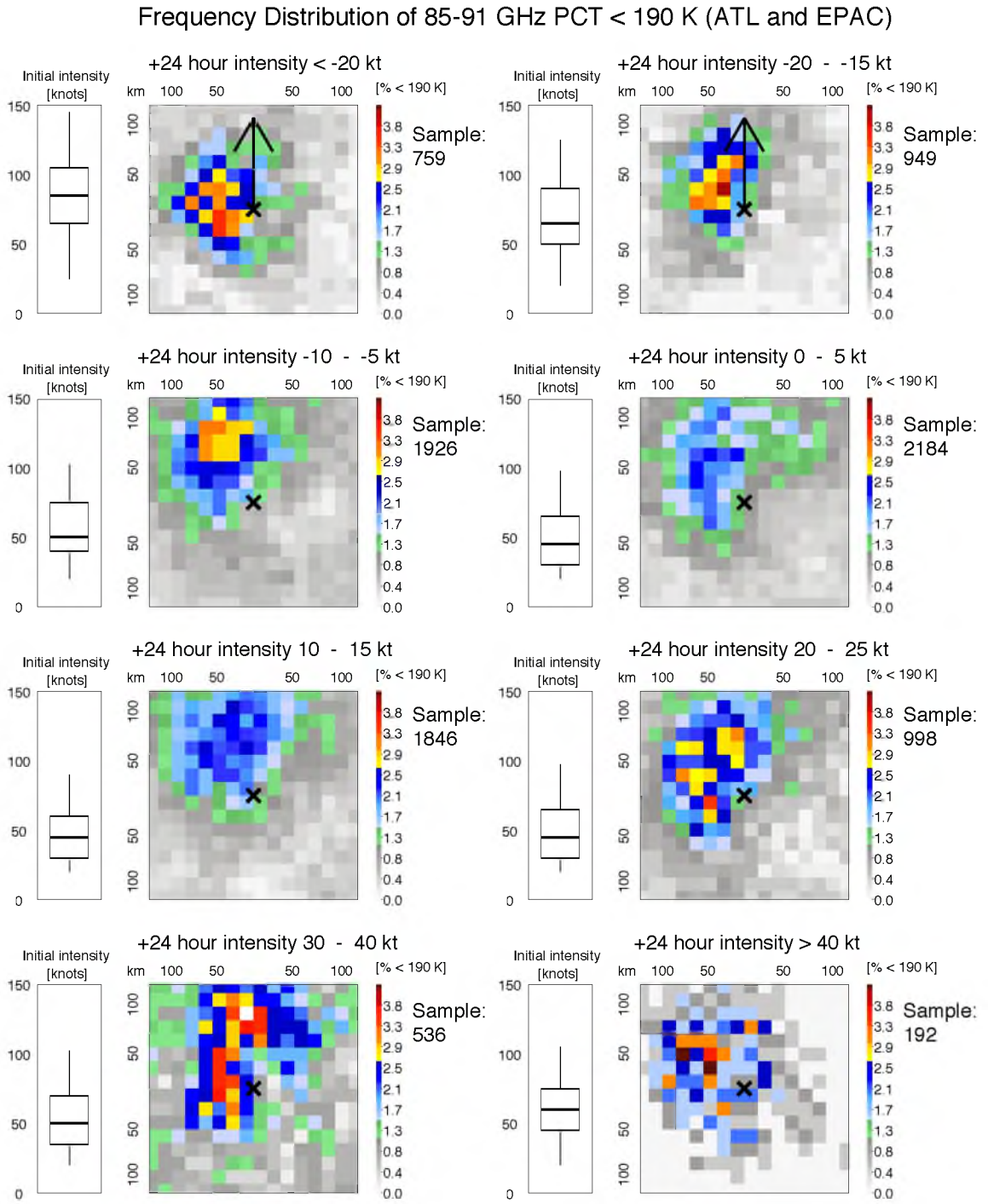

Figure 4.8. Eight-panel image of the frequency distribution of 85-91 GHz PCT < 190 K for all intensity change categories. All composites are constructed relative to the shear vector (pointing straight up). Boxplots of the initial intensities for each intensity change category are displayed. The lower quartiles that extend to "0" are simply a result of the boxplot calculation method; no storms below depression status are included.

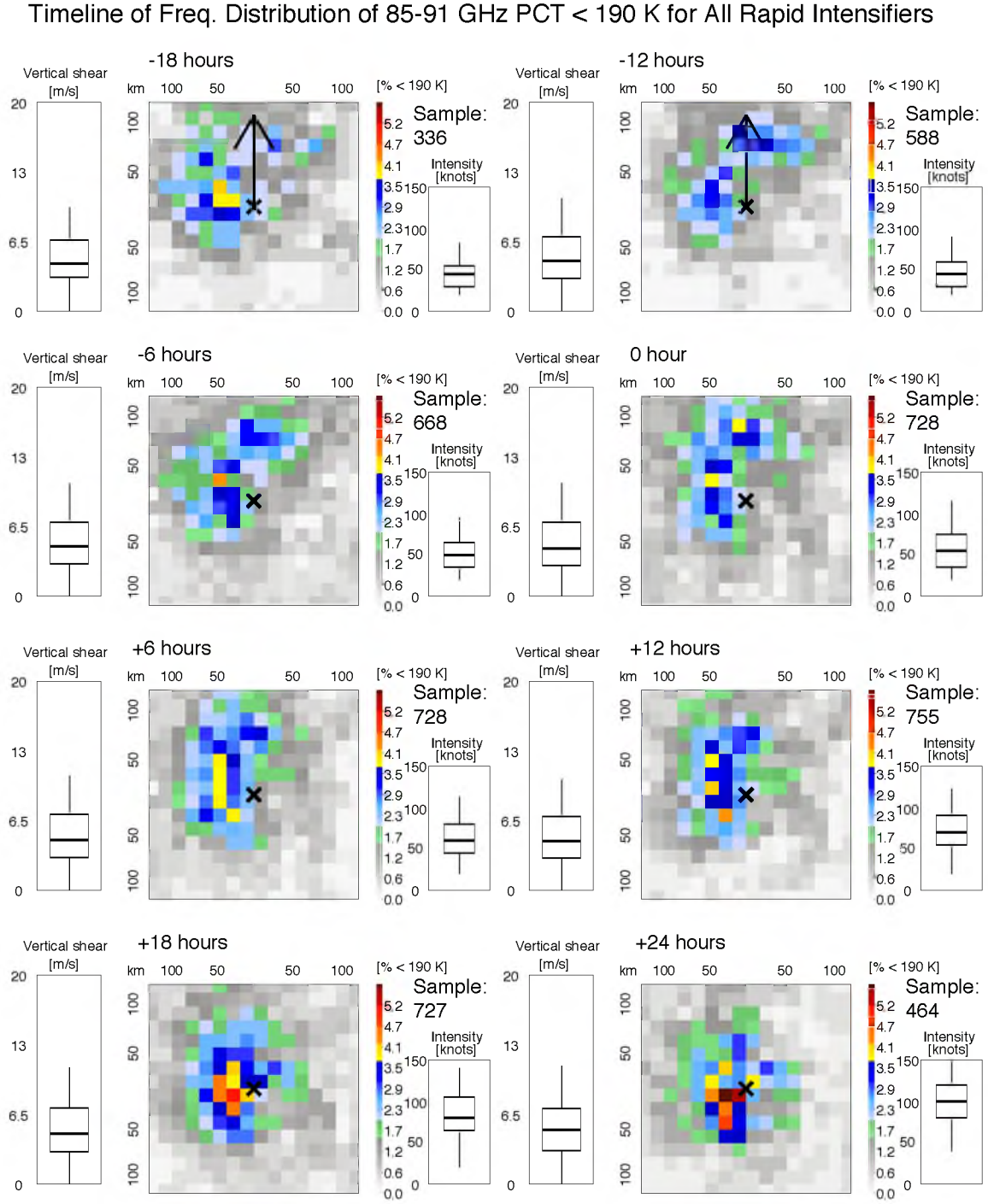

Figure 4.9. Eight-panel image of the frequency distribution timeline of 85-91 GHz PCT < 190 K for all rapid intensifiers. All composites are constructed relative to the shear vector (pointing straight up). Boxplots of the TC intensity and shear are displayed for each 6-hour interval. The 0-hour is the start of the +24 hour intensity change.

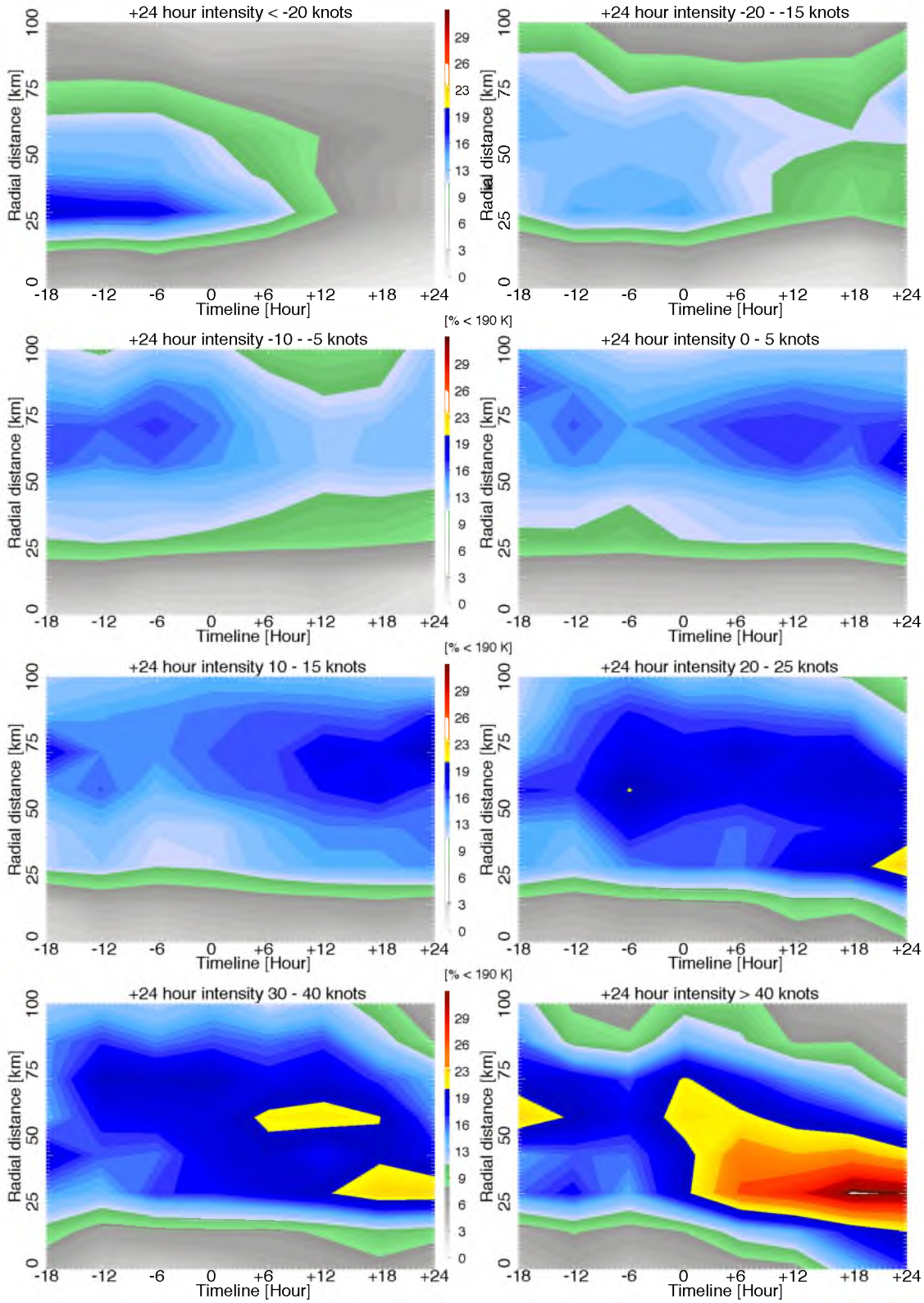

Figure 4.10 Hövmollers of 85-91 GHz PCT frequency distribution <190 K radially averaged within 1° of the center for all intensity change categories.

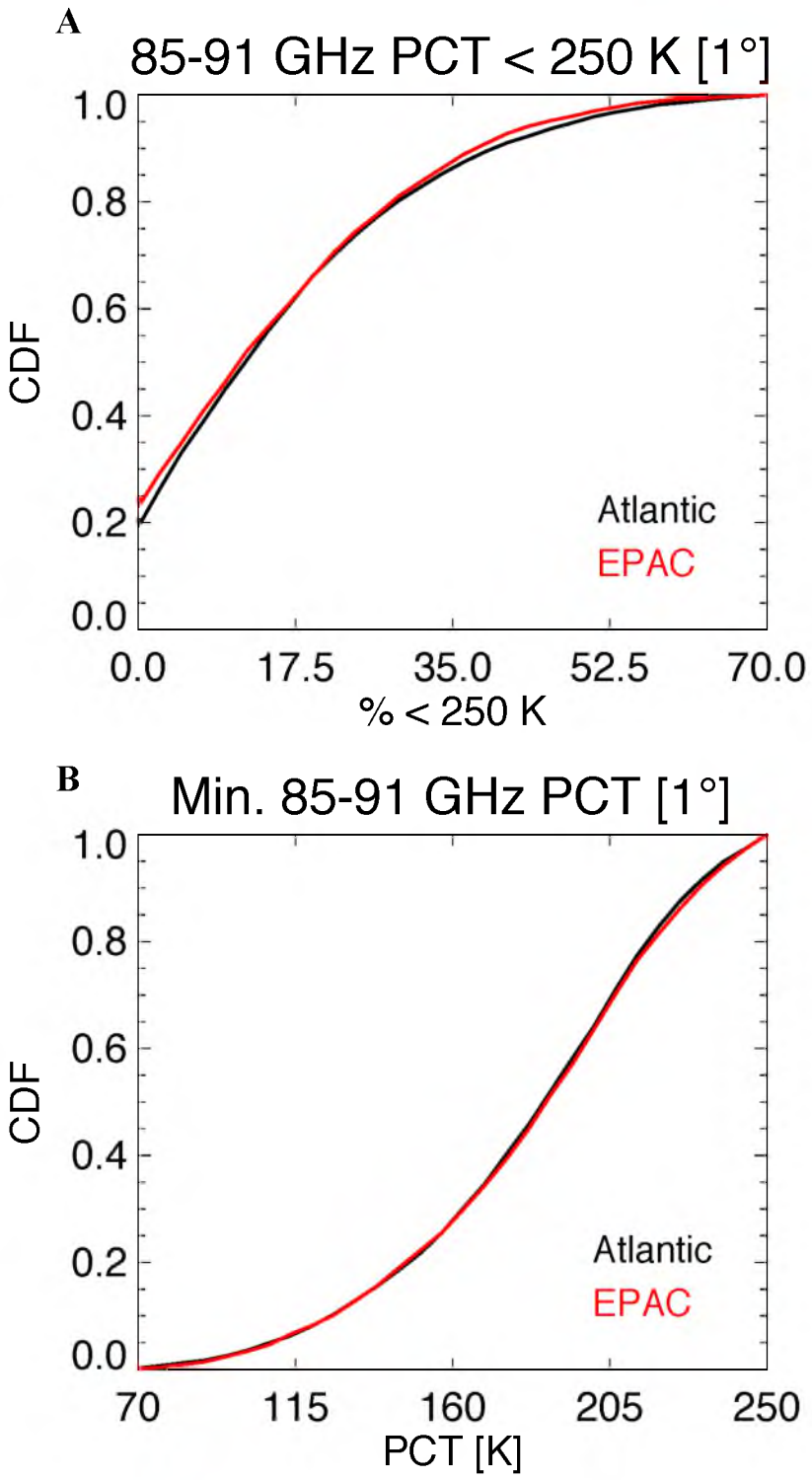

Figure 4.11. Basin comparison for percent of 85-91 GHz PCT < 250 K within 1° of the center for each overpass (A) and minimum 85-91 GHz PCT within 1° of the center (B).

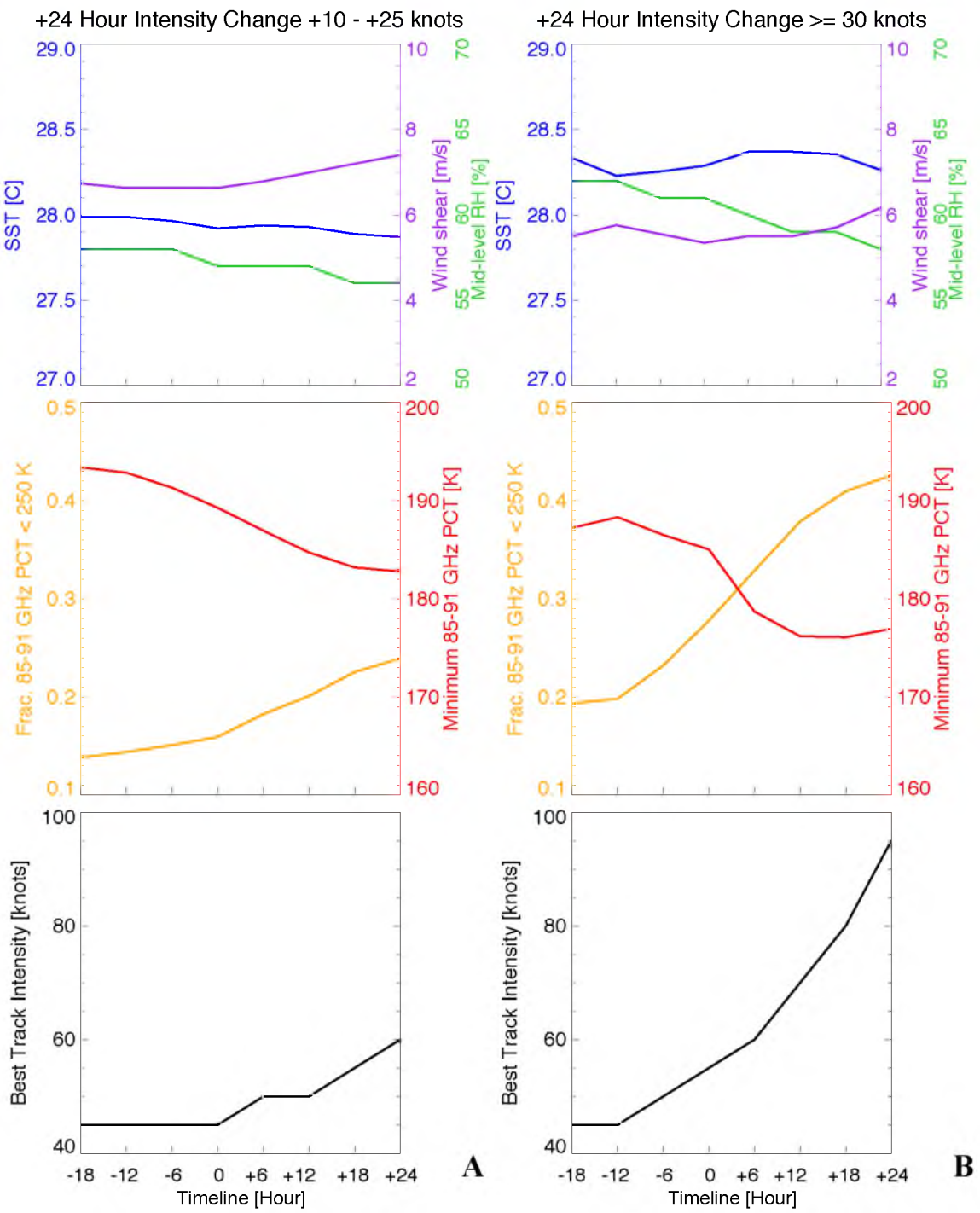

Figure 4.12. Timeline evolution of Atlantic median environmental parameters (midlevel RH: green; vertical wind shear: purple; SST: blue), convective parameters within 1° of the center (minimum 85-91 GHz PCT: red; fractional coverage of 85-91 GHz PCT < 250 K within 1° of the center: orange), and best track intensity (black) for slowly intensifying TCs (A) and rapidly intensifying TCs (B).

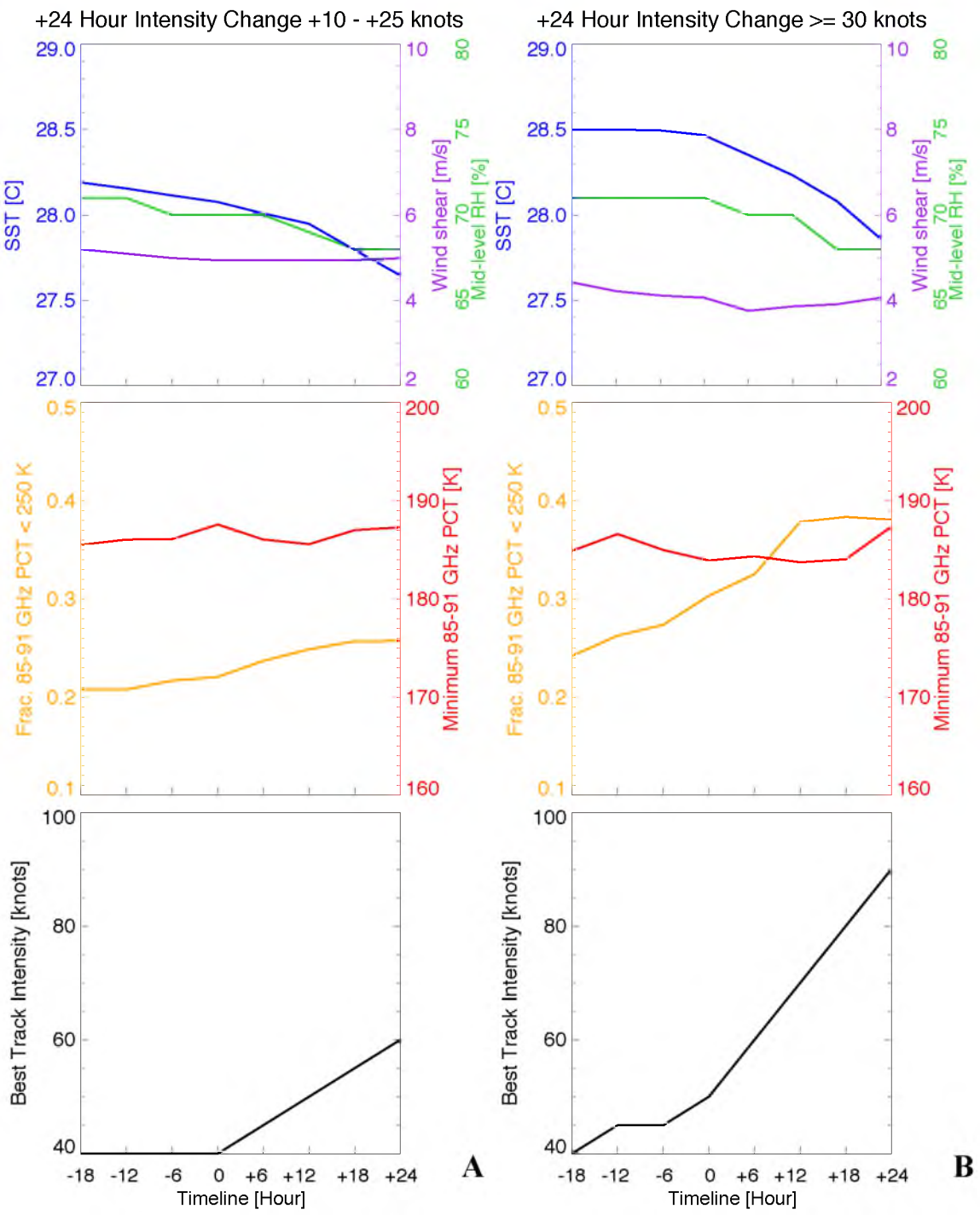

Figure 4.13. Timeline evolution of EPAC median environmental parameters (midlevel RH: green; vertical wind shear: purple; SST: blue), convective parameters within 1° of the center (minimum 85-91 GHz PCT: red; fractional coverage of 85-91 GHz PCT < 250 K within 1° of the center: orange), and best track intensity (black) for slowly intensifying TCs (A) and rapidly intensifying TCs (B).

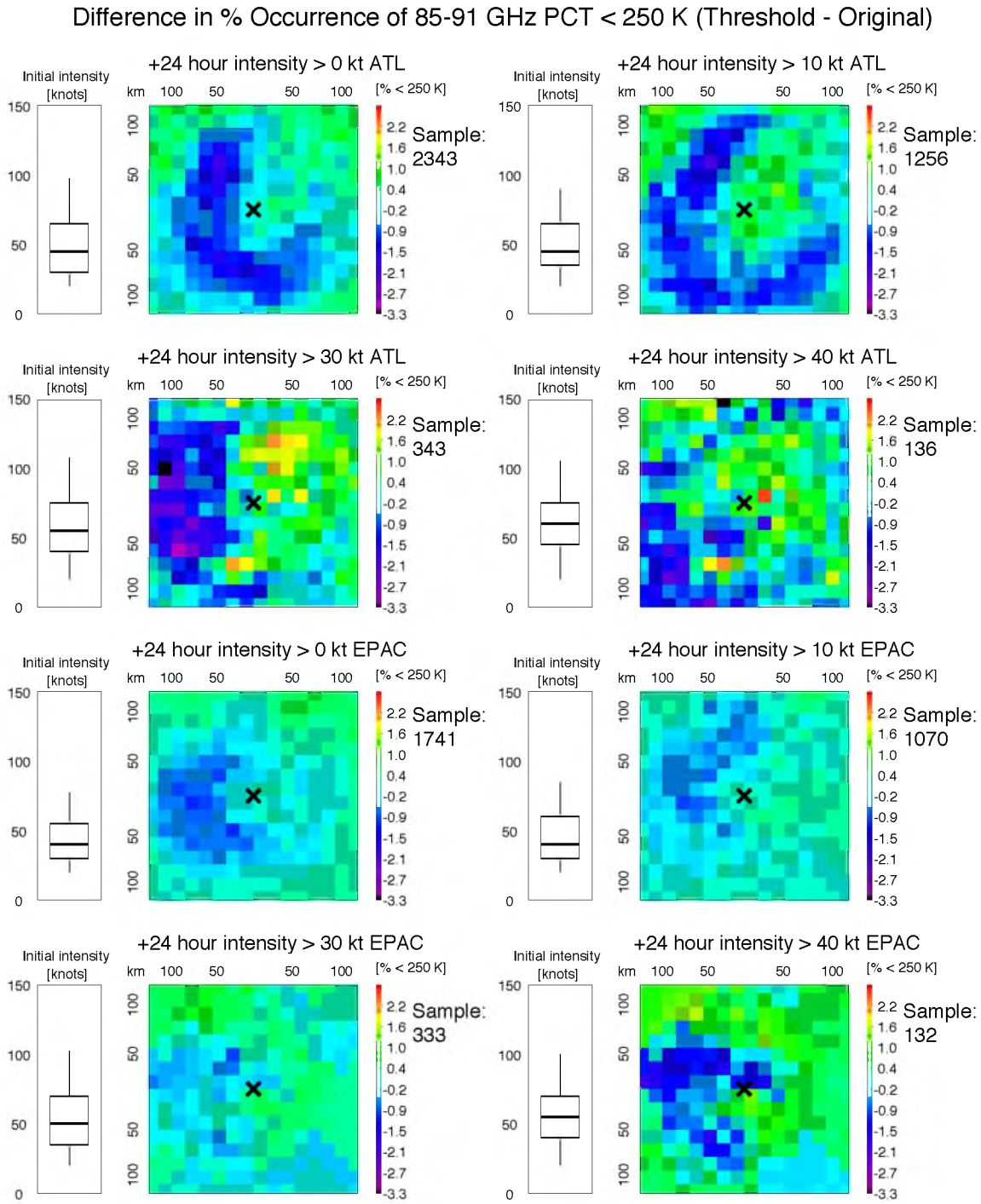

Figure 4.14. Eight-panel image of the difference in frequency distribution of 85-91 GHz PCT < 250 K between threshold and original composites for varying intensification rates in the Atlantic or EPAC. All composites are constructed relative to the shear vector (pointing straight up). Boxplots of the initial intensities for each intensity change category are displayed. The lower quartiles that extend to "0" are simply a result of the boxplot calculation method; no storms below depression status are included.

CHAPTER 5

CASE STUDIES

The previous parts of this study have dealt almost exclusively with the large dataset and examining composite statistics. This section will place a few well-sampled cases of TC intensification from recent hurricane field experiments within the context of the dataset. Cases examined include Hurricane Karl (2010), Hurricane Nadine (2012), and Hurricane Isaac (2012).

5.1 The Rapid Intensification of Hurricane Karl (2010)

On 16-17 September 2010 Karl rapidly intensified from a 45-kt tropical storm into a 105-kt major hurricane in less than 24 hours. Of particular importance, operational numerical models grossly underestimated Karl's intensification; though better than the models, the NHC intensity forecast also underestimated intensification (by greater than 30 kts for the 24-hour forecast). Dr. Michael Brennan, a forecaster for the NHC, stated in a personal communication that the lack of RI in official NHC forecasts is often due to lack of confidence and/or poor model guidance; the lack of knowledge about the current state of the storm and its environment can also attribute to lack of confidence. Additional motivation for investigating Hurricane Karl: an unprecedented six aircraft examined Karl's environment and inner core during the RI period. Data from the NOAA P-3, NASA Global Hawk, and NASA DC-8 are examined for a detailed analysis of Karl's

evolution during RI.

Figure 5.1 shows the evolution of Karl's convective properties and environmental characteristics from 1200 UTC 15 September to 1200 UTC 17 September 2010 with respect to the best track intensity. Karl traversed the Yucatan during the first 18 hours of the timeline; despite being over land during this period the TC only experienced modest weakening. In a correspondence with Dr. Michael Brennan from the NHC, he stated "there is considerable uncertainty in a situation like Karl, since over the Yucatan we don't really have much in situ data to tell us how strong the storm actually is." The Yucatan landfall at 1200 UTC on 15 September featured a remarkably intense (minimum 85-91 GHz PCT less than 135 K), large areal (fractional area less than 250 K of 40%) convective burst that subsided after landfall. With all environmental conditions deemed conducive for plausible intensification (and RI), upon emergence in the Bay of Campeche (0600 UTC 16 September), Karl immediately began rapid intensification. The NHC did not forecast RI despite accurate operational model guidance of the surrounding TC environment; plausible conditions were forecasted accurately days in advance. As previously stated, the lack of storm intensification in model guidance and uncertainties in initial storm intensity superseded a more aggressive intensity forecast (despite increasingly favorable convective properties). The RI is attributed to the already favorable state of the vortex, associated convection, and, as mentioned, favorable environment (midlevel RH > 70%, VWSH < 5 m s^{-1}, SST > 30 °C). The following paragraphs examine RI evolution and hypotheses of intensification causes.

During the RI period, all environmental parameters remained within the threshold for plausible rapid intensification (Table 3.1). Interestingly, the SSTs maximized during

the beginning of the RI period before decreasing to 28.5°C, a value still more than sufficient for intensification. Convective intensity maximized 6 hours prior to the onset of the RI period (and just prior to exiting the Yucatan into the Bay of Campeche), around 0000 UTC on 16 September; and again 6 hours after RI onset (1200 UTC), before decreasing throughout the remainder of the RI period. In addition, the areal coverage of 85-91 GHz PCT < 250 K increased throughout the RI period (except for the final few hours) and was actually already increasing prior to the storm exiting the Yucatan and beginning RI, as well as before the most intense burst of convection at 1200 UTC 16 September.

Data from the Airborne Precipitation Dual Frequency radar (APR-2) aboard the NASA DC-8 provides vertical cross sections of Karl's inner core during the "continuing" stages of RI (on station 1700 UTC - 0000 UTC). Figure 5.2 displays a SE to NW center pass at approximately 2000 UTC, during which the DC-8 over-flew a deep, intense convective burst in the SE quadrant. Coincidentally, the NOAA P-3 made a south to north transect across the center near the time of the DC-8 transect. Doppler velocity and in situ flight-level wind data from the P-3 reveal that the radius of maximum winds (RMW) was located at 20-25 km from the center and sloped outward with height. Figure 5.3 shows the radar reflectivity structure along with the approximate RMW locations. It is hypothesized that the strong convective burst, located in the S/SE quadrant within the radius of maximum winds, aided the intensification of Karl, a result consistent with Rogers et al. (2013).

The High Altitude MMIC Sounding Radiometer (HAMSR) aboard the Global Hawk provides additional data for evaluating the convective evolution. The 166 GHz

channel (one of HAMSR's 25 channels) is similar to the 85-91 GHz frequencies in that they are both sensitive to frozen hydrometeors; 166 GHz, however, responds more strongly to frozen hydrometeors of a smaller size and higher altitude (Skofronick-Jackson et al., 2008). Figure 5.4 displays brightness temperature (Tb) composites of the 166 GHz channel (Level 1) at 2100 UTC on 16 September; and 0100 UTC, 0400 UTC, 0800 UTC on 17 September. The composites encompass 4-hourly periods and include a minimum of 3 transects (of different orientation). The 2100 UTC composite (Fig. 5.4; 12-15 hours after RI onset) features a strong brightness temperature asymmetry, confirming the intense, asymmetric distribution of convection during the continuing stages of RI seen in Figures 5.2 and 5.3. Although shear is minimal (< 5 m/s) during this timeframe (Fig. 5.1), if the 2100 UTC composite is examined with respect to the observed south or southwestward pointing shear vector, the coldest brightness temperatures are located in the DL quadrant. This compares quite well to the overall TC-PMW dataset spatial frequency distribution of 85-91 GHz PCT (as a proxy for convective intensity in Figs. 4.3 and 4.9) in rapidly intensifying storms. While still asymmetric, the 0100 UTC composite reveals a trend towards a more symmetric distribution of 166 GHz Tbs and less intense convection (increasing minimum Tbs). The 0400 UTC and 0800 UTC time periods (bottom panels) show a continued evolution towards a less intense but more symmetric convective configuration during the latter stages of RI.

In addition to the level-1 HAMSR data providing a high spatial and temporal resolution of inner core brightness temperatures, the level-2 data yield derived temperature and moisture profiles for Karl's evolution. Figure 5.5 displays the vertical profile of the temperature anomaly for Hurricane Karl's eye during a portion of the RI

period (15-27 hours after onset). The anomaly is calculated by differencing mean temperatures within the precipitation-free eye with a mean environmental temperature profile (precipitation free at radii > 200 km). The warm core maximizes in the upper troposphere (above 300 hPa) during the continuing stages of RI (2100 UTC on 16 September). During the latter stages of RI, the warm core maximum in the upper troposphere intensifies and actually expands to lower altitudes; the temperature anomalies increase in the middle troposphere, a further indicator of overall vortex intensification. It is of great interest to know the warm core profile prior to the strong asymmetric burst(s) around 1200 - 2100 UTC on 16 September; unfortunately no in situ data are available from any aircraft during this period. Thus, it is difficult to hypothesize exact contributions of the intense convection to warm core and TC intensification during the initial onset of RI.

Using the aforementioned data along with additional satellite, radar, and reconnaissance data not shown here, several hypotheses regarding the under-prediction of intensification are investigated. The 0300 UTC 16 September NHC forecast advisory anticipated intensification upon Karl's reemergence in the Bay of Campeche, however, the intensification rate was underestimated. The NHC's conservative intensity forecast was partially attributed to a lack of significant intensification depicted in model guidance (despite favorable environmental conditions). It is possible that model guidance underestimated Karl's vortex strength and convective organization upon reemergence from the Yucatan. Figure 5.6 shows the 85 GHz Tb snapshot from TMI at 06 UTC 16 September. For having been over land approximately 18 hours, Karl featured a remarkably organized structure with well-defined inner core convection and an eye-like

feature. Though PMW snapshots were limited, this was also apparent in infrared satellite imagery. Forecasted environmental conditions did not change significantly prior to and following Karl's traverse across the Yucatan; thus it is believed that Karl's convective evolution (and particularly the vortex maintenance collocated with intense near-center convection) played a crucial role in "priming" the TC for RI.

5.2 Hurricane Nadine (2012): A Case Study of an Unusually Resilient TC

Nadine, an unusually long-lived tropical cyclone (fourth longest on record in the Atlantic basin), tracked across the eastern subtropical Atlantic from 10 September - 03 October, 2012 (Brown, 2013). This section focuses on the first half of Nadine's lifecycle. On 12 September, Nadine intensified 25 kts within a 24-hour period; the NHC accurately forecasted this period with intensification attributed to "favorable" environmental conditions and "deep convection and a possible CDO [central dense overcast] feature" that formed over the well-defined low-level center. SSTs of 28°C, midlevel RH greater than 60% and vertical wind shear less than 10 m/s (Fig. 5.7) all fell within the Atlantic thresholds for plausible rapid intensification (Table 3.1). The lack of intense convection is an interesting characteristic of Nadine's intensification; Figure 5.7 (2nd panel) shows the relatively warm minimum 85-91 GHz PCTs peaking around 190 K. The intensification period also featured a significant increase in areal coverage of precipitation and "moderate" convection, with fractional 85-91 GHz PCT < 250 K peaking near 50%. Figure 5.8 shows the distribution of Nadine's evolving convective symmetry and its radial contributions. The intensification period on 12 September featured a rapid increase in 85-91 GHz PCT < 250 K in all quadrants except UR (upper

panel) at all radial distances (< 100 km). Also, the bottom panel reveals that Nadine's convective asymmetry increased with a PCT minimum DR approximately 12-24 hours prior to intensification onset (around 00 UTC 12 September); this agrees with the findings in section 4.1.1 that higher 24-hour intensification rates commonly feature more significant asymmetries in the 18 hours prior. As Nadine begins to intensify, the index indicates an "increasing symmetry"; interestingly, however, the UL to DL and UR to DL differences actually increase (decreasing symmetry) at the middle portion of the intensification as convection increased upshear, likely a result of diurnal variations. The end of intensification, though, features the greatest symmetry with all differences nearest to 0; the main takeaway being the transformation from an asymmetric storm prior to RI.

Intensification quickly halted on 13 September as vertical wind shear increased to near 10 m s^{-1}, midlevel RH decreased to less than 60%, and SSTs began to decrease, though values remained within thresholds for plausible intensification. The following 24-48 hours (13 and 14 September) featured a relatively steady state period for TC intensity. During this time period, areal coverage of PCT <250 K decreased; coincidentally, vertical wind shear increased and midlevel RH and SST continued to decrease. "Intense" convection is observed at 1200 UTC 14 September with a minimum 85-91 GHz PCT around 110 K in the DL quadrant. Immediately following, the fractional area of precipitation increased from 25% to 50%. Only slight intensification (10 kts), however, occurs coincident with this burst and areal increase. The lack of more significant intensification is largely attributed to the continued increase in vertical wind shear (greater than 10-15 m s^{-1}). Additionally, SSTs and midlevel RH values become even more marginal following the convective burst. As some previous studies have cited, the

asymmetric burst and resulting structure may have actually been a result of high vertical wind shear (Molinari, 2012; Rogers, 2014). The burst was maximized in the DL quadrant but was 50-75 km from Nadine's center (Fig. 5.8), an additional possible hindrance.

Following the brief intensification on 14 September, Nadine's intensity changed very little for 24 hours. Thereafter, as midlevel RH plummeted below 40% but still remained within the "threshold for plausible intensification," Nadine weakened; vertical wind shear remained detrimental with values near 15 m s^{-1} (not within the threshold for plausible intensification). SSTs continually decreased as Nadine tracked farther northeastward over waters below 26°C. In addition to not meeting the environmental thresholds for plausible intensification, Nadine's fractional coverage of PCT <250 K decreased to 20% on 16 - 18 September, an additional likely culprit for the lack of intensification. From the 18th until the 21st Nadine's intensity was steady state; SSTs continued to decrease to below 24°C and midlevel RH remained around 35%. Vertical wind shear also remained unfavorable with values near 15 m s^{-1}. On the 20th values rapidly decreased, but unfavorable SSTs prevented the regeneration of convection leading to Nadine's brief but temporary demise.

Overall, important observations of Nadine's evolution include a more asymmetric convective pattern 18-24 hours prior to intensification, followed by increasing symmetry prior to onset. Nadine's primary intensification period (12 September) occurred in the presence of plausible environmental conditions for RI but featured a relative lack of "intense" convection. An increase in "intense" convection on 14 September, coincident with high (10 -15 m s^{-1}) vertical wind shear, only results in modest intensification (10 kts). Lower convective intensity after 14-15 September is attributed to lower SST and

mid-RH. An examination of additional satellite data reveal that Nadine maintained a shallow vortex with light precipitation during the steady state period (18 - 21 September) despite high vertical wind shear (> 15 m s^{-1}).

5.3 Hurricane Isaac's (2012) Over-Predicted Intensification

Isaac entered the southeastern Gulf of Mexico around 0000 UTC 27 August before moving northwestward towards the Louisiana coastline. Isaac's structure was characterized by a large wind field (National Hurricane Center) and gradually strengthened into a hurricane just prior to landfall. Despite having a near perfect lead-time with hurricane watches posted 48 hours prior to landfall, Isaac provides a unique scenario in which the NHC over-predicted intensification (forecasting 20-kt +24 hour intensification). NHC intensity errors on 27-29 August were about 15 kts higher than observed. The NHC attributed the overforecast intensification to an increasingly organized satellite appearance and developing eye in reconnaissance data coincident with a contracting RMW. Additionally, Isaac was passing over very warm waters (> 29° C) and was in a region of very favorable upper-level outflow (with vertical wind shear values < 5 m s^{-1}) 24-36 hours prior to landfall. This section investigates the interaction between Isaac's convective and environmental properties to hypothesize the cause for slower intensification.

Figure 5.9 shows Isaac's environmental and convective properties coincident with intensity from 0000 UTC 27 August to 0000 UTC 29 August. Isaac's intensity (Fig. 5.9) slowly increased (10 kt in 12 hours) on 27 August. No intensity change was observed for the next 12 hours, before being followed by an additional slow intensification period (10 kt in 12 hours, beginning 0600 UTC 28 August) prior to landfall. All environmental

parameters throughout the period were within the threshold for "plausible intensification," and even RI (Fig. 5.9 top panel). Initially (00 UTC 27 August), vertical wind shear was 8 m s^{-1}, but within 24 hours, decreased below 5 m s^{-1}; coincidentally, midlevel RH decreased by approximately 10%. Isaac's intensification did feature an increasing fractional area of 85-91 GHz PCT < 250 K; though, the areal coverage of precipitation was decreasing before onset. In addition, a general lack of intense convection was observed with the coldest PCTs at the beginning of the period.

A more detailed look at Isaac's convective evolution (Fig. 5.10) reveals a "strong burst" DL at 0000 UTC 27 August. The coldest PCTs were generally located at a radial distance greater than 50 km from Isaac's center. This burst also featured an anomalously large precipitation asymmetry within the inner core (Fig. 5.10 bottom panel). In the 12 hours following, convection propagated upshear and the TC symmetrized significantly. Despite what appeared to be favorable convective and environmental characteristics for RI based on results in this study, Isaac only intensified 10 kts. One possible cause is the rather broad radius of maximum winds; during this time period the RMW was greater than 50 km on average (though the RMW contracted to approximately 30 km during the first intensification period according to the NHC TC Report). While this study has documented the importance of convective location and intensity in conjunction with environmental conditions, the tangential wind profile, and particular location of the convection with respect to the RMW as suggested by Rogers et al. (2013) and Guimond et al. (2009), can also add valuable information and should be considered when available. A second "convective burst" occurs around 1200 UTC 28 August, at approximately the same radius as the previous episode (50 - 75 km). Following this burst the areal coverage

of PCT within 1° of the center increased (Fig. 5.9); the intense convection, however, was not located inside the RMW. Proximity to land also limited more substantial intensification.

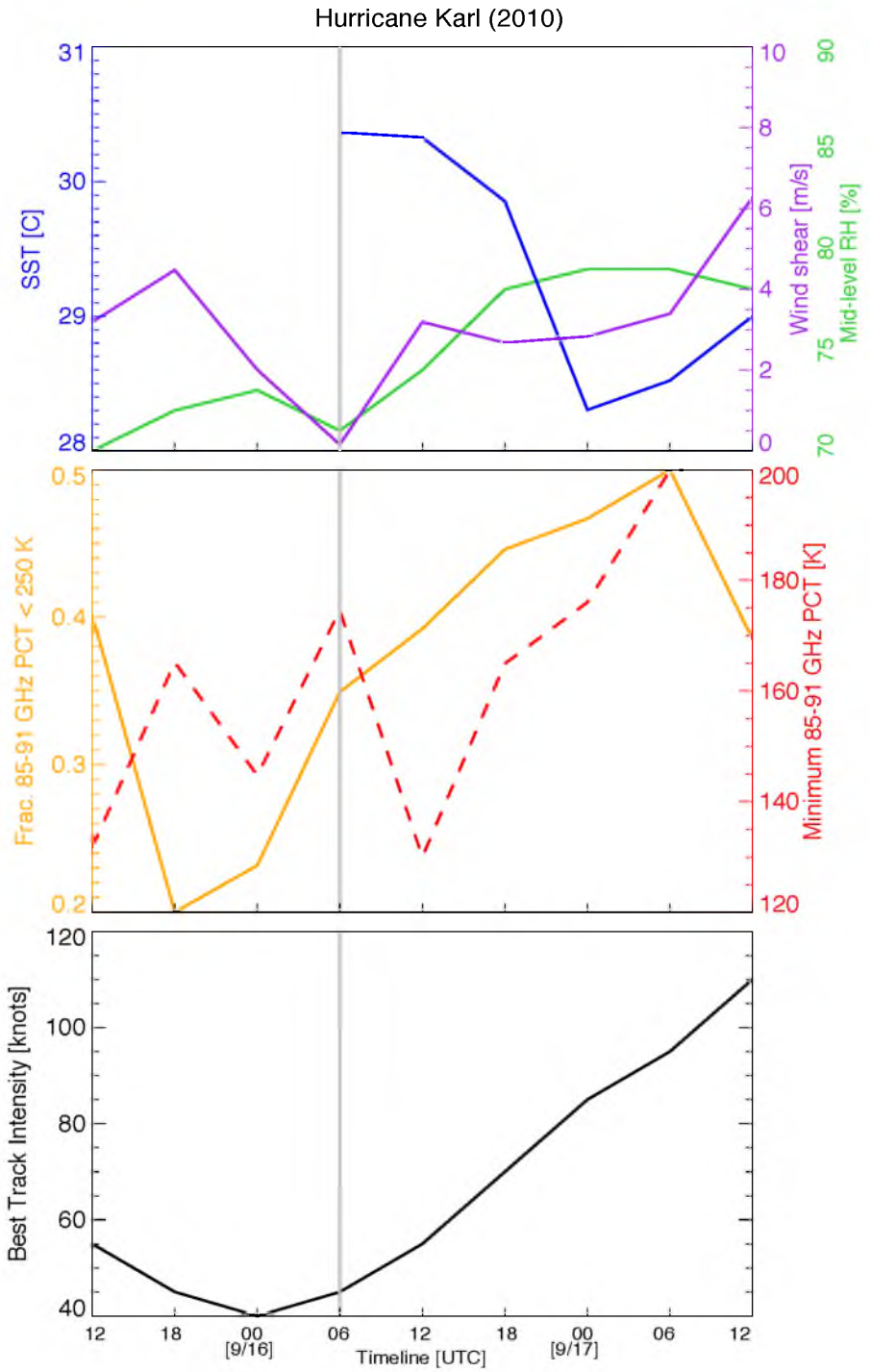

Figure 5.1 Evolution of Karl's environmental characteristics (SST: blue; vertical wind shear: purple; midlevel RH: green), convective properties (minimum 85-91 GHz PCT within 1° of the center: red; fractional coverage of 85-91 GHz PCT < 250 K: orange), and best track intensity (black). Karl traversed the Yucatan Peninsula beginning 15 September at 12 UTC before emerging in the Bay of Campeche on 16 September at 06 UTC.

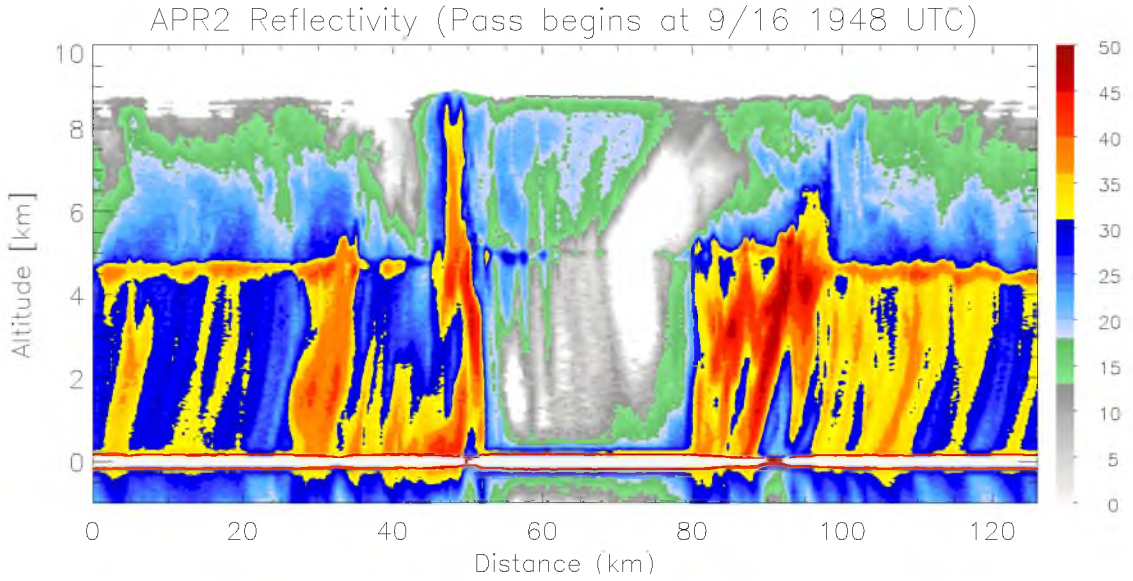

Figure 5.2 APR-2 cross section of Karl's inner core reflectivity (dBZ) on 16 September at 1948 UTC.

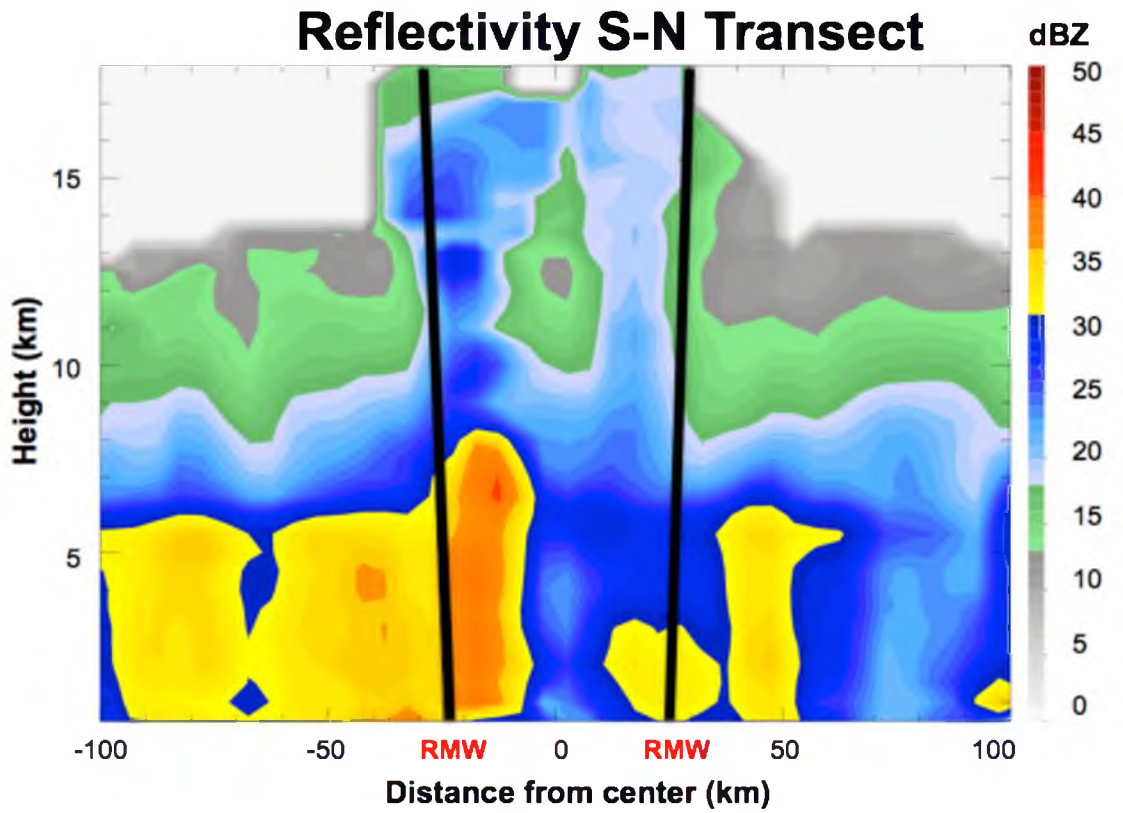

Figure 5.3 NOAA P-3 tail radar Doppler reflectivity from a S-N transect across Karl's center at approximately 1830 UTC on 16 September.

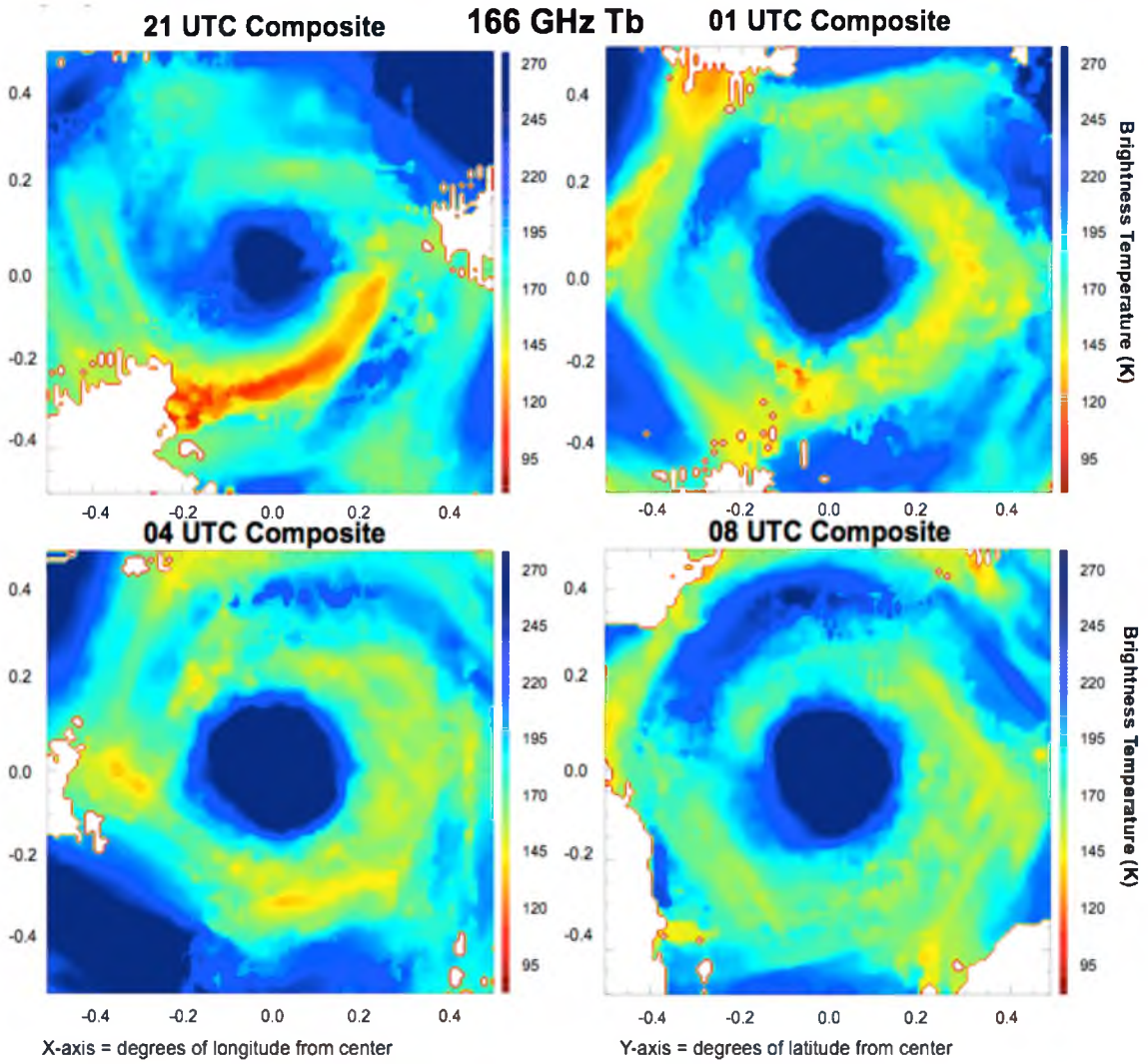

Figure 5.4 Brightness temperature [K] composites (166 GHz) from Level 1 HAMSR data aboard the NASA Global Hawk 16 - 17 September.

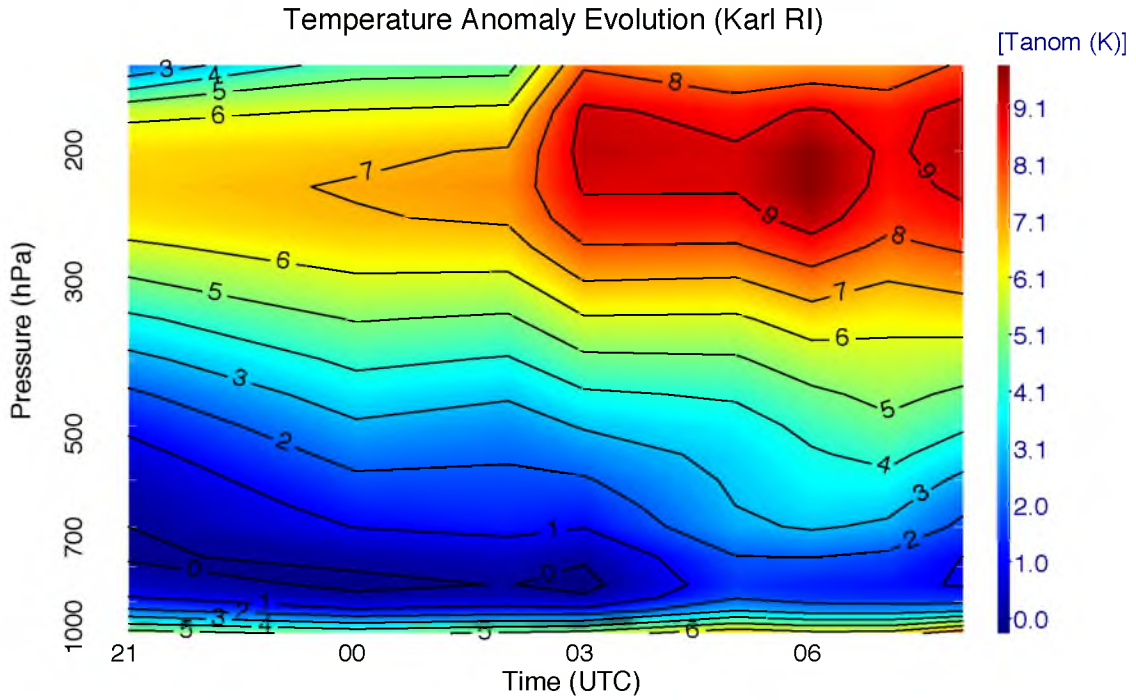

Figure 5.5. Reproduction of a figure from Brown et al. (2011) using HAMSR Level 2 derived eye temperatures to demonstrate the warm core evolution on 16-17 September during Karl's (2010) rapid intensification.

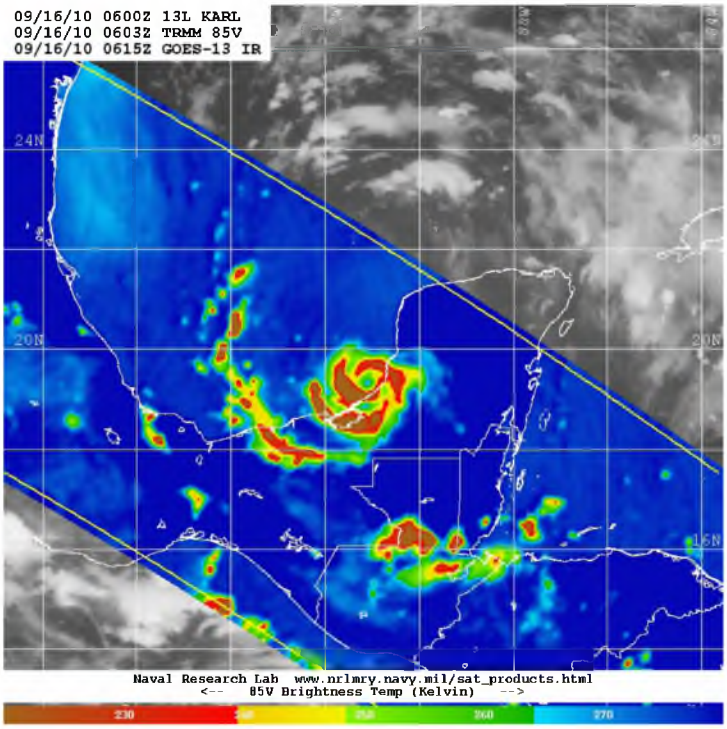

Figure 5.6. Tb (85 GHz) from TMI at 06 UTC 16 September. Image courtesy of Naval Research Laboratory. http://www.nrlmry.navy.mil/TC.html

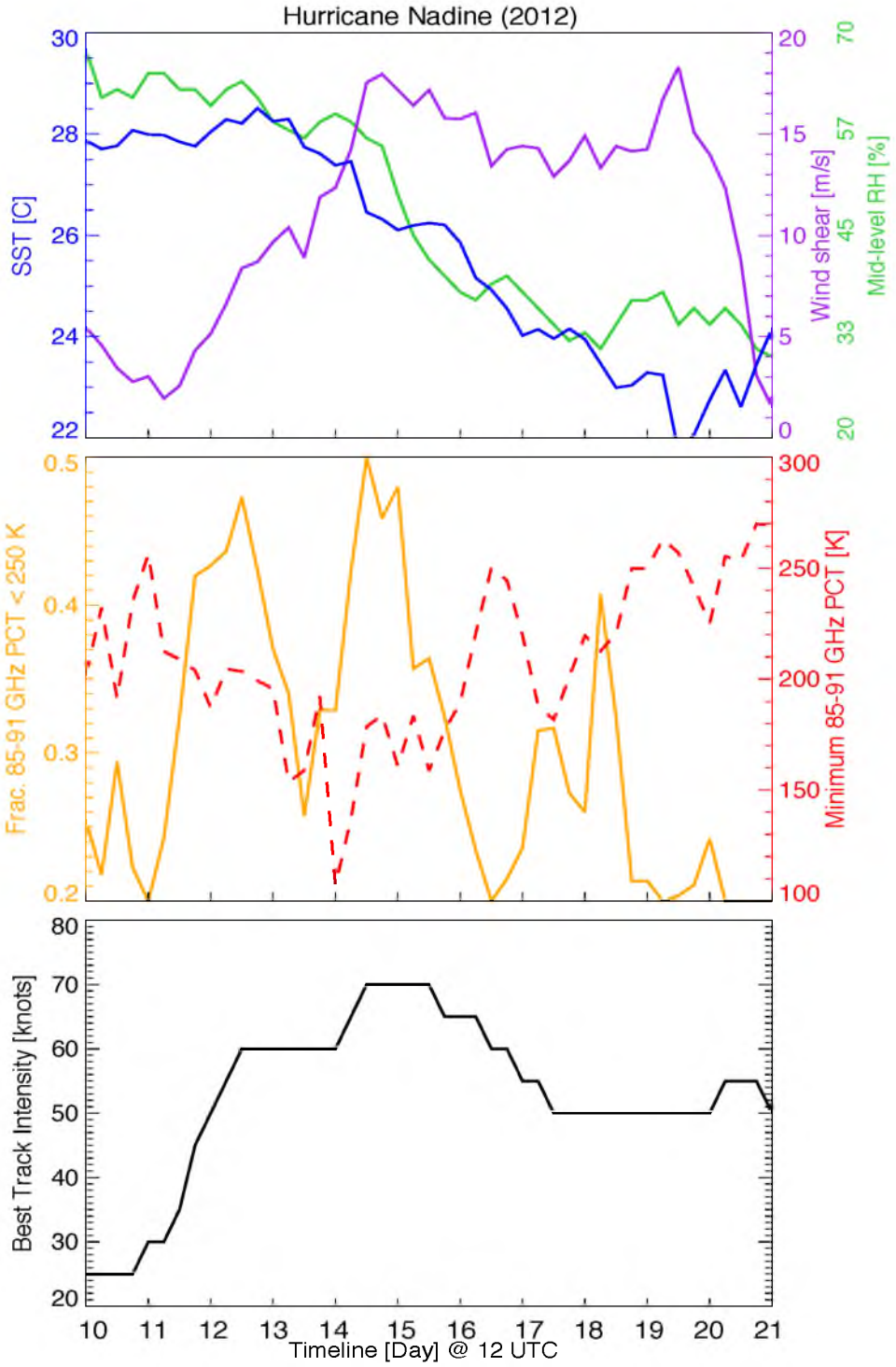

Figure 5.7. Evolution of Nadine's environmental characteristics (SST: blue; vertical wind shear: purple; midlevel RH: green), convective properties (minimum 85-91 GHz PCT within 1° of the center: red; fractional coverage of 85-91 GHz PCT < 250 K: orange), and best track intensity (black). Nadine intensified in the Subtropical Atlantic on 11-12 September; thereafter, Nadine was steady state until briefly dissipating into a remnant low on 21 September.

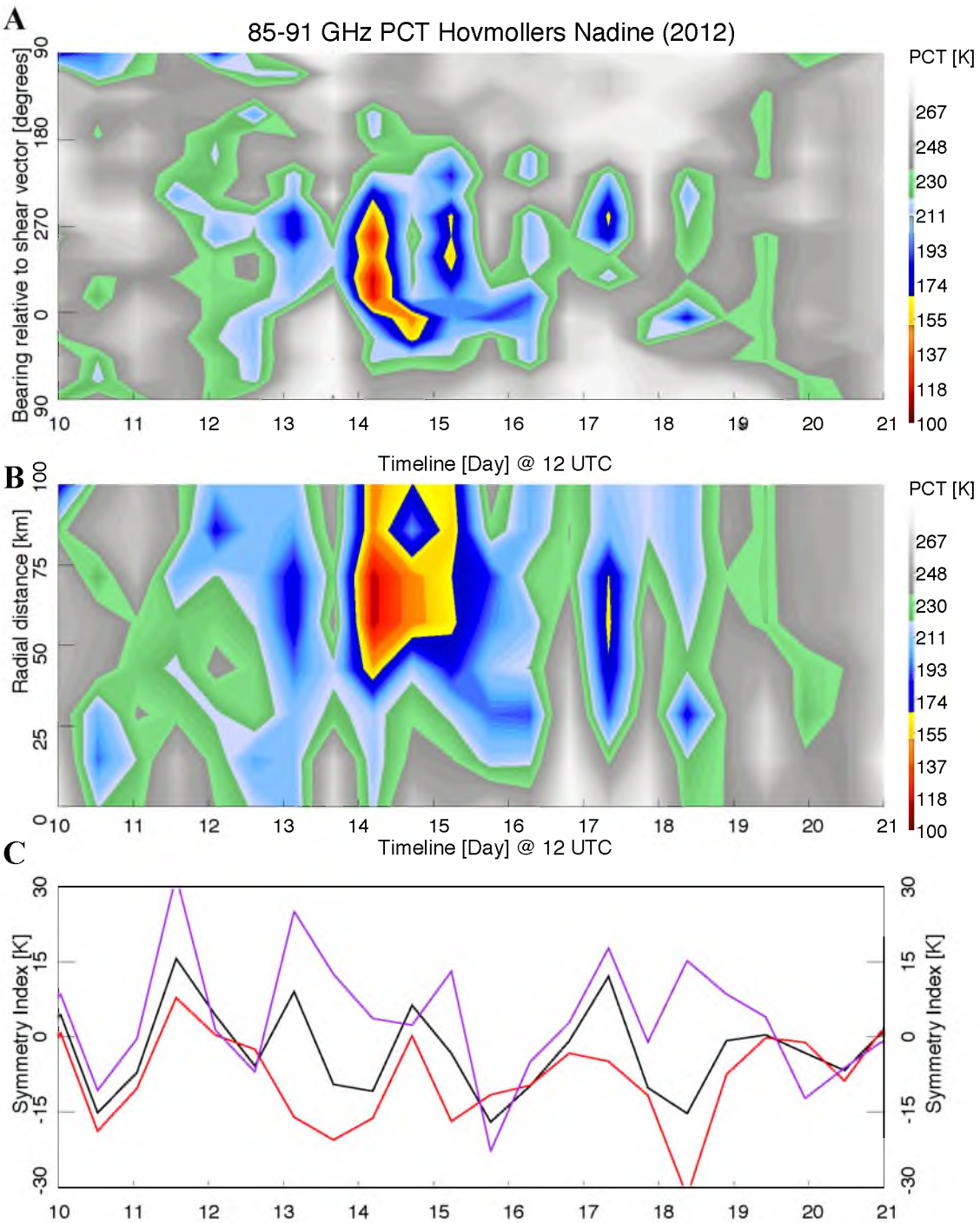

Figure 5.8. Hövmollers of Nadine's 85-91 GHz PCT symmetry (A) and radial distribution (B) evolution from 12 UTC 10 September to 21 September. (C) shows the symmetry index: Quadrants are oriented with respect to the shear vector; UL - DL (black); UL - DR (red); UR - DL (purple). Following previous methodology (Figs. 4.5 - 4.6), the symmetry index is calculated only using 85-91 GHz PCTs within 60 km of the center.

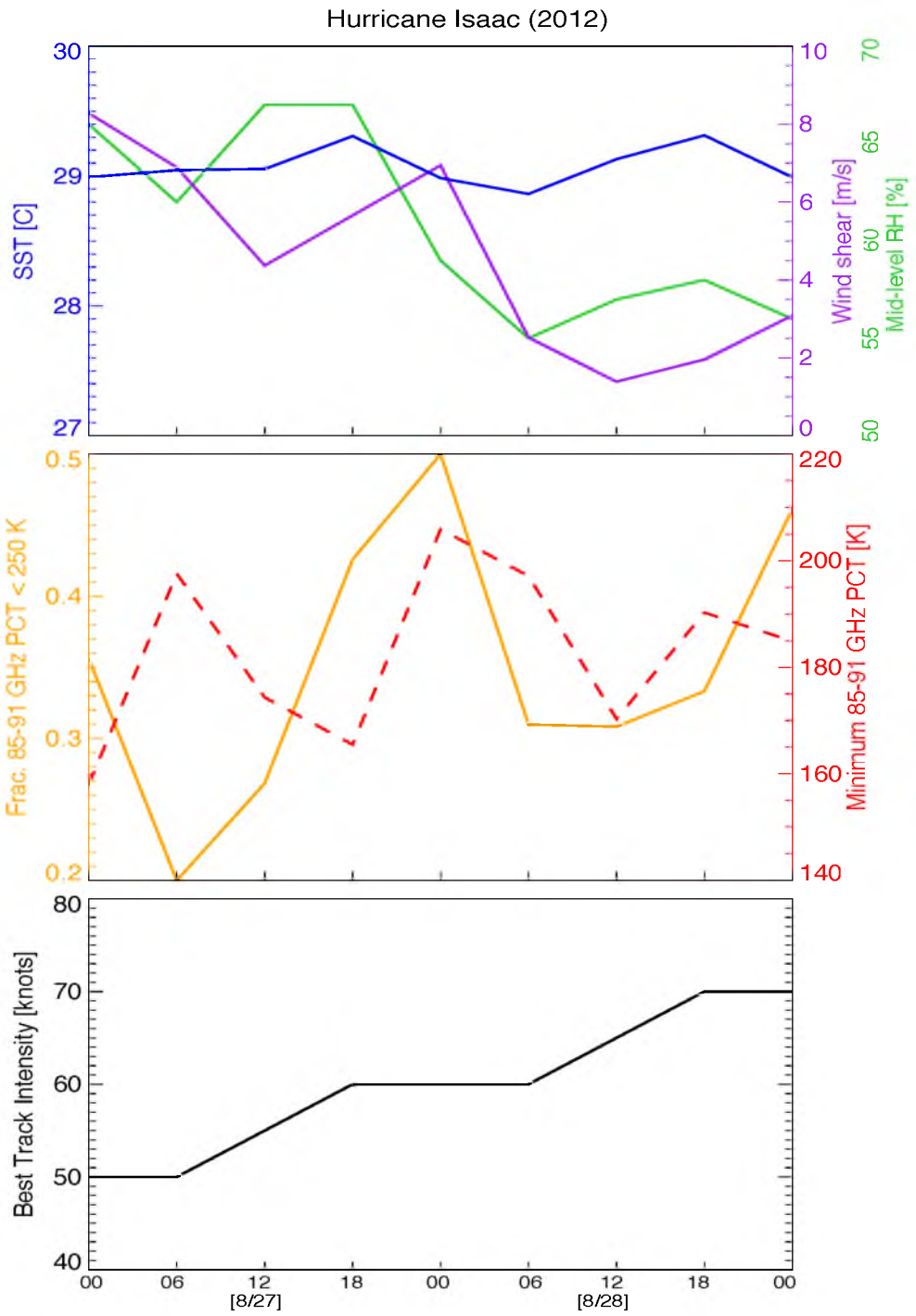

Figure 5.9. Evolution of Isaac's environmental characteristics (SST: blue; vertical wind shear: purple; midlevel RH: green), convective properties (minimum 85-91 GHz PCT within 1° of the center: red; fractional coverage of 85-91 GHz PCT < 250 K: orange), and best track intensity (black).

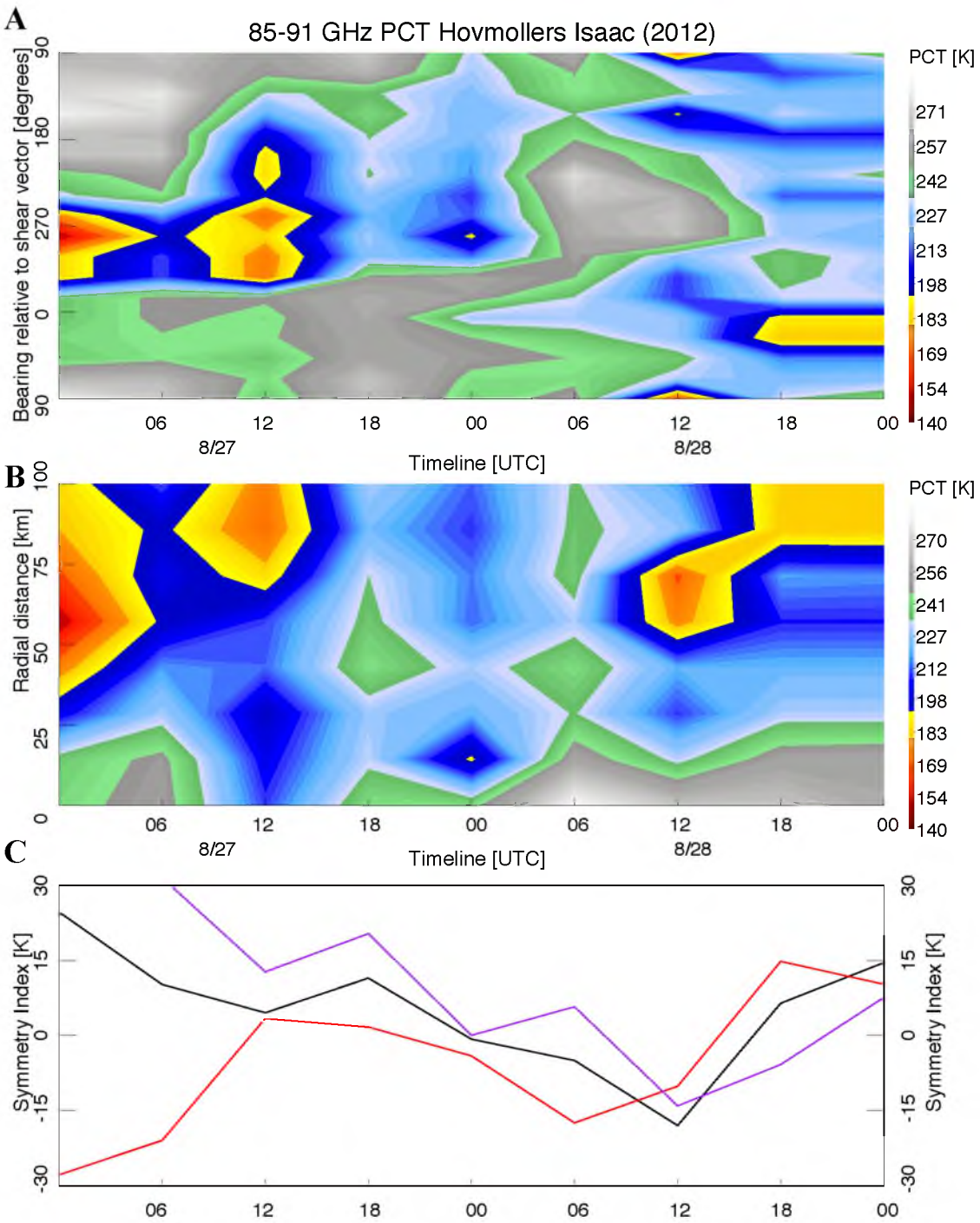

Figure 5.10. Hövmollers of Isaac's 85-91 GHz PCT symmetry (A) and radial distribution (B) evolution from 00 UTC 27 August to 29 August. (C) shows the symmetry index: Quadrants are oriented with respect to the shear vector; UL - DL (black); UL - DR (red); UR - DL (purple). Following previous methodology (Figs. 4.5 - 4.6), the symmetry index is calculated only using 85-91 GHz PCTs within 60 km of the center.

CHAPTER 6

SUMMARY AND CONCLUSIONS

Similar to previous studies (DeMaria and Kaplan 1994; Hendricks et al. 2010), the importance of environmental variables relative to 24-hour intensity changes was investigated. In addition, precipitation properties (relative to the shear vector following Cecil and Zipser, 1999; Jiang, 2012; Ramirez et al. 2013; Zagrodnik et al. 2014) were investigated using a TC-PMW dataset comprising overpasses from multiple basins (Atlantic and EPAC). Separating itself from previous studies, environmental parameters and convective distributions were examined not only during the period of intensification, but also uniquely in the period preceding intensification. The TC-PMW dataset used in this study utilized 15 years of data in the Atlantic and EPAC from multiple PMW sensors (AMSR-E, SSMI-[S], TMI) in the EPAC and Atlantic. In addition, PCT distributions, used as proxies for precipitation and convective intensity, were investigated both spatially (in shear-oriented quadrants) and quantitatively. New metrics for quantifying the symmetry of precipitation were also explored (a Symmetry Index and quadrant based standard deviations). Finally, while many previous studies have loosely categorized TCs as RI versus non-RI, this study attempted to analyze the entire spectrum of intensification rates when possible.

6.1 Environmental Characteristics

Similar to findings from Kaplan and DeMaria (2003, 2010), an examination of the most important environmental variables (vertical wind shear, SST, VMPI-$V_{current}$, OHC, midtropospheric RH) reveals that intensity change in both the Atlantic and EPAC is sensitive to changes in environmental characteristics. However, environmental variables alone do not consistently offer predictive value in distinguishing 24-hour intensity change in 10-kt increments. On average, storms that undergo RI begin (within 24 hours prior to onset) with a more humid environment over warmer waters and in lower vertical wind shear; investigation of slower intensification rates, though, reveals significant overlap in the spectrum of environmental characteristics.

Because statistically significant spatial and magnitude differences are identified between the basins, the Atlantic and EPAC are separated for examination of environmental properties. While both basins demonstrate environmental sensitivity with respect to intensity change, the EPAC is more sensitive to smaller changes in environmental variables. This coincides with the fact the Atlantic, as a whole, has a much more variable environment than the EPAC. This higher variability is attributed to an increased latitudinal extent of TC occurrence, and subsequent interactions with mid-latitude troughs.

6.2 Precipitation and Convective Properties

In agreement with Cecil and Zipser (1999), Ramirez et al. (2013), and Kieper and Jiang (2012), this study verified that the occurrence of inner core precipitation at the onset (0 hour) not only increases with intensification rate in all quadrants, but also that the symmetry (measured by the occurrence in the upshear quadrants) distinguishes those

that undergo RI (greater symmetry) versus those with slower intensification rates (less symmetry). Additionally, it is determined that symmetry is already increasing prior to the onset of RI, coincident with a median increase in intensity of 10 kts during this period. Removing those storms already intensifying, however, reveals a similar result. This can be attributed to the fact that storms without pre-onset intensification have a nearly identical VMPI-$V_{current}$ at the 0 hour to those already intensifying. Symmetry is also found to increase throughout the entire 42-hour period (18 hours before, to 24 hours after onset) with highest percent occurrences of PCT < 250 K (used as a proxy for a raining area) in the "RI continuing" stage (similar to findings from Zagrodnik et al. 2014). Since the magnitudes of the vertical wind shear change very little during the entire 42-hour period, the increase in precipitation symmetry, in a composite perspective, during RI is not attributed to decreasing wind shear. The spatial frequency distributions of PCT < 250 K also reveal that the maximum coverage actually increases and rotates from DL towards the upshear quadrants during RI (a result also found with case studies of Hurricane Earl (2010) by Rogers et al. 2014, Stevenson et al. 2014, and Susca-Lopata et al. 2014).

The symmetry indices developed for this study all reveal that the rate of symmetrization increases with increasing intensity change. During the 18-hour period preceding RI, storms have a significantly (at the 95% confidence level) greater asymmetry, according to the mean PCT and standard deviations in each quadrant, than those slowly intensifying. By the 0 hour, however, RI storms have a more symmetric distribution than those with slower intensification rates.

As intensification rates increase, the occurrence of "intense" convection (proxy using 85-91 GHz PCT < 190 K) noticeably increases. The period 18 hours prior to RI

onset also features a higher fractional occurrence of "intense" near-center (within 50 km) convection than all other periods prior to onset, and seems to be related to the amount of intensification. The frequency of intense, near-center convection does not increase after RI onset, and the "more intense" (PCT < 170 K) convection actually decreases. A reinvigoration of intense convection is noted during the "continuing RI" period, possibly a result of diurnal variations, a consolidating eyewall, or a reflection of varying pathways towards RI with different environmental interactions. While the results from this study clearly demonstrate important contributions from intense convection, similarly to Jiang (2012), because of its occurrence across the intensity change spectrum, it is concluded that hot towers (intense convection), alone, are neither a necessary nor sufficient condition for RI.

6.3 Case Studies: A Synthesis of Environmental and Precipitation Characteristics

Karl (2010) features a strong, prolonged asymmetric convective burst, located in the DL quadrant within the RMW. While it is hypothesized to have aided in the intensification of Karl, this cannot be verified solely from temporally limited in situ data. The "burst," at least in this case, however, agrees with results from the overall TC-PMW dataset. RI storms are more asymmetric 18 hours prior to RI onset, followed by a rapid symmetrization, though, the most significant symmetrization is slightly delayed until RI onset. Another interesting characteristic of Karl is that, while over the Yucatan Peninsula for approximately 18 hours, the TC features a remarkably organized structure with well-defined inner-core convection and an eye-like feature. This favorable organization over land likely allows Karl to immediately undergo RI upon emergence in the Bay of

Campeche. Because forecasted environmental conditions do not change significantly throughout Karl's lifecycle, it is believed that Karl's convective evolution plays a dominant role in RI.

Nadine (2012) features a high precipitation asymmetry 18-24 hours prior to intensification (12 September), followed by increasing symmetry prior to onset (similar to findings from the overall TC-PMW dataset). Interestingly, however, Nadine has a relative lack of intense convection during the first intensification period. "Intense" convection is observed during a weaker intensification period (10 kts on 14 September), but coincides with higher vertical wind shear (10-15 m s^{-1}) that may have promoted the "intense" convective initiation. Nadine also remains a resilient TC in the face of hostile environmental conditions, possibly due to the shallow/hybrid nature of the vortex.

Isaac (2012) reiterates the importance of using all available aircraft in situ and satellite data (RMW) when possible. Consistent with Rogers et al. (2013, 2014), the location of convective intensity maxima with respect to the RMW, identified to be unfavorable outside the RMW, appears to play an important role in the lack of intensification in Isaac; a lack of intensification that was not anticipated by NHC forecasters. Although it is difficult to make robust conclusions with any individual case study alone, when placed in a historical context, as done using the TC-PMW dataset, more confidence can be placed on the importance of particular properties observed before, and during, intensification events.

In summarization the most significant findings of this study include the determination that while intensification is sensitive to changes in environmental characteristics, these variables, alone, do not consistently offer predictive value in

distinguishing 24-hour intensity changes in 10-kt increments (hence the emphasis on convective and precipitation characteristics). In addition, an investigation of precipitation properties finds that higher intensification rates (including RI) have more "intense" near center convection and more asymmetric distributions of precipitation prior to intensification onset (but also a greater overall areal coverage). Also, while results clearly demonstrate important contributions from intense convection, similarly to Jiang (2012) it is concluded that hot towers, alone, are neither a necessary nor sufficient condition for RI. Of possibly greater importance, intensification is more strongly correlated to the evolution of the areal, radial, and rate of symmetrization of precipitation. Future work should include a focus on the quantification of these precipitation properties with potential uses in statistical intensity prediction.

REFERENCES

Bister, M., and K.A. Emanuel, 1998: Dissipative Heating and Hurricane Intensity. *Meteor. Atm. Phys.*, **52**, 233-240.

Black, M.L., J. F. Gamache, F. D. Marks Jr., C. E. Samsury, and H. E. Willoughby, 2002: Eastern Pacific Hurricanes Jimena of 1991 and Olivia of 1994: The Effect of Vertical Shear on Structure and Intensity. *Mon. Wea. Rev.*, **130**, 2291-2312.

Bosart, L.F., W.E. Bracken, J. Molinari, C.S. Velden, and P.G. Black, 2000: Environmental Influences on the Rapid Intensification of Hurricane Opal (1995) over the Gulf of Mexico. *Mon. Wea. Rev.*, **128**, 322-352.

Braun, S.A., J.A. Sippel, and D.S. Nolan, 2012: The Impact of Dry Midlevel Air on Hurricane Intensity in Idealized Simulations with No Mean Flow. *J. Atmos. Sci.*, **69**, 236-257.

Cecil, D.J., and E.J. Zipser, 1999: Relationships between Tropical Cyclone Intensity and Satellite-Based Indicators of Inner Core Convection: 85-GHz Ice-Scattering Signature and Lightning. *Mon. Wea. Rev.*, **127**, 103-123.

Cecil, D.J., and E.J. Zipser, 2002: Reflectivity, Ice Scattering, and Lightning Characteristics of Hurricane Eyewalls and Rainbands. Part II: Intercomparison of Observations. *Mon. Wea. Rev.*, **130**, 785-801.

Cecil, D.J., E.J. Zipser, and S.W. Nesbitt, 2002: Reflectivity, Ice Scattering, and Lightning Characteristics of Hurricane Eyewalls and Rainbands. Part I: Quantitative Description. *Mon. Wea. Rev.*, **130**, 769-784.

Chen, H., and D. Zhang, 2013: On the Rapid Intensification of Hurricane Wilma (2005). Part II: Convective Bursts and the Upper-Level Warm Core. *J. Atmos. Sci.*, **70**, 146-162.

Corbosiero, K.L., and J. Molinari, 2002: The Effects of Vertical Wind Shear on the Distribution of Convection in Tropical Cyclones. *Mon. Wea. Rev.*, **130**, 2110-2123.

DeHart, J.C., R.A. Houze Jr., and Robert F. Rogers, 2014: Quadrant Distribution of Tropical Cyclone Inner-Core Kinematics in Relation to Environmental Shear. *J. Atmos. Sci.*, **71**, 2713-2732.

DeMaria, M., and J. Kaplan, 1994: A Statistical Hurricane Intensity Prediction Scheme (SHIPS) for the Atlantic Basin. *Wea. Forecasting*, **9**, 209-220.

DeMaria, M., and J. Kaplan, 1999: An Updated Statistical Hurricane Intensity Prediction Scheme (SHIPS) for the Atlantic and Eastern North Pacific Basins. *Wea. Forecasting*, **14**, 326-337.

Emanuel, K.A., 1987: The Dependence of Hurricane Intensity on Climate. *Letters to Nature*, **326**, 483-485.

Emanuel, K.A., 1988: The Maximum Intensity of Hurricanes. *J. Atmos. Sci.*, **45**, 1143-1155.

Emanuel, K., C. DesAutels, C. Holloway, and R. Korty, 2004: Environmental Control of Tropical Cyclone Intensity. *J. Atmos. Sci.*, **61**, 843-858.

Gall, R., J. Franklin, F. Marks, E.N. Rappaport, and F. Toepfer, 2013: The Hurricane Forecast Improvement Project. *Bull. Amer. Meteor. Soc.*, **94**, 329-343.

Gopalakrishnan, S.G., F. Marks Jr., X. Zhang, J. Bao, K. Yeh, and R. Atlas, 2011: The Experimental HWRF System: A Study on the Influence of Horizontal Resolution on the Structure and Intensity Changes in Tropical Cyclones Using an Idealized Framework. *Mon. Wea. Rev.*, **139**, 1762-1784.

Gray, W. M., 1998: The Formation of Tropical Cyclones. *Meteor. Atmos. Phys.*, 67, 37-69.

Guimond, S.R., G.M. Heymsfield, and F.J. Turk, 2010: Multiscale Observations of Hurricane Dennis (2005): The Effects of Hot Towers on Rapid Intensification. *J. Atmos. Sci.*, **67**, 633-654.

Hanley, D., J. Molinari, and D. Keyser, 2001: A Composite Study of the Interactions between Tropical Cyclones and Upper-Tropospheric Troughs. *Mon. Wea. Rev.*, **129**, 2570-2584.

Hence, D.A., and R.A. Houze Jr., 2011: Vertical Structure of Hurricane Eyewalls as Seen by the TRMM Precipitation Radar. *J. Atmos. Sci.*, **68**, 1637-1652.

Hence, D.A., and R.A. Houze Jr., 2012: Vertical Structure of Tropical Cyclone Rainbands as Seen by the TRMM Precipitation Radar. *J. Atmos. Sci.*, **69**, 2644-2661.

Hendricks, E. A., M. T. Montgomery, and C. A. Davis, 2004: On the Role of "Vortical" Hot Towers in Formation of Tropical Cyclone Diana (1984). *J. Atmos. Sci.,* 61, 1209-1232.

Hendricks, E.A., M.S. Peng, B. Fu, and T. Li, 2010: Quantifying Environmental Control on Tropical Cyclone Intensity Change. *Mon. Wea. Rev.*, **138**, 3243-3271.

Heymsfield, G.M., J.B. Halverson, J. Simpson, L. Tian, and T.P. Bui, 2001: ER-2 Doppler Radar Investigations of the Eyewall of Hurricane Bonnie during the Convection and Moisture Experiment-3. *J. Appl. Meteor.*, **40**, 1310-1330.

Holliday, C.R., and A.H. Thompson, 1979: Climatological Characteristics of Rapidly Intensifying Typhoons. *Mon. Wea. Rev.*, **107**, 1022-1034.

Houze Jr., R.A., W. Lee, and M.M. Bell, 2009: Convective Contribution to the Genesis of Hurricane Ophelia (2005). *Mon. Wea. Rev.*, **137**, 2778-2800.

Houze Jr., R.A., 2010: Clouds in Tropical Cyclones. *Mon. Wea. Rev.*, **138**, 293-344.

Jiang, H., C. Liu, and E.J. Zipser, 2011: A TRMM-Based Tropical Cyclone Cloud and Precipitation Feature Database. *J. Appl. Meteor. Climatol.*, **50**, 1255-1274.

Jiang, H., 2012: The Relationship between Tropical Cyclone Intensity Change and the Strength of Inner-Core Convection. *Mon. Wea. Rev.*, **140**, 1164-1176.

Jiang, H., and E.M. Ramirez, 2013: Necessary Conditions for Tropical Cyclone Rapid Intensification as Derived from 11 Years of TRMM Data. *J. Climate*, **26**, 6459-6470.

Kaplan, J., and M. DeMaria, 2003: Large-Scale Characteristics of Rapidly Intensifying Tropical Cyclones in the North Atlantic Basin. *Wea. Forecasting*, **18**, 1093-1108.

Kaplan, J., M. DeMaria, and J.A. Knaff, 2010: A Revised Tropical Cyclone Rapid Intensification Index for the Atlantic and Eastern North Pacific Basins. *Wea. Forecasting*, **25**, 220-241.

Kieper, M., and H. Jiang, 2012: Predicting Tropical Cyclone Rapid Intensification Using the 37GHz Ring Pattern Identified from Passive Microwave Measurements. *Geophys. Res. Lett.*, **39**, L13804, doi:10.1029/2012GL052115.

Lambrigtsen, B., Brown, S., Behrangi, A., 2011: Observing Tropical Cyclones from the Global Hawk: HAMSR Results from GRIP. *Fall Meeting 2011*, San Francisco, CA, American Geophysical Union.

Lonfat, M., F.D. Marks Jr., and S.S. Chen, 2004: Precipitation Distribution in Tropical Cyclones Using the Tropical Rainfall Measuring Mission (TRMM) Microwave Imager: A Global Perspective. *Mon. Wea. Rev.*, **132**, 1645-1660.

Mainelli, M., M. DeMaria, L.K. Shay, and G. Goni, 2008: Application of Oceanic Heat Content Estimation to Operational Forecasting of Recent Atlantic Category 5

Hurricanes. *Wea. Forecasting*, **23**, 3-16.

Malkus, J.S., and H. Riehl, 1960: On the Dynamics and Energy Transformations in Steady-state Hurricanes. *Tellus*, 12, 1-20.

Miller, B.I., 1958: On the Maximum Intensity of Hurricanes. *J. Meteor.*, **15**, 184-195.

Mohr, K.I., and E.J. Zipser, 1996: Mesoscale Convective Systems Defined by Their 85-GHz Ice Scattering Signature: Size and Intensity Comparison over Tropical Oceans and Continents. *Mon. Wea. Rev.*, **124**, 2417-2437.

Molinari, J., J. Frank, and D. Vollaro, 2013: Convective Bursts, Downdraft Cooling, and Boundary Layer Recovery in a Sheared Tropical Storm. *Mon. Wea. Rev.*, **141**, 1048-1060.

Montgomery, M. T. and R. J. Kallenbach, 1997: A Theory for Vortex Rossby-waves and its Application to Spiral Bands and Intensity Changes in Hurricanes. *Q. J. R. Meteorol. Soc.*, **123**, 435-465.

National Hurricane Center, Brown, Daniel P., 2013: Tropical Cyclone Report - Hurricane Nadine. [Available online at http://www.nhc.noaa.gov/data/tcr/AL142012_Nadine.pdf.]

Nolan, D. S. and M. T. Montgomery, 2002: Nonhydrostatic, Three-dimensional Perturbations to Balanced, Hurricane-like Vortices. Part I: Linearized Formulation, Stability and Evolution. *J. Atmos. Sci.*, **59**, 2989-3020.

Nolan, D.S., and L.D. Grasso, 2003: Nonhydrostatic, Three-Dimensional Perturbations to Balanced, Hurricane-Like Vortices. Part II: Symmetric Response and Nonlinear Simulations. *J. Atmos. Sci.*, **60**, 2717-2745.

Palmén, E., 1948: On the Formation and Structure of Tropical Hurricanes. *Geophysica*.

Rogers, R., S. Chen, J. Tenerelli, and H. Willoughby, 2003: A Numerical Study of the Impact of Vertical Shear on the Distribution of Rainfall in Hurricane Bonnie (1998). *Mon. Wea. Rev.*, **131**, 1577-1599.

Rogers, R., P. Reasor, and S. Lorsolo, 2013: Airborne Doppler Observations of the Inner-Core Structural Differences between Intensifying and Steady-State Tropical Cyclones. *Mon. Wea. Rev.*, **141**, 2970-2991.

Rogers, R., P. Reasor, and J. Zhang, 2014: Multiscale Structure and Evolution of Hurricane Earl (2010) During Rapid Intensification. *Mon. Wea. Rev.* doi:10.1175/MWR-D-14-00175.1, in press.

Shapiro, L.J., and H.E. Willoughby, 1982: The Response of Balanced Hurricanes to

Local Sources of Heat and Momentum. *J. Atmos. Sci.*, **39**, 378-394.

Shay, L.K., G.J. Goni, and P.G. Black, 2000: Effects of a Warm Oceanic Feature on Hurricane Opal. *Mon. Wea. Rev.*, **128**, 1366-1383.

Shea, D.J., and W.M. Gray, 1973: The Hurricane's Inner Core Region. I. Symmetric and Asymmetric Structure. *J. Atmos. Sci.*, **30**, 1544-1564.

Sitkowski, M., and G.M. Barnes, 2009: Low-Level Thermodynamic, Kinematic, and Reflectivity Fields of Hurricane Guillermo (1997) during Rapid Intensification. *Mon. Wea. Rev.*, **137**, 645-663.

Skofronick-Jackson, G., A. Heymsfield, E. Holthaus, C. Albers, and M.-J. Kim (2008), Nonspherical and Spherical Characterization of Ice in Hurricane Erin for Wideband Passive Microwave Comparisons, *J. Geophys. Res.*, 113, D06201, doi:10.1029/2007JD008866.

Spencer, R.W., H.M. Goodman, and R.E. Hood, 1989: Precipitation Retrieval over Land and Ocean with the SSM/I: Identification and Characteristics of the Scattering Signal. *J. Atmos. Oceanic Technol.*, **6**, 254-273.

Stevenson, S.N., K.L. Corbosiero, and J. Molinari, 2014: The Convective Evolution and Rapid Intensification of Hurricane Earl (2010). *Mon. Wea. Rev.*, **142**, 4364-4380.

Susca-Lopata, G.A., E.J. Zipser, and R. Rogers 2014: Evaluating Different Convective Indicators of Tropical Cyclone Rapid Intensification: The Case of Hurricane Earl (2010). *AMS Tropical Meeting 2014*, San Diego, CA, American Meteorological Society.

Wang, Y., 2009: How Do Outer Spiral Rainbands Affect Tropical Cyclone Structure and Intensity? *J. Atmos. Sci.*, **66**, 1250-1273.

Wingo, M.T., and D.J. Cecil, 2010: Effects of Vertical Wind Shear on Tropical Cyclone Precipitation. *Mon. Wea. Rev.*, **138**, 645-662.

Zagrodnik, J.P., and H. Jiang, 2014: Rainfall, Convection, and Latent Heating Distributions in Rapidly Intensifying Tropical Cyclones. *J. Atmos. Sci.*, **71**, 2789-2809.

Zipser, E., 2003: Some Views on ''Hot Towers'' After 50 Years of Tropical Field Programs and Two Years of TRMM Data. Cloud Systems, Hurricanes, and the Tropical Rainfall Measuring Mission (TRMM)—A Tribute to Dr. Joanne Simpson, Meteor.Monogr., No. 29, *Amer. Meteor. Soc.*, 49-58.